1   Introduction

This draft report is being provided to the Modeling Workgroup for review prior to the July meeting. The modeling workgroup members will be asked for approval of certain sections of this document pertaining to topics considered complete by the modeling team. Each section will have notes requesting review of the appropriate topics. Other topics are provided as draft for information purposes. You may find the topics for review by searching for "MWG review"

MWG Review: The introduction will provide useful background, however review and approval of section 1 and its subsections are not necessary

1.1   Partnership Decision Context

The EPA and the Chesapeake Bay Program (CBP) partnership put in place the Chesapeake Bay TMDL in 2010, setting allocation limits on nitrogen, phosphorus, and sediment from each jurisdiction and major basin (U.S. EPA 2010). The modeling for the TMDL was performed using a hydrologic averaging period, 1991-2000, that was judged to represent long term average precipitation, temperature, and meteorology. The critical period for meeting dissolved oxygen water quality standards is a wetter period within that span, 1993-1995, representing a three-year period with a 10-year recurrence interval.

The averaging period and critical period represent long term climate norms that will no longer be representative of average conditions or a 10-year recurrence interval condition. The strategy for incorporating climate change as of 2025 is to examine the changes expected due to long term trends between 1995 and 2025. The 30-year change in climate is to be applied to the CBP modeling data sets and the environmental change assessed. For information and planning purposes, the partnership will also examine change expected by 2035, 2045, and 2055.

The CBP partnership's 2017 Midpoint Assessment process resulted in updates to nutrient and sediment planning targets consistent with the 2010 Chesapeake Bay TMDL allocations. The new planning targets were based on updates to the CBP's suite of models, accounting for the influence of the changing conditions in the Conowingo Reservoir, and consideration of future population and land use change. Consideration of the effects of climate change on the CBP partnership's ability to reach water quality goals in the bay was part of the 2017 Midpoint Assessment process as well, however, the partnership decided to delay decisions until additional modeling could be completed.

The CBP's Principals' Staff Committee (PSC) met in March 2018 and agreed that the jurisdictions' Phase III Watershed Implementation Plans (WIPs) would address climate change narratively and numerically. Specifically, the WIPs would include a narrative strategy describing the jurisdictions' current action plans and strategies to address climate change. The partnership further committed to adopting numerical climate change targets by 2021 using the CBP's modeling tools. Initial estimates were that climate change effects on dissolved oxygen

standards were equivalent to an increase of 9 million pounds of nitrogen and 0.5 million pounds of phosphorus. Jurisdictions may include numerical adjustments to account for climate change within their current WIPs if they choose.

The PSC agreed to refine the climate modeling and assessment framework based on improved understanding of the science of the impacts of climate change. Research needs will be identified, particularly with regard to a better understanding of BMP responses. New, enhanced, and resilient BMPs that better address climate change conditions such as increased storm intensity are a focus point.

In March 2021, the Partnership will consider results of updated methods, techniques, and studies and develop an estimate of pollutant load changes (nitrogen, phosphorus, and sediment) due to 2025 climate change conditions.   In September 2021 jurisdictions will account for additional nutrient and sediment pollutant loads due to 2025 climate change conditions in a Phase III WIP addendum and/or 2-year milestones beginning in 2022.   Starting with the 2022-2023 milestones, the Partnership will determine how climate change will impact the BMPs included in the WIPs and address these vulnerabilities in the two-year milestones.

Oversight of the climate change assessment development process will be handled by groups within the CBP management structure. The management questions involving climate change will be articulated by the PSC, the Management Board (MB), and the Water Quality Goal Implementation Team (WQGIT). Technical direction for the climate change analysis will be handled by workgroups of Scientific, Technical Assessment & Reporting (STAR). The Modeling Workgroup and Climate Resiliency Workgroup (CRWG) will direct the CBPO's modeling team on technical issues of input data set and modeling response development with the advice of the Scientific and Technical Advisory Committee (STAC), the MB, the WQGIT, and workgroups of the WQGIT. Figure 1-1 shows a simplified timeline of the climate analysis.

2018	2019	2020	2021
STAC Workshop Partnership Decisions on schedule	The Modeling WG and Climate Resiliency WQ direct the Modeling team to develop climate change assessment for TMDL	Technical Review of Models	Climate change considerations will be implemented into the 2022-2023 milestones.
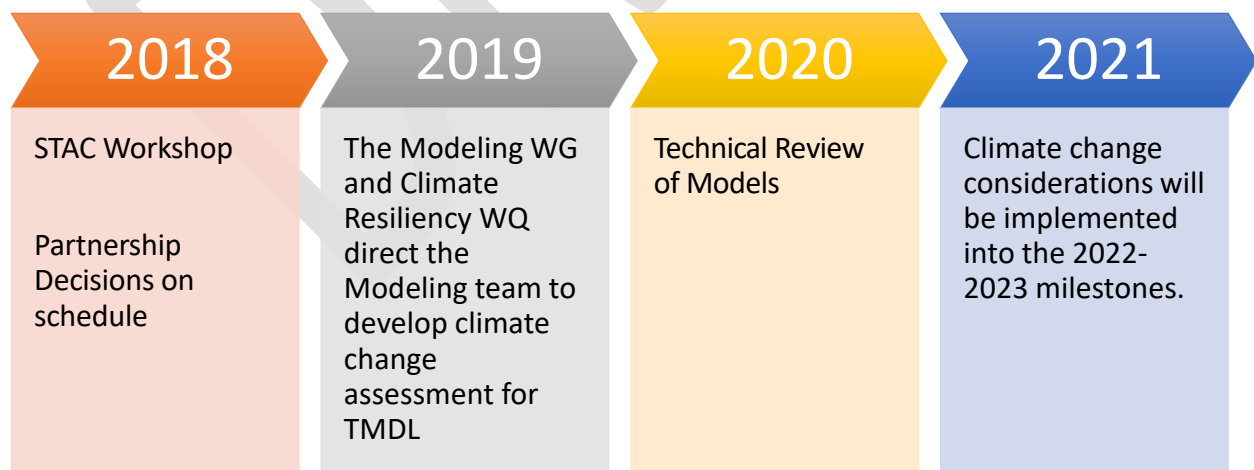
Figure 1-1: Climate assessment timeline

1.2   Modeling Framework

The CBP used a linked system of airshed, land use, watershed, and estuarine models for the 2010 TMDL (U.S. EPA 2010), the 2011 Phase II WIPs, and the 2017 Midpoint Assessment. The CBP has used similar systems dating back to decisions in the 1980s and 1990s (Linker et al, 2002). Figure 1-2 shows a schematic of the system, which is designed to address questions of how Chesapeake Bay water quality will respond to changes in management actions. The CBP Land Use Change Model predicts changes in land use, sewerage, and septic systems given changes in land use policy. The Airshed Model, a combination of a regression model of National Atmospheric Deposition Program (NADP) data and a national application of the Community Multiscale Air Quality (CMAQ) Model, predicts changes in deposition of inorganic nitrogen due to changes in emissions. The Watershed Model combines the output of these models with other data sources, such as the US Census of Agriculture, and predicts the loads of nitrogen, phosphorus, and sediment that result from the given inputs. The estuarine Water Quality and Sediment Transport Model (WQSTM) predicts changes in Bay water quality due to the changes in input loads provided by the Watershed Model.
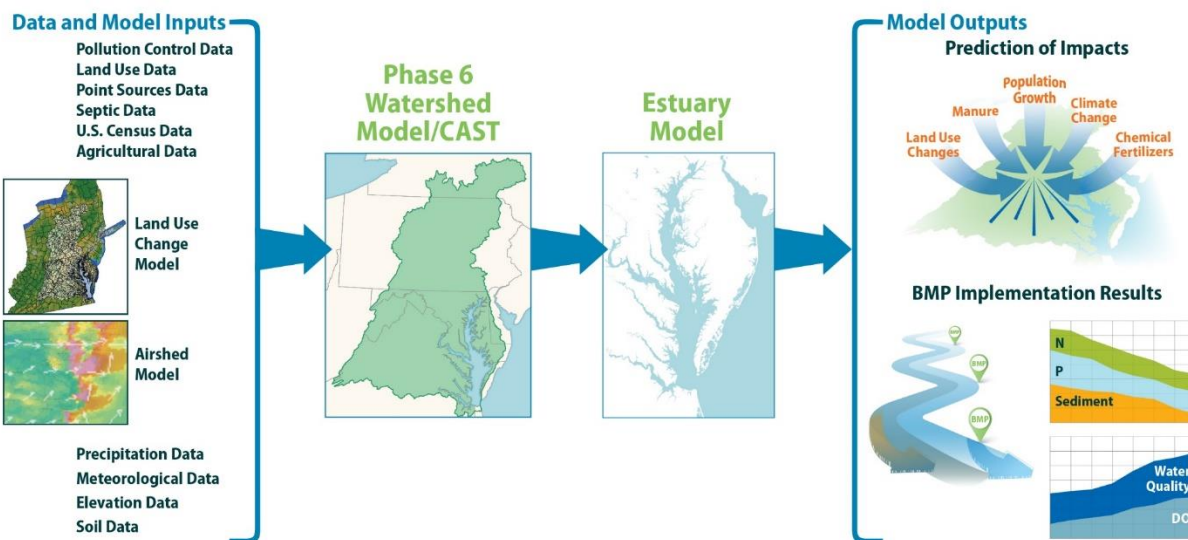

Figure 1-2: the Chesapeake Bay Program partnership's modeling system

The Phase 6 Watershed Model consists of two parallel models: a time-averaged model and a dynamic model, which is constrained to match the time-averaged model over the long term. The time-averaged model, known as the Chesapeake Assessment Scenario Tool (CAST) (Chesapeake Bay Program 2017) is used as the primary model for decision making. Stakeholders and other users can access CAST through a web interface at http://cast.chesapeakebay.net/. The dynamic model is used in calibration of the Phase 6 system, to translate CAST scenarios into hourly loads of nutrients and sediment for the estuarine model, and to perform research. For the climate change analysis, changes will be

made to both CAST and the dynamic model. The dynamic model will run with projected precipitation and meteorology input data to predict changes in hydrology and sediment. These changes will be used in CAST, along with additional investigation using multiple lines of evidence, to predict changes in nitrogen and phosphorus loads delivered to large rivers. Finally, the modeling team will use the dynamic model to temporally disaggregate the predictions of CAST, simulate the effects in large rivers, and pass loads to the estuarine model. Further description of the Phase 6 watershed model is available on the CAST documentation page (http://cast.chesapeakebay.net/Documentation/ModelDocumentation). The relationship between CAST and the dynamic model is described in Section 1. The dynamic model is described in section 10.

The modeling system used for all analyses December 2017 through July 2018 that resulted in the phase III planning targets is in large part the same system used for the climate assessment. Some significant changes were made to accommodate climate-related analysis as detailed in this document. Other minor changes such as the inclusion of new land use and BMP information for future scenarios may also be included per partnership decisions unrelated to climate change. Due to the changes made to the modeling system, the scenarios are not directly comparable to scenarios that were run during the Midpoint Assessment. The climate change analysis will consist of new scenarios that will be compared to estimate the overall effect of climate change on dissolved oxygen water quality standards.

Models, by nature, are not perfect representations of reality and are based on the best available data, knowledge, and computational power available at the time of their use. The analysis for the 2021 climate decisions will represent the current best estimate. It is anticipated that the CBP will reassess the TMDL progress relative to climate change and other factors in 2025.

1.3   Climate Effects Simulated
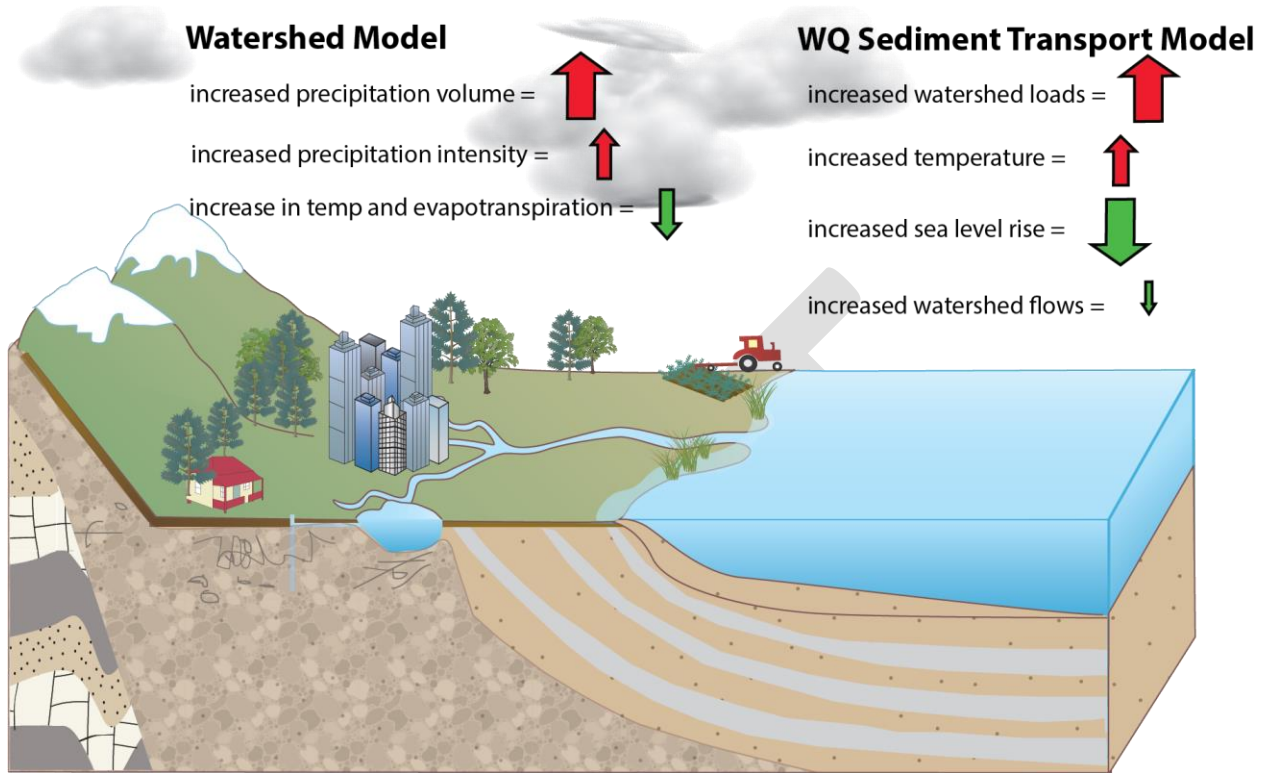
Figure 1-3: Simplified conceptual model of climate effects on dissolved oxygen water quality standards. Red arrows denote an increase in violation of standards. Green arrows denote a decrease.

Figure 1-3 has been used by the CBP partnership to communicate the main effects of climate change on the dissolved oxygen water quality. Increased precipitation volume is expected to increase the runoff of nitrogen, phosphorus, and sediment, which in isolation would lead to an increase in non-attainment of dissolved oxygen water quality standards. This is indicated in the figure by a red arrow. An increase in evapotranspiration caused by an increase in temperature will load to a decrease in runoff, which in turn will lead to a decrease in nutrients and sediment and a decrease in non-attainment of standards, indicated by a green arrow. Increased precipitation intensity in isolation would cause an increase in sediment and phosphorus runoff. An overall increase in watershed loads would lead to an increase in non-attainment. Increased temperatures in the Bay lowers solubility of oxygen which has a negative effect on attainment. Sea level rise and increased watershed flows, in isolation, increase the circulation in the Bay, leading to improved attainment of standards.
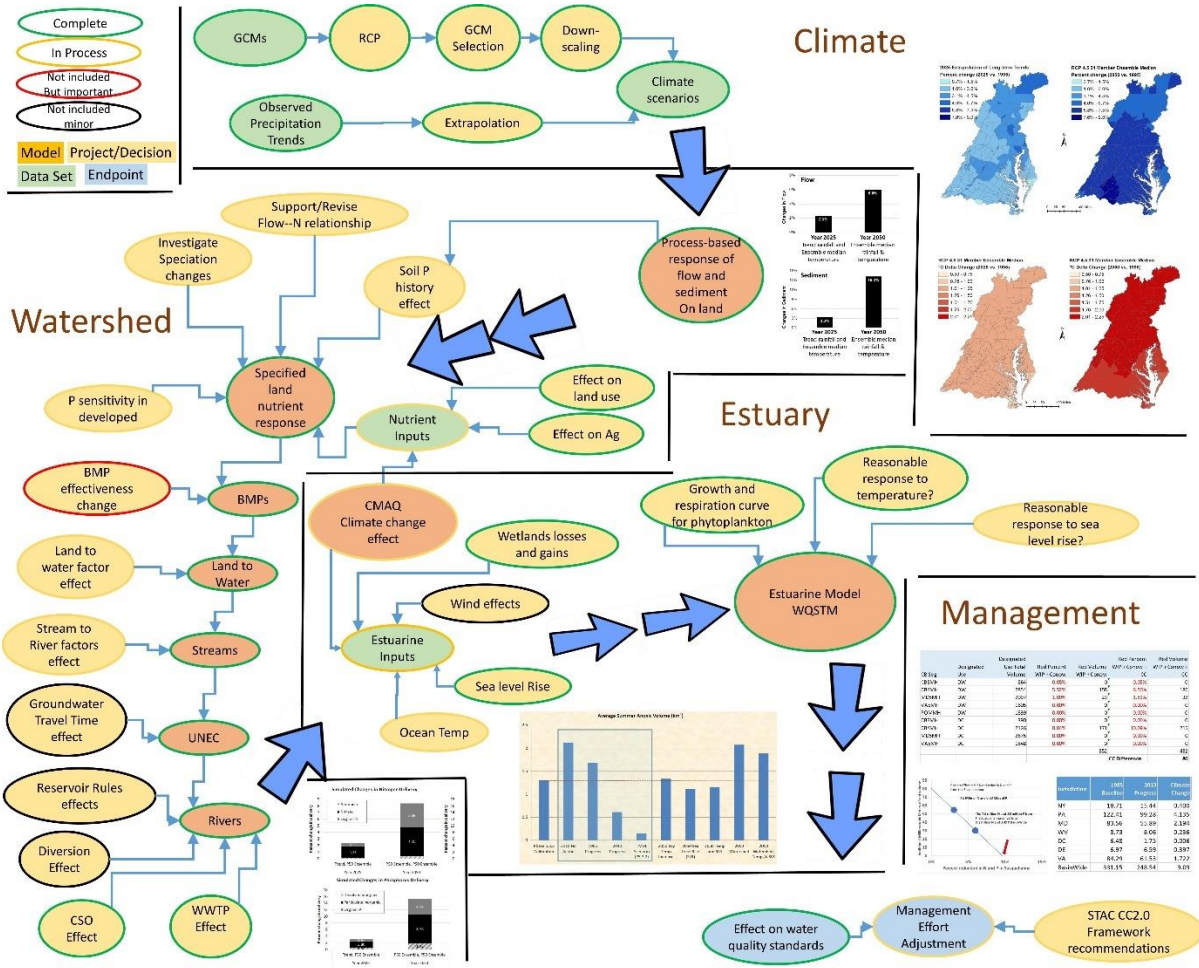
Figure 1-4: Detailed conceptual model of processes affecting dissolved oxygen water quality standards, indicating inclusion or non-inclusion in the CBP climate assessment

Figure 1-4 is a detailed conceptual model of the processes considered in the CBP climate assessment. The above figure was used to guide the CBP in determining the effects to directly include in the analysis. Climate change affects the majority of the inputs and processes in the modeling system. The CBP considered a wide array of effects and made decisions to include those processes which were both well understood and judged to have a significant effect on water quality standards. Some processes left out of the analysis could be important but are without sufficient data and understanding to include them.

For the assessment of climate change impacts in the Chesapeake watershed, the primary variables considered were precipitation volume, precipitation intensity, temperature, and evapotranspiration. Estimates of the influence of sea level rise, increased ocean inflow, air temperature, and tidal wetland loss were incorporated into the Water Quality and Sediment Transport Model (WQSTM) of the tidal Bay and are documented there (Cerco and Noel 2017).

1.4 Input from the CBP's Scientific and Technical Advisory Committee

The CBP's Scientific and Technical Advisory Committee (STAC) has conducted several assessments of climate science and has recommended processes for integrating consideration of climate change into the Bay Program's management framework. STAC proactively authored a report on the likely effects of climate change (Pyke et al. 2008). STAC encouraged the CBP to consider the effects of sea level rise, temperature, and increasing variability of salinity and hydrology on hypoxia and on living resources including algal, submerged aquatic vegetation, and fish communities. STAC asked the CBP to understand the implications of climate change for important management decisions, update monitoring systems, and take action to mitigate the effects of climate change.

A 2011 STAC workshop on climate change (Pyke 2012; Pyke et al. 2012) produced a recommendation that climate change be embedded within the CBP decision-making structure. The response from the CBP (DiPasquale 2014) indicated that the CBP agreed and that a new climate resiliency position was being created and that the concept was consistent with the 2009 executive order (Office of the President, 2009) and the 2014 Bay Agreement (Chesapeake Executive Council 2014). The 2014 agreement explicitly called for climate change considerations to be part of all CBP goals and outcomes. STAC recommended focusing on specific problems, identified through assessments of vulnerability, and developing the technical capacity to address these issues. The inclusion of climate change in the 2017 Midpoint Assessment follows these principles. The recommendations were communicated to the CBP's Executive Council as well (STAC 2011).

A 2016 STAC workshop on climate projections assessed available climate data for use in the CBP decision process (Johnson et al. 2016; Wainger 2016). STAC recommended that the assessment should be as comprehensive as possible. Specific recommendations included the use of historical precipitation trends for 2025 while carefully considering evapotranspiration. For assessments after 2017, STAC recommended a 2050 time frame using multiple models to estimate response. The recommendations and guidance provided by the Chesapeake Bay Program's Climate Resiliency Workgroup (CRWG) (CBP 2016) rely heavily on the 2016 STAC workshop. A follow-up 2017 STAC workshop, not published as of this writing, generated specific near-term and long-term recommendations for watershed and estuarine modeling, and methods of model application.

2 Estimates of Changes in Meteorology and Precipitation

MWG Review: The entirely of section 2 and all its subsections require review

2.1 Climate Change Scenarios

Climate change assessments for the years 2025 and 2050 rely on robust estimates of changes in precipitation and temperature, and the CBP has utilized a combination of trend analysis and

global climate models (GCMs) for these projections. The CBP's methods for developing the climate projections are based on recommendations provided by the 2016 STAC workshop *The Development of Climate Projections for Use in Chesapeake Bay Program Assessments* (Johnson et al. 2016). The recommendation of STAC was to use long-term observed precipitation trends instead of climate model projections to assess expected changes in precipitation for the year 2025, as the uncertainty of the models introduced more variability for this near future than extrapolation of the trend. For 2050 precipitation estimates, STAC recommended climate models used for assessing anticipated changes in precipitation that were based on the Coupled Model Intercomparison Project Phase 5 (CMIP5) set of Global Climate Models (GCMs) as outlined in the Intergovernmental Panel on Climate Change's Fifth Assessment Report (IPCC AR5, 2013). It was also recommended that these models be employed in the assessment of expected temperature change for both 2025 and 2050, as the model projections of temperature change are much less variable for both the short and long-term projections. Decisions by the Chesapeake Bay Program's Modeling Workgroup on 4/2/2019 affirmed the recommendations of the STAC workshop (Johnson et al, 2016).

Subsequent to the STAC workshop, the years 2025, 2035, 2045, and 2055 were selected for the climate change impacts assessment by the Modeling Workgroup rather than 2025 and 2050. The Watershed Model was used to assess expected changes in 2025 precipitation based on historical observed trends within the watershed. Climate models were used precipitation in 2050 and beyond, while 2035 and 2045 were interpolated between the two approaches. Expected changes in 2025, 2035, 2045, and 2055 temperatures were extracted from the models

The GCM projections of rainfall and temperature changes used in the assessment were based on the Representative Concentration Pathway (RCP) 4.5. Forcings for the GCMs are determined by RCP, which are each characterized by potential future socio-economic and natural conditions. The RCPs are defined according to the additional radiative forcing generated by the year 2100 measured in watts per square meter (W/m^2); for example, RCP 4.5 projects an increase in radiative forcing of 4.5 W/m^2. Additional analyses based upon RCP 2.6 and RCP 8.5 could be used to further develop the assessment to include a range of potential future climates. However, due to computational constraints only a limited number of key climate scenarios were simulated with the linked watershed and estuarine models to quantify the range of climate change impacts.

2.1.1   Long-term Observed Trends in Precipitation

The STAC Workshop Report, "The Development of Climate Projections for Use in the Chesapeake Bay Program Assessments" (Johnson et al. 2016), recommends using long-term observations to estimate the 30-year (1995 - 2025) change in precipitation volume that can be attributed to climate change. Precipitation trends for model land segments (counties) were developed by analyzing Parameter-elevation Relationship on Independent Slope Model (PRISM, Daly et al., 2008) rainfall data. A linear trend analysis was conducted with annual PRISM rainfall

data as recommended by Jason Lynch, EPA, and Karen Rice, USGS. The PRISM dataset is a reanalysis product that uses point data measurements at rain gauges and incorporates a conceptual framework to address spatial variably in rainfall due to orographic and other processes. The long-term PRISM dataset (1895-1980) is modeled at 30 arc second (approx. 800 m) grid cell resolution but then upscaled to provide monthly total rainfall at 2.5 arc minute (approx. 4-km) grid cell resolution for the conterminous U.S. The annual PRISM dataset for the years 1927 to 2014 (i.e. 88 years) were used in the linear regression trend analysis. The selection of the 88-year period was made because of easy accessibility of the dataset. For the analysis, gridded PRISM data were first spatially aggregated to each Phase 6 land segment, and then for each segment, a linear trend line was fitted to the annual rainfall data.

Figure 2-1 shows the regression analysis for two counties, where the linear slopes indicate 2.67% and 3.14% increases in average annual rainfall volumes as compared to the reference 1991-2000 conditions. Since regression analysis was done for annual rainfall volumes, the resulting linear slope does not provide information on changes at monthly or seasonal time scale. Therefore, the percent change in average annual rainfall was used for every month. Figure 2-15 shows the increase in annual rainfall over the 30-year period between 1995 and 2025 estimated using the trends for the land segments in the Chesapeake Bay watershed.
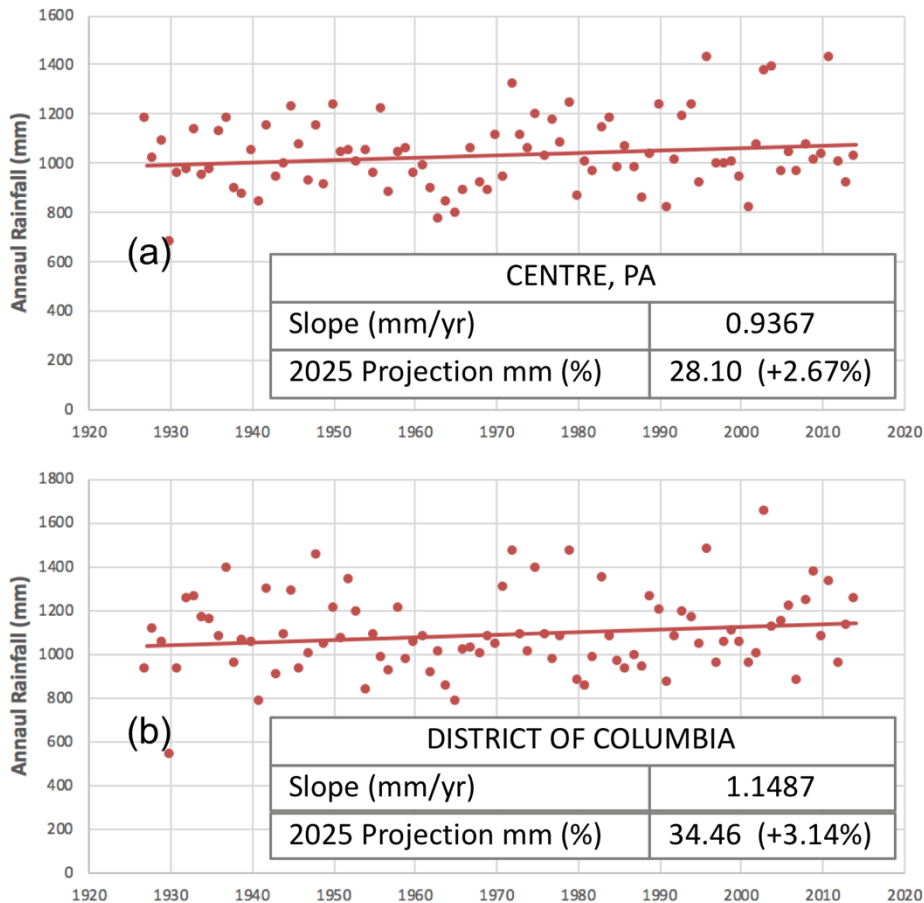

9

Figure 2-1: Annual rainfall volumes for the 88-year period linear regression lines are shown in red for the two land segments (counties) – (a) Centre County in Pennsylvania and (b) District of Columbia. The values for the slope of the regression lines, and the corresponding 30-year projections in the rainfall volume (1995 to 2025) are also shown.

Trend information derived from a short-term (e.g. 30 years) rainfall dataset may be influenced by decadal-scale variations in climate as well as weather anomalies. The influence of such variations can be more easily detected and reduced using longer-term data, however, it was not clear if the use of an 88-year record would be sufficient for overcoming such decadal-scale variabilities. The CBPO modeling team conducted an analysis of long-term rainfall data to investigate this. Different lengths of historical observations were used for estimating the linear trend and the corresponding percent change in annual rainfall over a 30-year period. A total of 59 sets ranging between most recent 30 years to 88 years of historical observations were analyzed. The goal was to test the influence of number of years on the linear trend estimate, and on how the decadal and natural variabilities impacted the resulting trend. A set of same color dots in Figure 2-2 shows the estimated percent change in annual rainfall volume for 30 years based on linear trends calculated from those 59 sets for a land segment (or county). The analysis was repeated for several counties (Figure 2-2). It was found that, although not perfect, the 88-year record came pretty close to overcoming cyclical climatic variabilities as the estimated percent change became more stable. It is noted that for a given county the estimated change varied quite a bit when data for 30 to 60 years were selected but became stable for greater numbers of years, as shown in Figure 2-2.
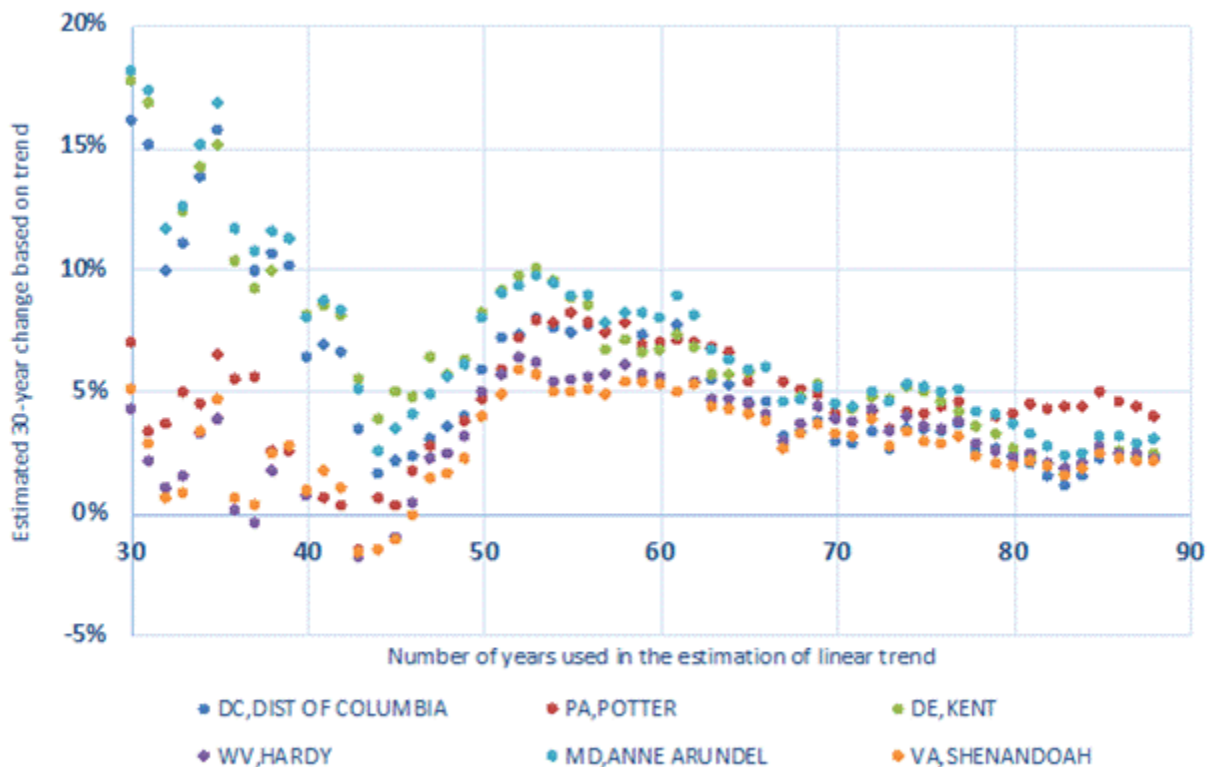
Figure 2-2: Estimated change in rainfall based on the extrapolation of linear trends are shown. For the estimation of linear trends historical observations ranging between last 30 to 88 years used. It was shown that a level of consistency was achieved after more than 80 years of observations were used in the estimation of linear trend.

2.1.2 General Circulation Models and Representative Concentration Pathways

General circulation models (GCMs) included in the most recently completed Coupled Model Intercomparison Project Phase 5, CMIP5 (Taylor et al. 2012) were used for the rainfall and temperature projections. As compared to CMIP3, the CMIP5 dataset provides incrementally refined climate projections that include more comprehensive models with a broader set of experiments, higher spatial resolution for models, and an expanded set of output variables for both the near-term (decadal predictions) and long-term (century time scale). The list of GCMs and model runs included in the CMIP5 is provided in Table 2-1.

The set of climate models in the U.S. Climate Resilience Toolkit (CRT) (NOAA 2014) (accessed 2016) were used in the development of climate scenarios for the Phase 6 application except that the CBP did not use the BNU-ESM model, which was unavailable for download. Statistically downscaled climate models and corresponding realizations were retrieved from an online archive accessed through the Geo Data Portal (Bureau of Reclamation, 2013). The decision to use an existent downscaled dataset rather than either developing or applying a tailored statistical climate downscaling process was based upon the recommendations of the STAC workshop (Johnson et al. 2016). The Bias Corrected Spatial Disaggregation (BCSD) downscaling methodology was chosen for the assessment because of its commonality among numerous datasets including the U.S. Climate Resilience Toolkit and the NASA Earth Exchange (NEX) Downscaled Climate Projections (NEX-DCP30), its extensive review in peer-reviewed literature in comparison with other downscaling methodologies (Gutmann et al. 2014; Mizukami et al. 2016), and its relative ease of access and flexibility in choosing models and realizations to be incorporated into analyses. The downscaled dataset was among the ones recommended by the data.gov climate data catalog. Still, it may benefit future regional climate assessment to consider other datasets based on downscaling techniques that are also capable of producing reliable correlations with observed precipitation and temperature such as the Multivariate Adaptive Constructed Analogs (MACA) or Localized Constructed Analogs (LOCA) methodologies (Demirel and Moradkhani 2016; Pierce and Cayan 2015).

The GCMs utilize forcings based on potential future socio-economic and natural scenarios defined as Representative Concentration Pathways (RCPs). The RCPs are categorized according to the additional radiative forcing generated by the year 2100 relative to pre-industrial values as measured in Watts per square meter (Wm^{-2}). The additional radiative forcing is a measure of the cumulative impact of future anthropogenic greenhouse gas emissions. The four RCPs, RCP 2.6, RCP 4.5, RCP 6.0, and RCP 8.5 were adopted by the IPCC in its Fifth Assessment Report (AR5) to represent possible future trajectories of greenhouse gas concentrations. These concentration pathways are used in the climate model simulations to estimate four possible climate futures. However, it has been shown that the spread across RCPs in the near term for a

single climate model is typically smaller than the difference between climate models under a single RCP scenario (Kirtman et al. 2013).

Table 2-1: A multi-model ensemble of statistically downscaled CMIP5 projections was used. "Downscaled CMIP3 and CMIP5 Climate and Hydrology Projections" archive at http://gdodcp.ucllnl.org/downscaled_cmip_projections was used for obtaining rainfall and temperature projections that were statistically downscaled using Bias Corrected Spatially Disaggregated method (Maurer et al., 2007). The symbol "Y" represents the member "model-runs" that were included as the ensemble analysis, whereas "x" indicates data for the model-run that were available but not included, and "o" indicates data for the model-run that were unavailable.

WCRP CMIP5 Modeling Workgroup	WCRP CMIP5 Climate Model	Model Run											
		R1	R2	R3	R4	R5	R6	R7	R8	R9	R10	R11	R12
Commonwealth Scientific and Industrial Research Organization and Bureau of Meteorology, Australia	ACCESS1-0	Y	o	o	o	o	o	o	o	o	o	o	o
	ACCESS1-3	x	o	o	o	o	o	o	o	o	o	o	o
Beijing Climate Center, China Meteorological Administration	BCC-CSM1-1	Y	o	o	o	o	o	o	o	o	o	o	o
	BCC-CSM1-1-M	Y	o	o	o	o	o	o	o	o	o	o	o
College of Global Change and Earth System Science, Beijing Normal University	BNU-ESM	o	o	o	o	o	o	o	o	o	o	o	o
Canadian Centre for Climate Modelling and Analysis	CanESM2	Y	x	x	x	x	o	o	o	o	o	o	o
National Center for Atmospheric Research	CCSM4	Y	x	x	x	x	o	o	o	o	o	o	o
Community Earth System Model Contributors	CESM1-BGC	Y	o	o	o	o	o	o	o	o	o	o	o
	CESM1-CAM5	Y	x	x	o	o	o	o	o	o	o	o	o
Centro Euro-Mediterraneo per I Cambiamenti Climatici	CMCC-CM	Y	o	o	o	o	o	o	o	o	o	o	o
Centre National de Recherches Météorologiques/ Centre Européen de Recherche et Formation Avancée en Calcul Scientifique	CNRM-CM5	Y	o	o	o	o	o	o	o	o	o	o	o
Commonwealth Scientific and Industrial Research Organization, Queensland Climate Change Centre of Excellence	CSIRO-Mk3-6-0	Y	x	x	x	x	x	x	x	x	x	x	x
EC-Earth consortium, representing 22 academic institutions and meteorological	EC-EARTH	o	Y	o	o	o	o	o	x	o	o	o	x

services from 10 countries in Europe													
Laboratory of Numerical Modeling for Atmospheric Sciences and Geophysical Fluid Dynamics, Institute of Atmospheric Physics, Chinese Academy of Sciences, and Center for Earth System Science, Tsinghua University	FGOALS-g2	Y	o	o	o	o	o	o	o	o	o	o	o
Laboratory of Numerical Modeling for Atmospheric Sciences and Geophysical Fluid Dynamics, Institute of Atmospheric Physics, Chinese Academy of Sciences	FGOALS-s2	o	x	o	o	o	o	o	o	o	o	o	o
The First Institute of Oceanography, State Oceanic Administration, China	FIO-ESM	Y	x	x	o	o	o	o	o	o	o	o	o
NOAA Geophysical Fluid Dynamics Laboratory	GFDL-CM3	Y	o	o	o	o	o	o	o	o	o	o	o
	GFDL-ESM2G	Y	o	o	o	o	o	o	o	o	o	o	o
	GFDL-ESM2M	Y	o	o	o	o	o	o	o	o	o	o	o
NASA Goddard Institute for Space Studies	GISS-E2-H-CC	x	o	o	o	o	o	o	o	o	o	o	o
	GISS-E2-R	Y	x	x	x	x	o	o	o	o	o	o	o
	GISS-E2-R-CC	x	o	o	o	o	o	o	o	o	o	o	o
Met Office Hadley Centre (additional HadGEM2ES realizations contributed by Instituto Nacional de Pesquisas Espaciais)	HadGEM2-AO	Y	o	o	o	o	o	o	o	o	o	o	o
	HadGEM2-CC	Y	o	o	o	o	o	o	o	o	o	o	o
	HadGEM2-ES	Y	x	x	x	o	o	o	o	o	o	o	o
Institute for Numerical Mathematics	INM-CM4	Y	o	o	o	o	o	o	o	o	o	o	o
Institut Pierre-Simon Laplace	IPSL-CM5A-LR	Y	x	x	x	o	o	o	o	o	o	o	o
	IPSL-CM5A-MR	Y	o	o	o	o	o	o	o	o	o	o	o
	IPSL-CM5B-LR	Y	o	o	o	o	o	o	o	o	o	o	o
Japan Agency for Marine-Earth Science and Technology, Atmosphere and Ocean Research Institute (The University of Tokyo), and	MIROC-ESM	Y	o	o	o	o	o	o	o	o	o	o	o
	MIROC-ESMCHEM	Y	o	o	o	o	o	o	o	o	o	o	o

National Institute for Environmental Studies													
Atmosphere and Ocean Research Institute (The University of Tokyo), National Institute for Environmental Studies, and Japan Agency for Marine-Earth Science and Technology	MIROC5	Y	o	o	o	o	o	o	o	o	o	o	o
Max-Planck-Institut für Meteorologie (Max Planck Institute for Meteorology)	MPI-ESM-LR	Y	x	x	o	o	o	o	o	o	o	o	o
	MPI-ESM-MR	Y	o	o	o	o	o	o	o	o	o	o	o
Meteorological Research Institute	MRI-CGCM3	Y	o	o	o	o	o	o	o	o	o	o	o
Norwegian Climate Centre	NorESM1-M	Y	o	o	o	o	o	o	o	o	o	o	o
	NorESM1-ME	x	o	o	o	o	o	o	o	o	o	o	o

2.1.3   Bias Correction and Downscaling of the Climatic Projections

The Bias Corrected and Spatially Disaggregated (BCSD) statistically downscaled CMIP5 climate projections were downloaded from the "Downscaled CMIP3 and CMIP5 Climate and Hydrology Projections" archive available at http://gdo-dcp.ucllnl.org/downscaled_cmip_projections/ (Maurer et al. 2007; Reclamation 2013). The online data archive provides output of GCMs that were statistically downscaled using the BCSD methodology that employed a quantile mapping technique for several GCMs. The archive also included several "model-runs" or "realizations" for a number of GCMs. The "model-runs" incorporate perturbations of initial conditions to provide a spread of possible outcomes. However, the selection of several GCMs over several model-runs for a particular GCM provides wider variability that enables an ensemble analysis to capture a fuller range of uncertainties in model projections (Pierce et al. 2009). In addition, selecting one realization per model constrains biases for models with more realizations. Subsequently, 31 GCMs that were included in the ensemble analysis are shown in Table 2-1. The selection was based on models used by the U.S. Climate Resiliency Toolkit (which itself relies upon the NASA NEX-DCP30 database) and the recommendation of the Chesapeake Bay Program's Climate Resiliency Workgroup.

Bias correction methods remove systematic climate model errors at regional scales, whereas the downscaling methods resolve finer scale climatological features, providing an improved dataset for applications in local scale impact analyses. The bias corrected data for every GCM are is forced to match the monthly cumulative density functions of observed rainfall at the regional scale. This is shown in Figure 2-3, where the dashed black lines represent the observed data, the red lines represent the hindcast simulations for the period 1950-1999 simulated by

GCMs at a spatial grid of 2°, and the green lines represent the bias corrected dataset for all GCMs. The green line for all of the GCMs and the observations are situated on top of one another demonstrating that the bias corrected GCMs match the observed distributions. The quantile maps, which establish a tabular relationship between the rank probability and bias in the hindcast dataset, were applied to the future projections. This approach preserves the same relative changes projected by the GCMs in mean, variance, and other statistical moments of the data.

Dynamical downscaling, which involves the use of a finer scale regional climate model (RCM), offers a better representation of a local study area nested within a GCM domain and can simulate local fine-scale feedback processes that are not anticipated by statistical downscaling. However, for hydrological applications, statistically downscaled climate projections using the BCSD method have been shown to exhibit comparable fidelity as compared to other statistical and dynamical methods (Wood et al. 2004). Moreover, the climate change projections obtained using BCSD have been found to provide similar strengths and weaknesses as compared to Bias Correction Constructed Analogues, BCCA, and Multivariate Adaptive Constructed Analogues (MACA) (Maurer et al. 2010; Abatzoglou and Brown 2011).
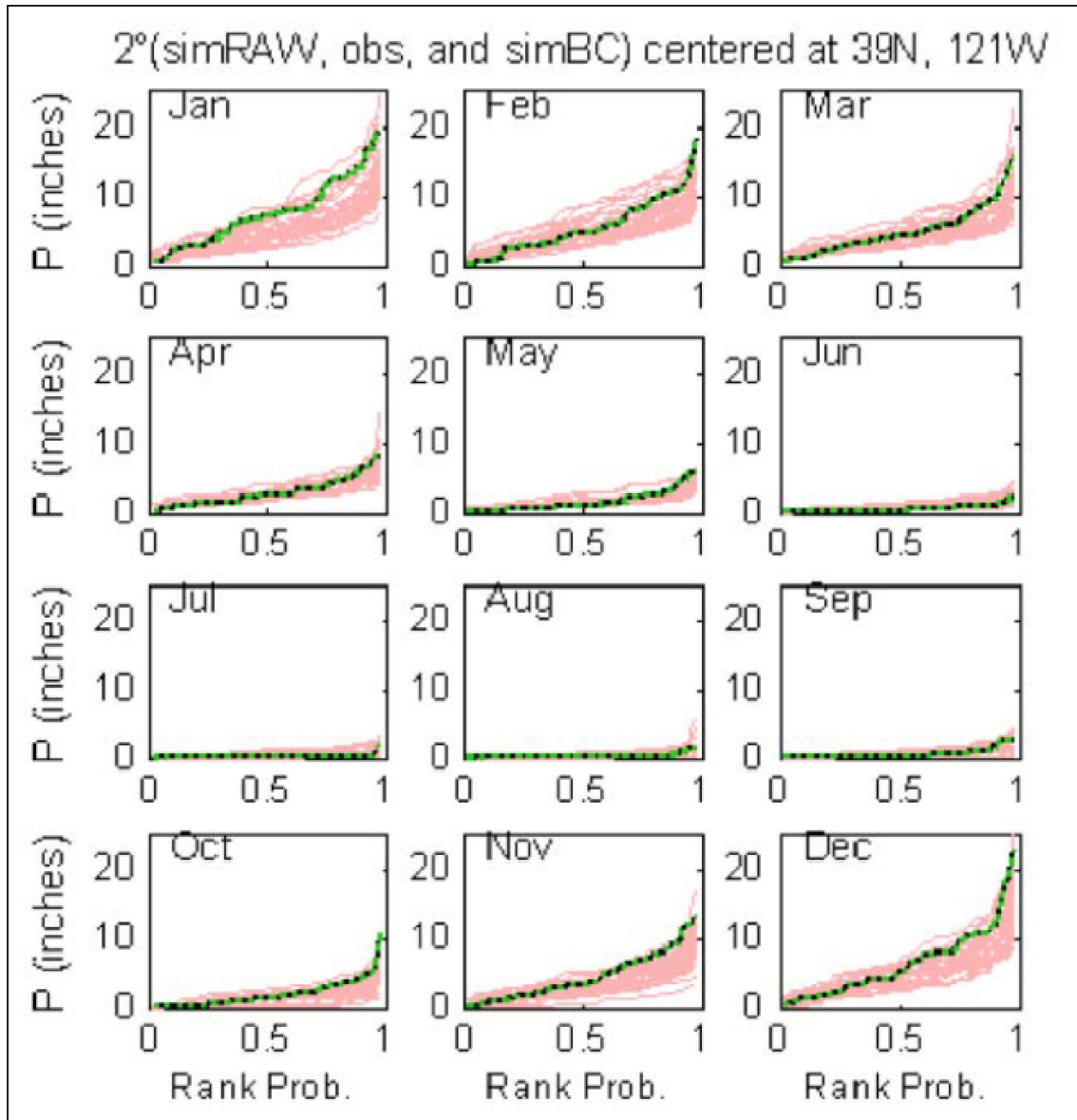
Figure 2-3: Bias corrected GCM outputs. Monthly bias corrections of rainfall data using a quantile mapping technique are shown (from Reclamation, 2013). Red lines show model output, dashed black lines show observations, and the green lines show the bias corrected GCM outputs.

2.1.4 The Ensemble Analysis

A widely used technique in climate change assessments involving the use of projections from multiple climate models is to combine ensembles of predictions from a collection of models. This approach allows increasing the sampling of both initial conditions and model properties in the subsequent climate change assessment. Furthermore, it has been shown that multi-model ensemble means generally exhibit higher skill, e.g., in capturing Atlantic Multi-decadal Variability, as compared to a single-model projection (Garcia-Serrano and Doblas-Reyes 2012; Kim et al. 2012; Kirtman et al. 2013).

Figure 2-4 shows monthly percent changes in rainfall volume and temperature changes in degrees Celsius for the 31-member ensemble described in Table 2-1. The modeled change between the years 2050 (2036-2065) and 1995 (1991-2000) are shown. The median change of the ensemble members for each month are also shown. For the ensemble median scenario, changes in monthly rainfall volume and temperature for each land segment were applied to the 1991-2000 rainfall and temperature dataset, respectively.
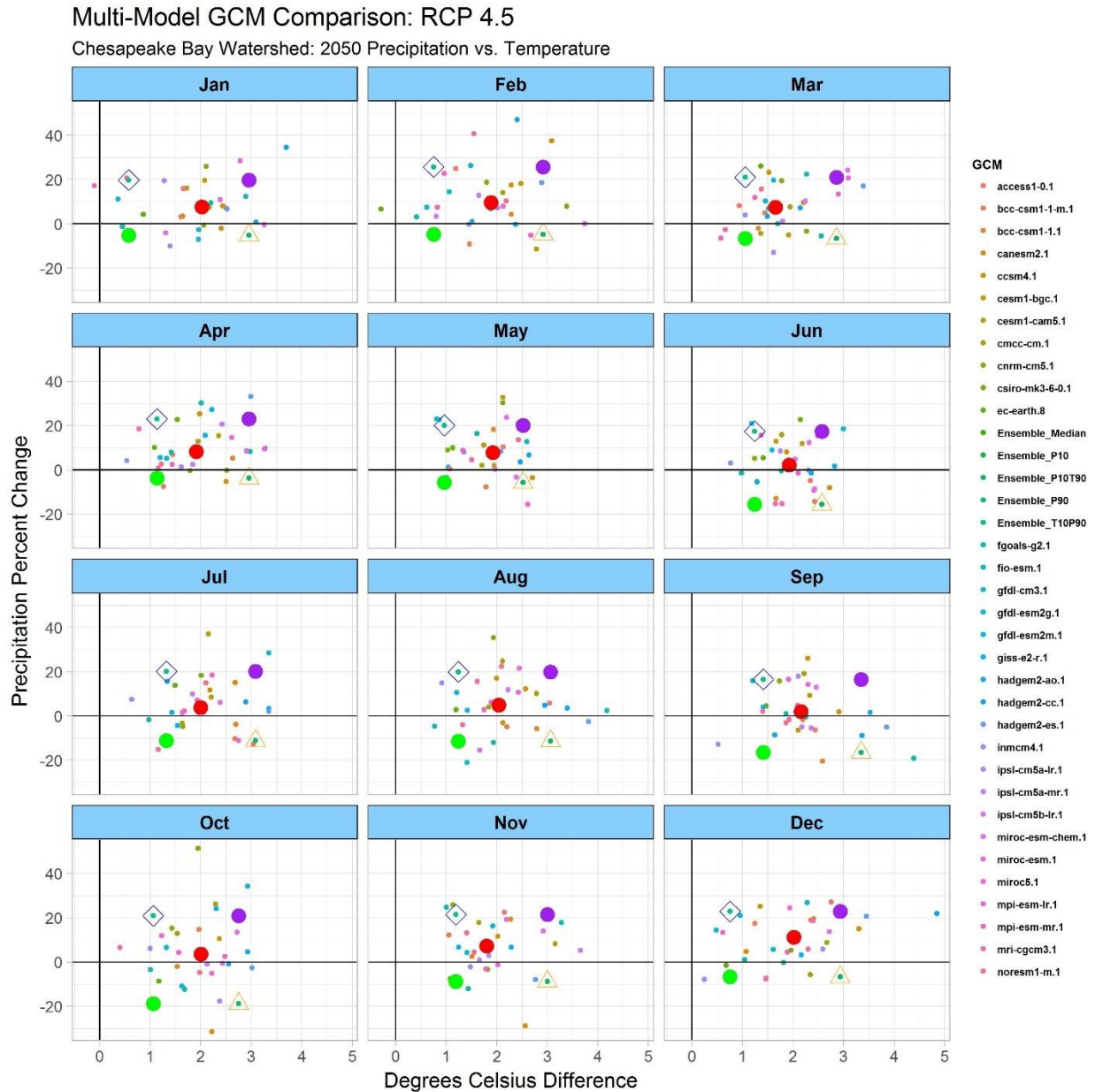
Figure 2-4: The monthly percent change in rainfall volume and degrees Celsius difference for the 31-member ensemble of the RCP 4.5 scenario are shown. Each data point represents the monthly difference between the average monthly temperature and precipitation volume between the periods 2036-2065 and 1981-2010. For year 2050, monthly median ensembles were used as the central tendency for the climate change assessment, whereas the 10th and 90th percentiles were used for uncertainty quantification.

Figure 2-5 and Figure 2-6 show the spatially averaged changes in precipitation and temperature, respectively, for the Chesapeake Bay watershed. Projected changes are compared for the years 2025 and 2050 relative to 1995 for three emission scenarios RCP 2.6, RCP 4.5, and RCP 8.5. The box plots show the ensemble distribution of projected change based on the ensemble of GCMs. Figure 2-5 shows that, for precipitation, the ensembles medians of different RCPs are similar and that the range between the 10th and 90th percentiles of RCP 4.5 includes the interquartile ranges of RCP 2.6 and RCP 8.5 for both 2025 and 2050. Figure 2-6 shows that, for temperature change between 1995 and 2025, the 10th, 50th, and 90th percentiles for the three emission scenarios are all similar. Projections for the year 2050 show large differences in ensemble medians for the emission scenarios, however the uncertainty range for RCP4.5 considerably overlaps the RCP 2.6 and RCP 8.5 range. For both precipitation and temperature, and in both 2025 and 2050, the variability due to model selection is greater than the variability due to emission scenarios and therefore the RCP 4.5 is used for the CBP climate projections for 2025, 2035, 2045, and 2055.
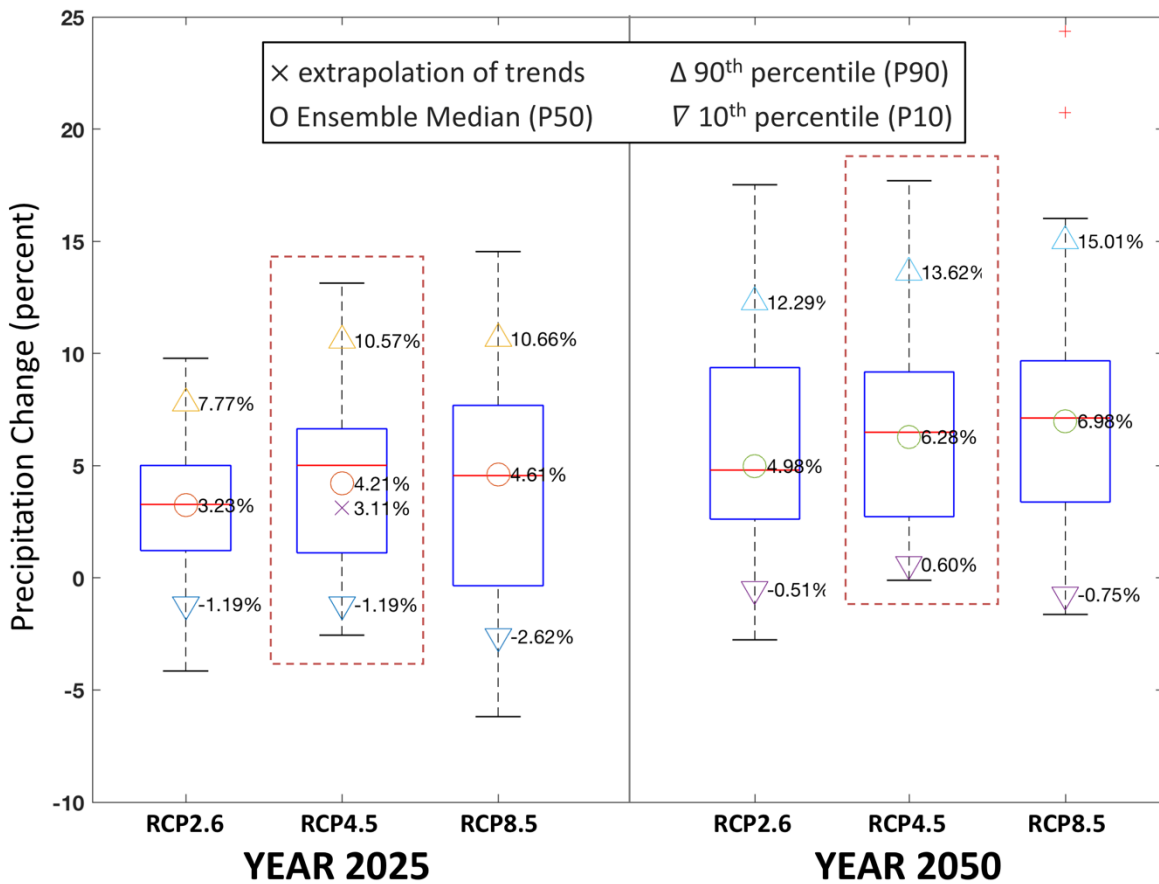
Figure 2-5: Percent change in rainfall volume for the Chesapeake Bay watershed for the years 2025 and 2050 relative to 1995 are shown. Box plots show variability in the ensemble of GCM projections. Ensemble median (circles) and 10th and 90th percentile (triangles) range are shown.
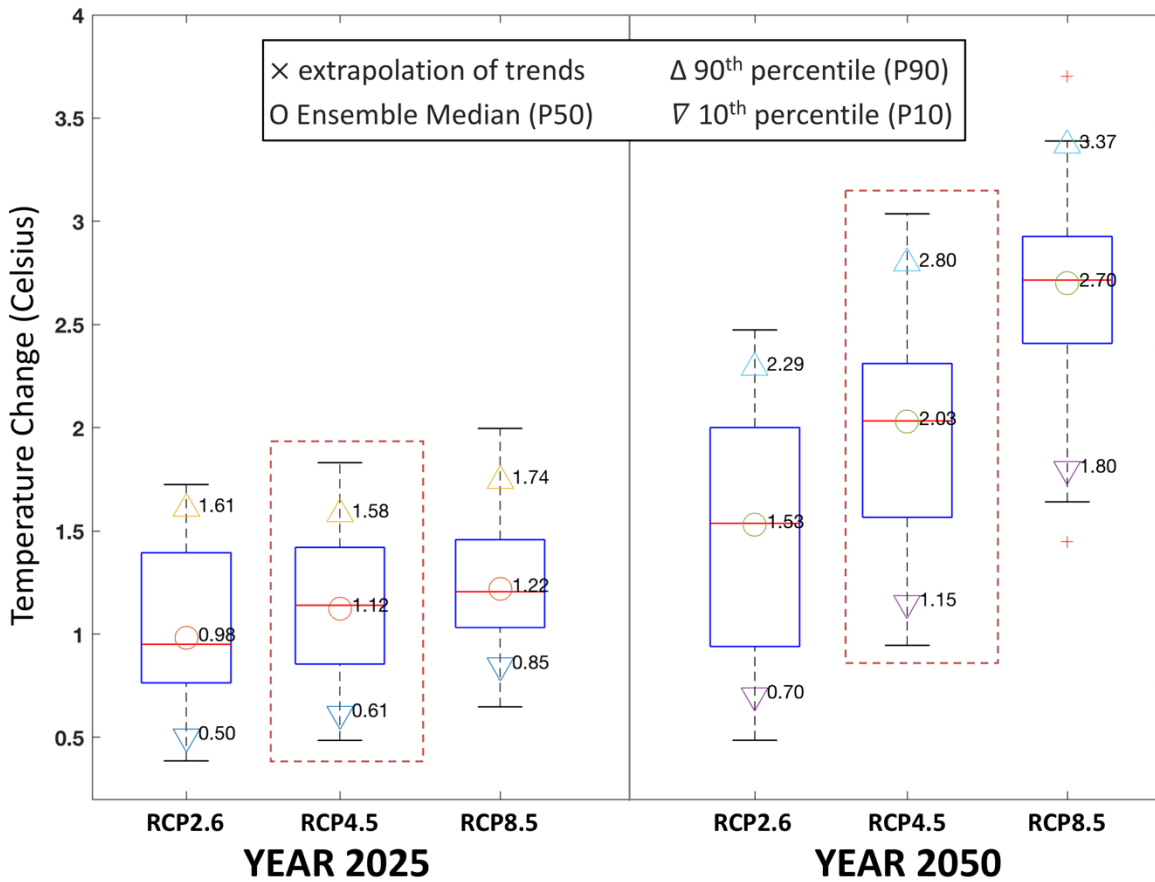
Figure 2-6: Percent change in temperature for the Chesapeake Bay watershed for the years 2025 and 2050 relative to 1995 are shown. Box plots show variability in the ensemble of GCM projections. Ensemble median (circles) and 10th and 90th percentile (triangles) ranges are shown.

2.1.5   Projected Changes in Precipitation Intensity

The capability to change precipitation by deciles was incorporated into the analysis. Changes in rainfall volume were divided among intensity deciles based on documented changes in intensity and frequency of precipitation events using a century of observations (Groisman et al. 2004; Groisman et al. 2001; Karl and Knight 1998, Gordon et al. 1992). The observed increases in larger precipitation events (Groisman et al. 2004) was the basis for assigning the total percent change in precipitation volume disproportionately to intensity deciles. Following Groisman et

al. (2004), the larger share of the increase in estimated precipitation volume due to climate change was placed in the highest decile (90 to 100 percent) of intensity (Figure 2-7).

For comparison, a model sensitivity scenario was also developed that applied a uniform distribution for the increased rainfall volume estimate due to climate change among intensity deciles. In future, further analysis of rainfall intensity should explore the alteration of precipitation intensities based upon different downscaled projections and its subsequent impacts on the watershed responses.
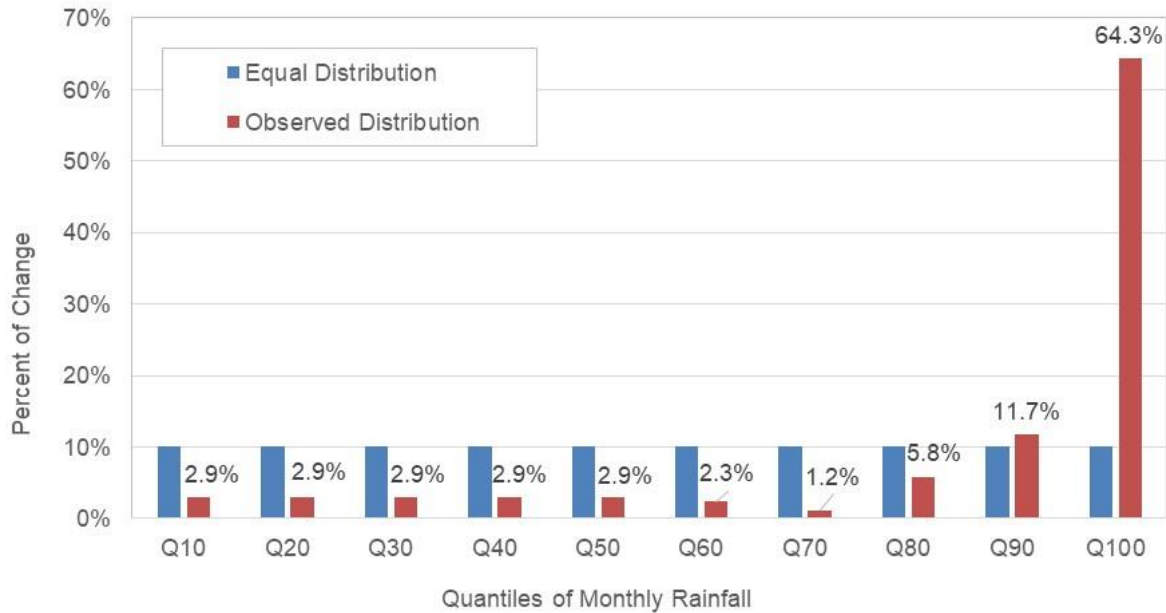
Figure 2-7: Observed changes in rainfall intensity over the last century (based on Figure 10 in Groisman et al. 2004). The equal allocation distribution (blue) is contrasted with the distribution obtained based on observed changes (red).

2.1.6   Application of the Delta Method

For hydrological applications and the impact analysis of linked natural systems, it is critical to maintain physically plausible spatial and temporal relationships between rainfall and other meteorological variables. Therefore, it is important that multiple variables are simultaneously downscaled at the regional scale. However, these relationships are not maintained by most of the statistical downscaling methods. The delta method is the creation of future meteorological time series by starting with a historical observed time series and applying change factors calculated from a modeled or statistical estimate of the effects of climate change. The use of a delta change method preserves the spatial and temporal relationship between the rainfall and meteorological variables in the observed reference data that was used for model calibration.

The Phase 6 Watershed Model was calibrated to the rainfall and meteorological data obtained from the NLDAS-2 database (Xia et al. 2012). Monthly changes to the NLDAS temperature data

for future climate scenarios were calculated based on the median change in the model ensemble as described in Section 2.1.4. Monthly changes to the NLDAS precipitation data for the 2050 climate scenarios were calculated based on the median change in the model ensemble as described in Section 2.1.4. Monthly changes to the NLDAS precipitation for 2025 were based on long-term trends as described in section 2.1.1. Changes in the precipitation data for the years 2035 and 2045 were interpolated between the two methods.

An appropriate selection of time-disaggregation procedures is needed for the application of monthly delta change to the reference dataset. For the time-disaggregation of monthly rainfall change, the monthly change in volume was divided into 10 rainfall intensity deciles based on an *a priori* distribution (Figure 2-7). Two methods were used for the quantile distributions (Figure 2-7). In the first method, additional precipitation volume was divided equally among the 10 quantiles, whereas in the second method the documented changes in observed rainfall intensities over the last century were used. As a result, the second method allocates more rainfall volume to the 10th decile (largest 10% events) of rainfall in the average hydrology period from 1991-2000 (Figure 2-8). In both methods, the change in rainfall is applied as a monthly factor multiplying each hour of rainfall. For all scenarios, the change in temperature is applied as a monthly-varying additive value.
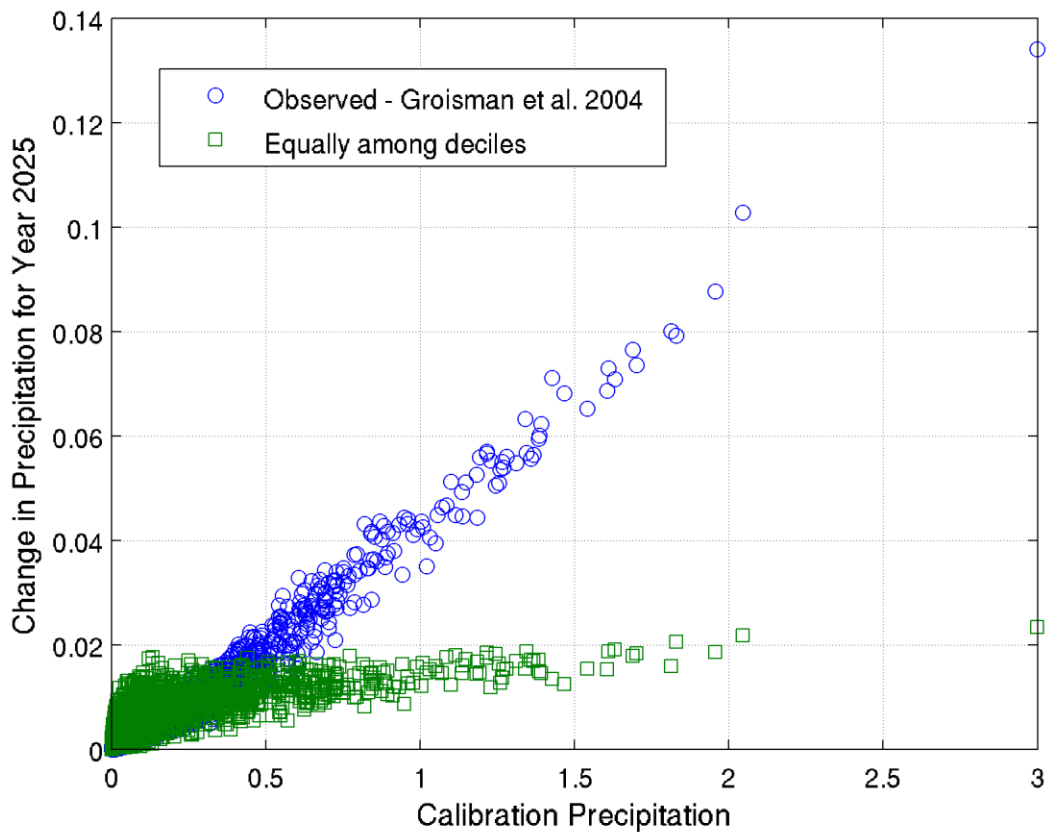
Figure 2-8: Additional rainfall added to the baseline daily rainfall over the 10-year period for a Phase 6 land segment (Potter, PA) is shown. In the method based on observed intensity trends, more volume is added to 10th decile resulting in higher intensity events become stronger.

2.1.7   Altered CO_2 Concentrations

Anticipated values of carbon dioxide concentrations were compiled from the IPCC's 5th Assessment Report for different emission scenarios (Figure 2-9). Carbon dioxide concentration levels of approximately 423 ppm and 487 ppm were obtained for the Representative Concentration Pathway (RCP) 4.5 for 2025 and 2050, respectively (IPCC, 2013: Annex II, Table AII.4.1). This is compared to 363 ppm for the average concentration for the years 1991-2000. Going forward, modifications to CO_2 concentrations based upon different RCP scenarios could also be simulated, depending upon the year and scenario of choice.
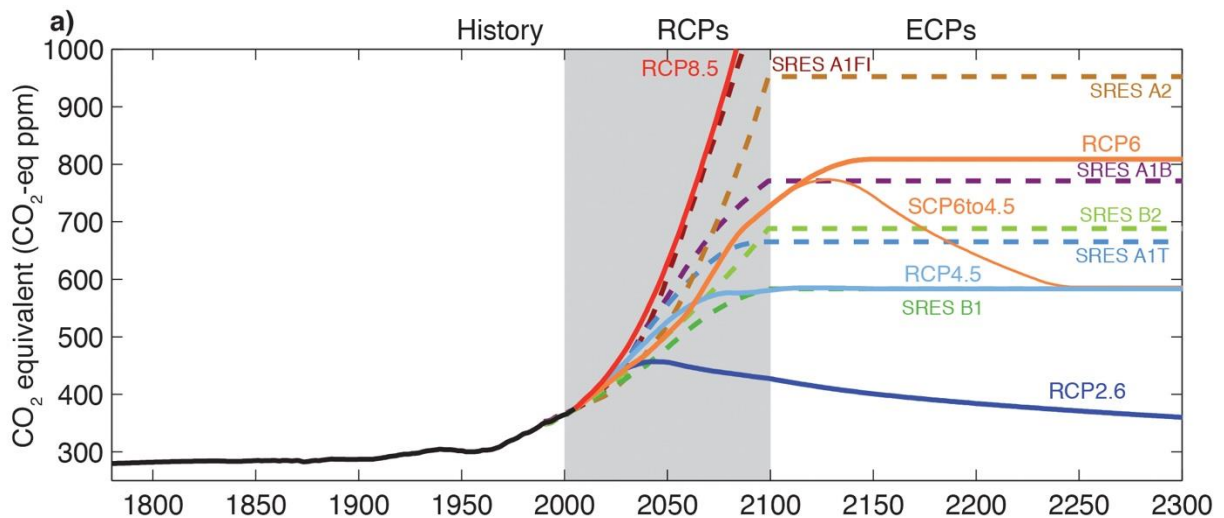
Figure 2-9: Equivalent CO2 concentration from IPCC 5 Worgking Group 1 report (Cubasch et al. 2013)

Table 2-2: CO_2 abundance table AII.4.1 of IPCC, 2013: Annex II: Climate System Scenario Tables In: Climate Change 2013: The Physical Science Basis

Year	Observed	RCP2.6	RCP4.5	RCP6.0	RCP8.5
PI	*278 ± 2*	*278*	*278*	*278*	*278*
2011 obs	*390.5 ± 0.3*				
2000		368.9	368.9	368.9	368.9

2005	378.8	378.8	378.8	378.8
2010	389.3	389.1	389.1	389.3
2020	412.1	411.1	409.4	415.8
2030	430.8	435.0	428.9	448.8
2040	440.2	460.8	450.7	489.4
2050	442.7	486.5	477.7	540.5
2060	441.7	508.9	510.6	603.5
2070	437.5	524.3	549.8	677.1
2080	431.6	531.1	594.3	758.2
2090	426.0	533.7	635.6	844.8
2100	420.9	538.4	669.7	935.9

2.1.8 Estimates of Potential Evapotranspiration

Potential evapotranspiration (PET) is generally estimated as a function of temperature, dew point temperature, wind speed, stomatal resistance, and other factors. The Phase 6 Model calibration uses the Hamon method for the estimation of PET (Equation 2-1). In the early development stages of the Phase 6 Model, the Hamon method was used for estimating changes in PET with climate change, specifically in response to changes in temperature, which was consistent with methods of climate change assessment in the Phase 5 Model. In response to the climate change simulation of Phase 5 Model as well as some of the early assessment using Phase 6 Model, STAC recommended careful considerations of the PET methods (Johnson et al. 2016).

$$Hamon\ Daily\ PET\ =\ 0.0055 \times VD_{sat} \times \left(Daily\ light\ hours/_{12}\right)^2$$

<div align="right">*Equation 2-1*</div>

$$VD_{sat} = 216.7 \times \frac{VP_{sat}}{\left(T_{avg} + 273.3\right)}$$

$$VP_{sat} = 6.108 \times e^{\frac{17.26939 \times T_{avg}}{T_{avg} + 237.3}}$$

Where:
PET = potential evapotranspiration, mm/day

VDsat = saturated vapor density, gram/m^3
Tavg = average daily temperature, degree Celsius
VPsat = saturated vapor pressure, millibars

To a large extent the simulated impact of climate change on the water budget of the watershed relies on the estimated PET. Therefore, the selection of PET method plays a very critical role. The Hamon method relies upon the temperature, the saturated water vapor density (also a function of temperature), and the number of daylight hours as inputs in calculating PET (Equation 2-1). As a result, the estimation of climate effects on PET in the Hamon method is solely a function of temperature. Milly (2016) showed an analysis of different PET methods, which demonstrated that Hamon method overestimated the impact of temperature change on the PET as compared to other methods, including Penman-Monteith (Figure 2-10). The Penman-Monteith equation is frequently relied upon for the estimation of PET in several watershed models for its more physically based approach. However, the Penman-Monteith equation requires several additional meteorological variables which are often hard to obtain. That was particularly the case for the downscaled climate change inputs that were available. The Hargreaves-Samani approach (Equation 2-2), on the other hand, uses readily available parameter variables as with Hamon but provides an estimated relationship of PET with temperature more similar to Penman-Monteith (Figure 2-10). For that reason, the Hargreaves-Samani method was used for estimating the change in PET. The estimated daily change was added as a factor to the hourly reference PET dataset. The Phase 6 Model simulation showed improved simulation results that were more consistent with streamflow trends (U.S. EPA. 2016a; Rice et al., 2017) when the change in PET was estimated using Hargreaves-Samani method rather than Hamon, which produced unrealistically drier conditions due to higher sensitivity to temperature.

Equation 2-2: Hargreaves-Samani PET equation

$$H\_S\ Daily\ PET = 0.0135 \times R_s \times (T_{avg} + 17.8)$$

$$R_s = KT \times R_a \times T_{del}^{1/2}$$

$$T_{del} = T_{max} - T_{min}$$

$$KT = 0.00185 \times T_{del}^2 - 0.0433 \times T_{del} + 0.4023$$

Where:
PET = potential evapotranspiration, mm/day
Rs = solar radiation, mm/day
KT = empirical coefficient
Ra = Extraterrestrial radiation, mm/day
Tdel = maximum minimum temperature difference, degree Celsius
Tmax = maximum daily temperature, degree Celsius
Tmin = minimum daily temperature, degree Celsius

Tavg = average daily temperature, degree Celsius
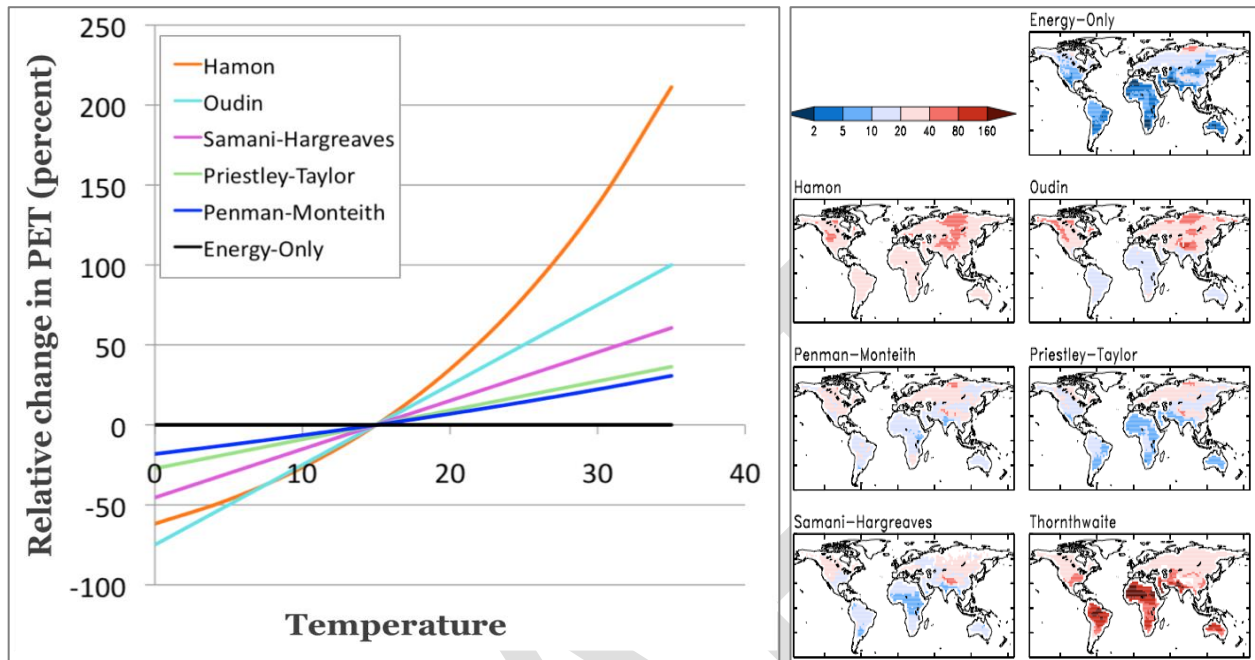
Figure 2-10: (a) Relative change in estimated change in potential evapotranspiration due to change in temperature is shown from different methods. It shows temperature alone can introduce considerable differences in estimation of potential evapotranspiration with the selection of method. (b) Estimate percent changes in potential evapotranspiration using different methods for RCP 8.5 for the late 21st century are shown (adapted from Milly 2016).

Both the Hamon and Hargreaves-Samani PET methods were evaluated for estimating change in potential evapotranspiration (PET). The average annual changes in PET over the watershed for the years 2025 and 2050 using the two methods are shown in Figure 2-11. The ensemble median of the change for the potential evapotranspiration data for short reference cover from the downscaled datasets are also shown, which is based on the Penman-Monteith equation. Short reference is defined as a hypothetical reference vegetative cover with an assumed height of 0.12 m, a fixed surface resistance of 70 s/m and an albedo of 0.23. Due to the similarities between estimated changes produced by the Hargreaves-Samani and Penman-Monteith methods, along with guidance provided by CBP STAC, and the recommendation of the Modeling Workgroup, Hargreaves-Samani was used for the CBP climate simulations. It is noted that estimated change using Hargreaves-Samani method falls between the estimated changes for open water and short reference.
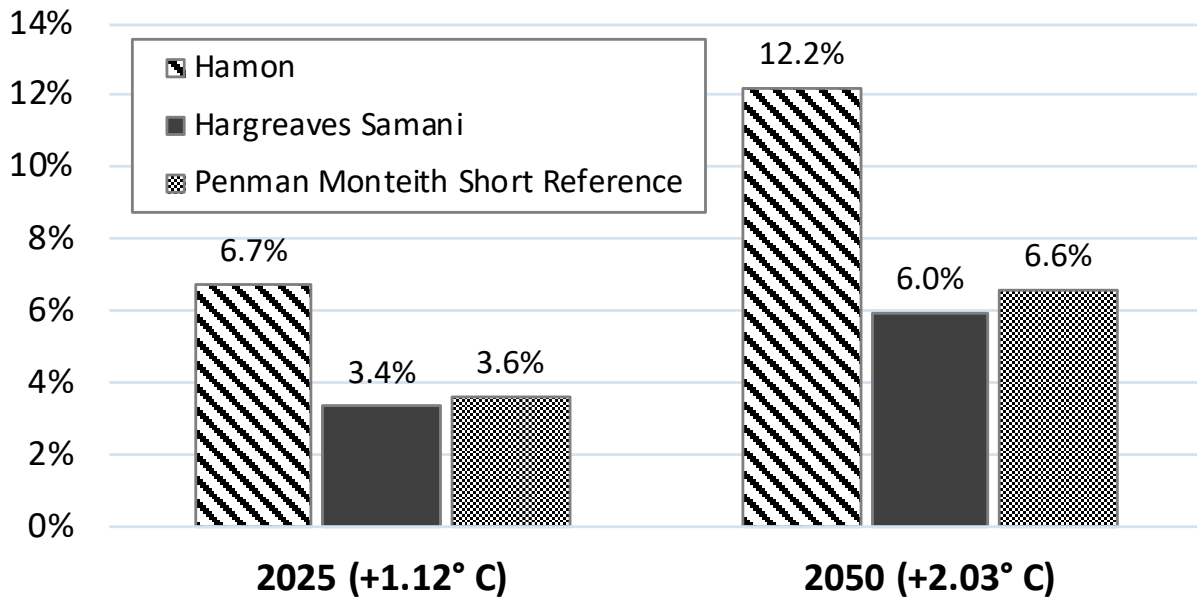
Figure 2-11: The relative difference in PET produced by using either the Hamon or Hargreaves-Samani methods are shown here. In 2025 projections produced by the WSM, the Hamon method simulated an increase in PET that was 3.36 percent greater than that simulated with the Hargreaves-Samani method. The change was more pronounced in 2050 simulations where the Hamon method outpaced the PET rate of Hargreaves-Samani by 6.26 percent.

2.2   Climate Scenario Input Summary

2.2.1   2025, 2035, 2045, and 2055 Temperature

Temperature change projections for 2025, 2035, 2045, and 2055 were obtained from an ensemble of statistically downscaled GCMs and were incorporated using the delta method (Section 2.1.6). For each model land segment, the average monthly change in temperature (in degree Celsius) was calculated for the GCMs, and the median change for each month was used as the central tendency of the projected future. Estimates for the 10th and 90th percentiles were also developed to define the range of uncertainty in projected future. As per the 31-member ensemble median for the RCP 4.5 scenario, the average annual increase in temperature for the Chesapeake Bay watershed in 2025, 2035, 2045, and 2055 were 1.12°C, 1.45°C, 1.84°C, and 2.12°C respectively. Spatial variability in average annual change for the land segments within the Chesapeake Bay watershed is shown in Figure 2-12. An elevation gradient in temperature increase is apparent for all scenarios, i.e. increases in air temperature are relatively lower at lower elevations. Figure 2-13 shows the ranges for monthly change in temperature averaged over the watershed from 31 GCMs for the RCP 4.5 scenario. The black line in the figure shows the spatial aggregation of the land segment ensemble median (P50) of monthly temperature changes. It shows a gradual increase in air temperature between 2025 to 2055 from 1.12°C to 2.12°C, where the increase in air temperature is almost the same across all months.
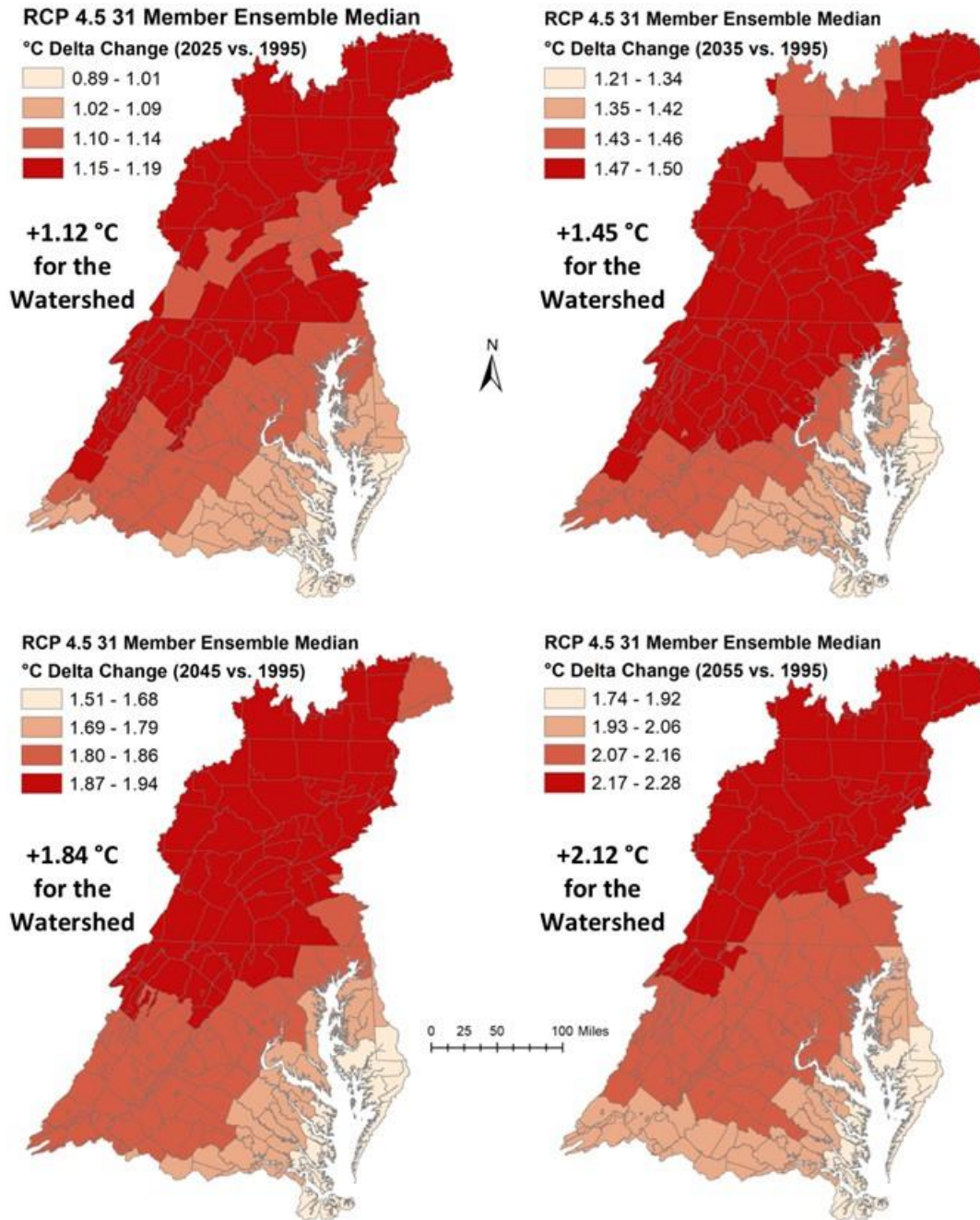
Figure 2-12: Estimated average annual change in temperature (°C) for the land segments (counties) in the Chesapeake Bay Watershed are shown for 2025 (top-left) 2035 (top-right), 2045 (bottom-left) and 2055 (bottom-right). The change in temperature with respect to 1995 are based upon 31-member ensemble median of downscaled Global Climate Models for RCP 4.5 scenario.
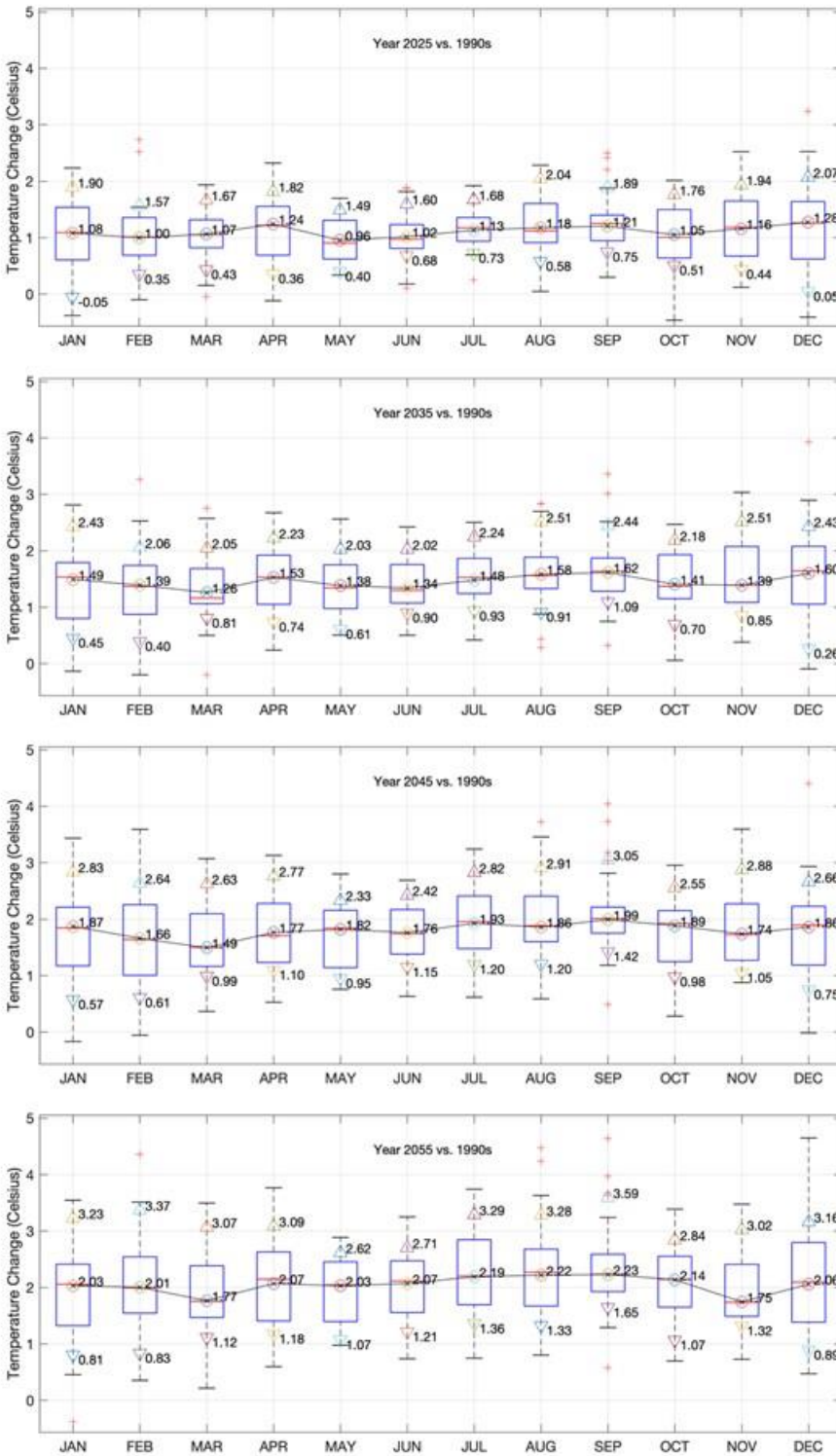
Figure 2-13: Monthly change in temperature for the Chesapeake Bay Watershed is shown. Box plots show the projected monthly change based on 31-member ensemble of downscaled Global Climate Models for RCP 4.5 for the years 2025, 2035, 2045 and 2055. Additional three markers show 10th percentile (P10), ensemble median (P50), and 90th percentile (P90) range for the spatially aggregated land segment data. The black line is spatial aggregation of the ensemble median (P50) of the RCP 4.5 GCMs for the land segments.

2.2.2   2025, 2035, 2045, and 2055 Precipitation

Precipitation change projections for 2025, 2035, 2045, and 2055 were developed using long-term rainfall trends and the ensemble of statistically downscaled GCMs and incorporated using the delta method (Section 2.1.6). For each land segment, the average monthly change in precipitation was calculated for each GCM, and the median change for each month was used as the central tendency of the projected future. Estimates for the 10th and 90th percentiles were also developed to define the range of uncertainty in projected future. The trend and GCM projections were reconciled using a hybrid approach, where the weight for trend varied linearly from 1 to 0 between 2025 and 2050, and weight for the GCM varied linearly from 0 to 1 between 2025 and 2050. As a result, rainfall projection for 2025 was entirely based on the extrapolation of rainfall trends, 60/40 hybrid of trend and GCMs for 2035, 20/80 hybrid of trend and GCMs for 2045, entirely based on GCMs for 2055. During the weighted averaging of trend and ensemble median of GCMs additional considerations were given to the seasonality. As discussed previously, information regarding seasonality was not directly available since rainfall trends were assessed using annual data. Therefore, before the trend data were combined with the ensemble median, the monthly percent change for trend data were calculated such that percent change in annual volume estimated by trend remained unchanged while the seasonal variability as seen in the ensemble median data was incorporated. As per these selections, the average annual increases in precipitation volume for the Chesapeake Bay watershed in 2025, 2035, 2045, and 2055 were 3.11%, 4.21%, 5.34%, and 6.91% respectively. Spatial variability in average annual change for the land segments within the Chesapeake Bay watershed is shown in Figure 2-15. Although the increase in rainfall gradually increases between 2025 and 2055 the spatial variability in rainfall do not show a consistent pattern. Figure 2-14 show an incremental increase in rainfall volume across all months between 2025 and 2055. Also, a relatively greater percent increase in rainfall during winter months (December to March) is evident as compared to July to September. Nonetheless, the representative scenario that is shown using the black line has an increase in rainfall volume for all months. The range or variability in monthly projections for rainfall change between the GCMs is considerably higher (Figure 2-14) as compared to variability seen for the changes in air temperature (Figure 2-13).
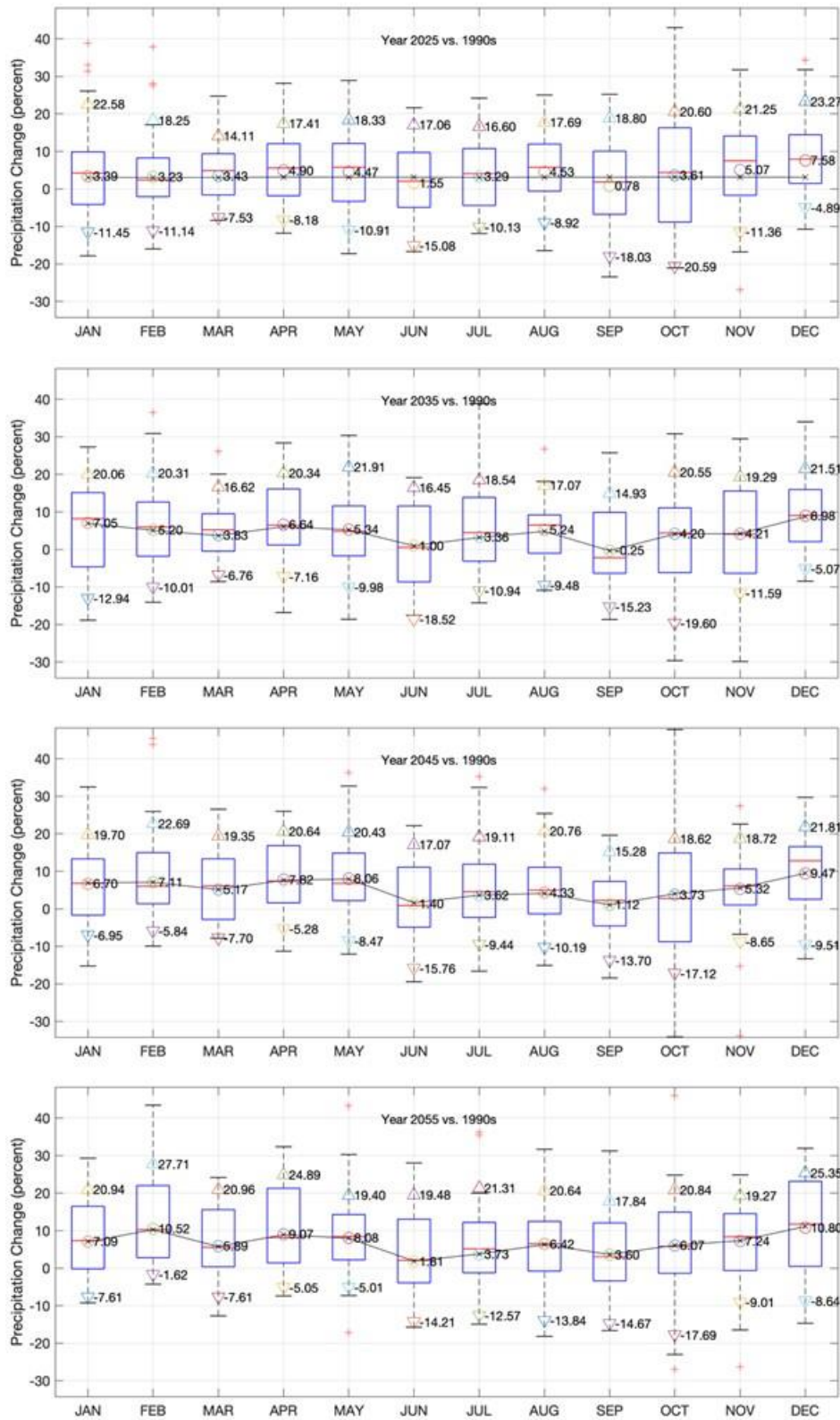
Figure 2-14: Monthly change in precipitation volume for the Chesapeake Bay Watershed is shown. Box plots show the projected monthly change based on 31-member ensemble of downscaled Global Climate Models for RCP 4.5 for the years 2025, 2035,

2045 and 2055. Additional three markers show 10th percentile (P10), ensemble median (P50), and the 90th percentile (P90) range for the spatially aggregated land segment data. The black lines show the monthly change after the estimated change from trend and GCMs were reconciled.
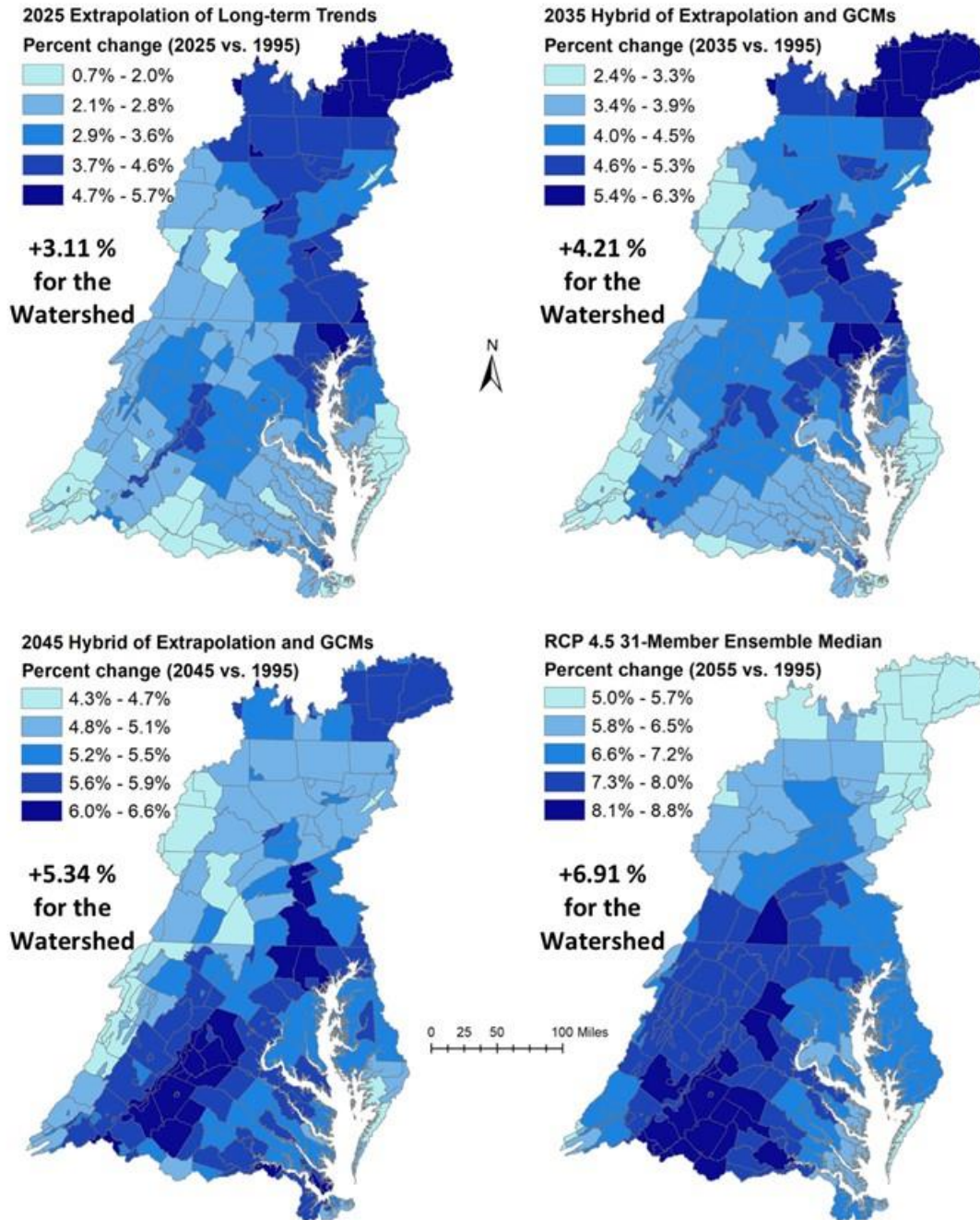
Figure 2-15: Estimated average annual change in precipitation volume (as percent change) for the land segments (counties) in the Chesapeake Bay Watershed are shown for 2025 (top-left), 2035 (top-right), 2045 (bottom-left) and 2055 (bottom-right). The change in rainfall volume with respect to 1995 are based on a specified combination of extrapolation of long-term trends and 31-member ensemble median of downscaled Global Climate Models for RCP 4.5 scenario.

2.2.3   2025, 2035, 2045, and 2055 Potential Evapotranspiration (PET)

Estimates for PET changes for 2025, 2035, 2045, and 2055, as discussed in Section 2.1.8, were developed using the Hargreaves Samani method and the temperature change from statistically downscaled GCMs (Section 2.1.6) that were incorporated using the delta method with the NLDAS temperature. Daily factor change in PET was calculated using Hargreaves Samani method and applied to the hourly calibration PET data. For each model land segment, the monthly median change in temperature was used as the central tendency of the projected future in the estimation of PET. Estimates for the 10th and 90th percentiles were also developed to define the uncertainty in projected future. As per the 31-member ensemble median for the RCP 4.5 scenario, the average annual increase in PET for the Chesapeake Bay watershed in 2025, 2035, 2045, and 2055 were 3.36%, 4.43%, 5.54%, and 6.35%, respectively. Spatial variability in average annual change for the land segments within the Chesapeake Bay watershed is shown in Figure 2-17. An elevation gradient in estimated changes in PET is seen across the watershed same as for the changes in air temperature. Figure 2-17 show monthly changes in PET using Penman Monteith method from Variable Infiltration Capacity (VIC) hydrologic simulations using 31-member ensemble of downscaled GCMs for RCP 4.5 for the years 2025, 2035, 2045 and 2055. The changes in PET corresponding to the ensemble median temperature estimated using Hargreaves Samani method.
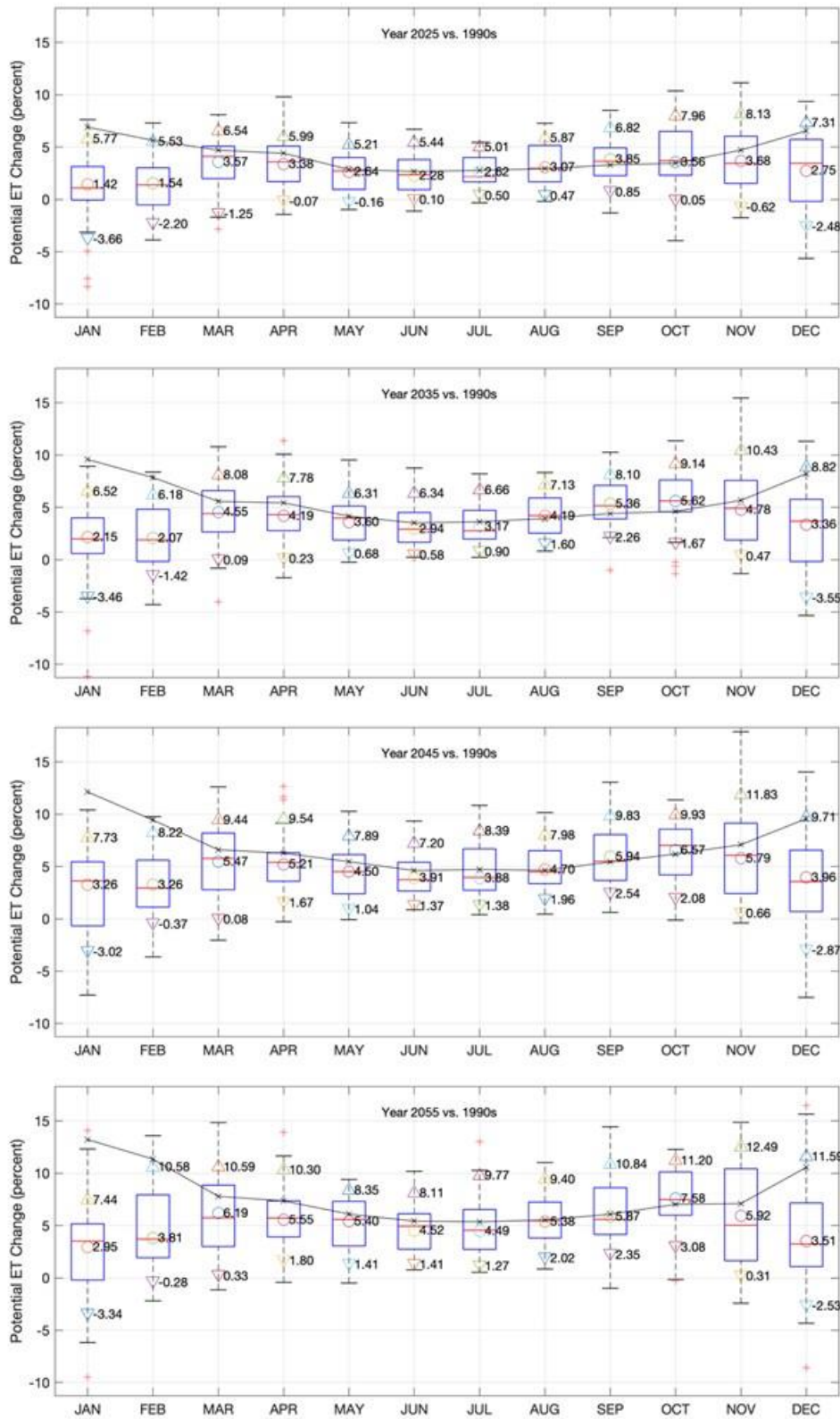
Figure 2-16: Monthly change in potential evapotranspiration for the Chesapeake Bay Watershed is shown. Box plots show the estimated monthly change using Penman Monteith method from VIC hydrologic simulation using 31-member ensemble of

downscaled Global Climate Models for RCP 4.5 for the years 2025, 2035, 2045 and 2055. Additional three markers show 10th percentile (P10), ensemble median (P50), and 90th percentile (P90) range for the spatially aggregated land segment data. The black line show the changes in PET estimated using the Hargreaves Samani method using the ensemble median (P50) temperature change.
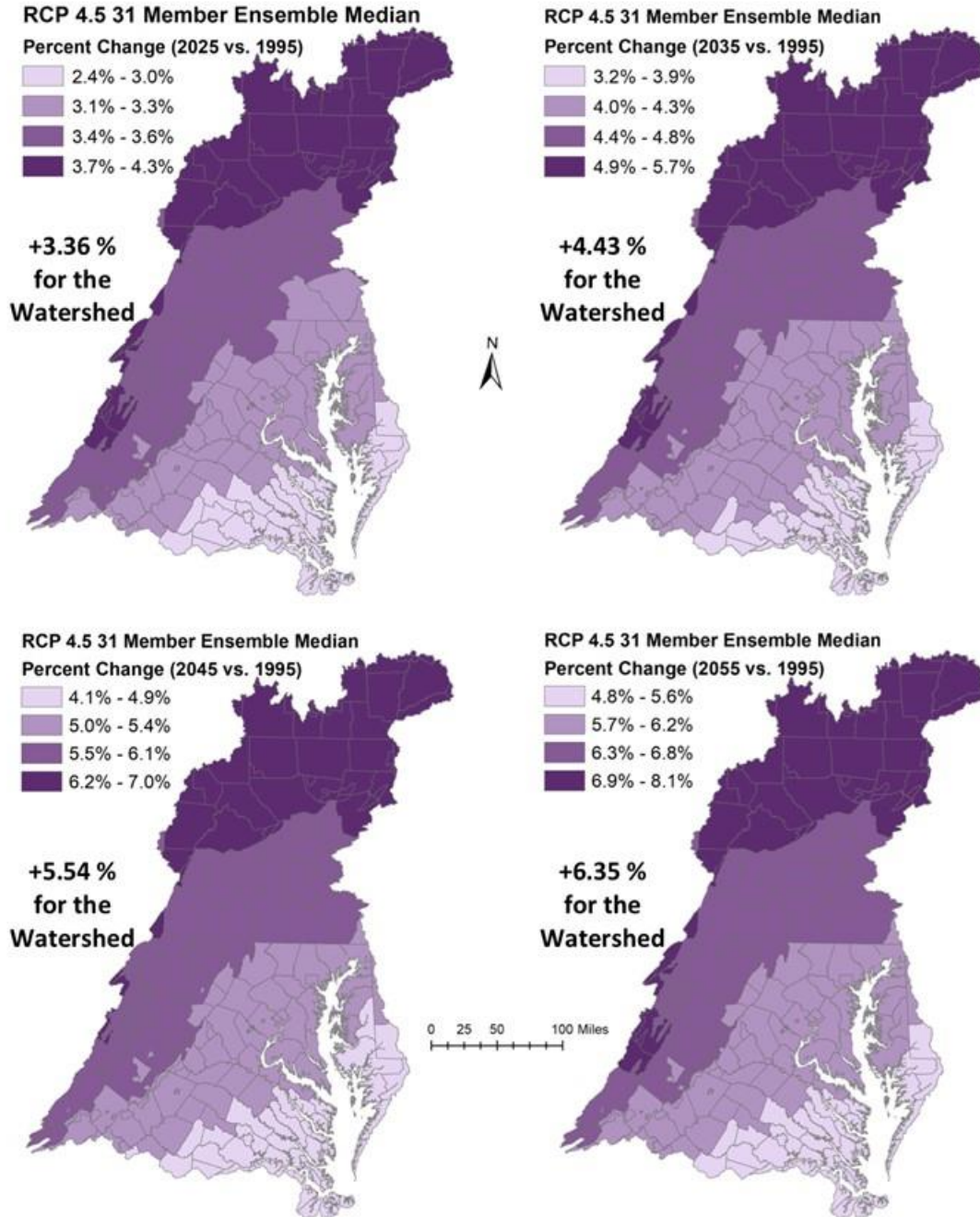
Figure 2-17: Estimated average annual change in potential evapotranspiration (as percent change) for the land segments (counties) in the Chesapeake Bay Watershed are shown for 2025 (top-left), 2035 (top-right), 2045 (bottom-left) and 2055 (bottom-right). The change in potential evapotranspiration with respect to 1995 are based on a Hargreaves-Samani Method and 31-member ensemble median temperature change of downscaled Global Climate Models for RCP 4.5 scenario.

3   Nutrient Inputs Response to Climate Change

MWG Review: Certain subsections of section 3 require review as marked

3.1   Atmospheric Deposition

MWG Review: no review necessary at this time

The modeling team is expecting to develop a relationship between precipitation and deposition from CMAQ.

3.2   Land Use

MWG Review: Requires review for July

Climate and land use are linked in complex ways – land use choices have effects on the release of greenhouse gasses, climate trends can affect human choices about land cover and land use, and both can be driven by the same societal choices.

Climate change may result in a change in the frequency and severity of droughts, heat waves, tropical storms and other weather hazards which may affect the patterns of development. Additionally, agriculture will react by planting a different combination of crops more suited to the future weather patterns. (Grimm, et al 2013, Brown, et al 2014)

Climate and land use are both changing through time; however, they are not the primary drivers of each other at the scale of the Chesapeake watershed. Land use changes in the watershed would have a small effect on the global carbon budget and the primary drivers of land use change within the Chesapeake are based on the local economy, regulation, conservation, and other factors that are not primarily driven by climate change.

Although the climate effect on land use change is likely small, the effect is already subsumed within the land use data set that has been developed by the CBP land data team detailed in Section 5 of the CAST documentation (CBP 2017). The land use data set is provided from 1985 through 2017 and projected through 2025 using trends and population projections that are based on observations occurring during a period of climate change, and therefore climate-induced changes in land use are already included in the data set. Climate effects are not separable from land use changes from other drivers, however. Land use projections will be provided through 2050. Climate effects will be included in these estimates to the extent that they are a continuation of current trends in land use.

3.3   Agricultural Inputs

MWG Review: Requires review for July

Agricultural practices are highly dependent on expected weather and therefore will change in response to climate trends. Alterations in production due to climate have already occurred and have been estimated in the literature (e.g. Gammas et al, 2017). The National Climate Assessments (Hatfield et al, 2014, Gowda, et al, 2018) found that increased climate stressors such as droughts, extreme precipitation, and extreme temperatures will likely have negative effects on production systems. Other studies have found beneficial effects of increased carbon dioxide concentrations (e.g. Deryng et al, 2016). Meanwhile adaptations in cropping methods and technologies tend toward increasing agricultural yields in the Chesapeake region.

The CBP uses data from the census of agriculture (e.g. USDA-NASS 2014) and other sources (CBP 2017, section 3) to estimate changes in production systems, animal populations, and yields through years of interest. The 2017 census of agriculture will be projected through 2022 and held constant for future years according to methods approved by the CBP partnership (CBP 2017, section 3).   The observed changes to agriculture in the census include changes due to climate, although the CBP does not break out agricultural change due to climate specifically. Currently, no method has been identified to include climate influences in land use or agricultural projections to 2035, 2045, and 2055.

3.4   Direct Loads

3.4.1   Combined Sewer Overflows

MWG Review: Requires review for July

Changes in Combined Sewer Overflow (CSO) volumes expected because of climate change were obtained by first estimating the expected changes in rainfall volume and intensity under a set of climate change scenarios and then using an empirical regression between rainfall and daily CSO volume. This regression was developed by Tetra Tech and previously used to estimate CSO inputs for the Phase 6 Watershed Model (see Section 8 of the Phase 6 CAST and Watershed Model documentation, Chesapeake Bay Program 2017).

Projected changes in average monthly volumes of rainfall for different climate change scenarios (2025, 2035, 2045 and 2055) were obtained through a combination of observed long-term historical trends in local rainfall and results from climate models as described in detail in Section 0. For each climate change scenario, the overall change in rainfall volume projected in each month was distributed across the historical (1991–2000) daily precipitation events exceeding 0.01 inches occurring in that month. As described in more detail in Section 0, the projected change in rainfall volume was not distributed uniformly across all daily precipitation events. Instead, the set of precipitation events > 0.01 inches occurring in each month was divided into deciles, and precipitation events falling into the highest deciles were assigned a

larger fraction of the overall rainfall change projected for that month. For example, if a climate change scenario predicted a 3% increase in rainfall volume for the month of March and the observed rainfall volume for March in 1991-2000 was 7 inches, then 7 inches x 3% = 0.21 inches of total rainfall volume should be added to March rainfall. This added volume is distributed unevenly across rainfall deciles, with events falling in the highest decile of the distribution for March precipitation events receiving around 65% of 0.21 inches, events falling in the second highest decile receiving around 10% of 0.21 inches and events falling in smaller deciles receiving the remaining amount of volume. This approach was designed to account for the fact that previous literature has shown uneven increases in precipitation events in this area, with larger rainfall events increasing more compared to smaller ones (Groisman et al., 2004). As described in Section 0, climate-driven changes in monthly rainfall volumes vary geographically, and as a result, CSO service areas received somewhat different projected rainfall changes depending on their location in the watershed.

After generating new time series (1991–2000) of daily precipitation events for each CSO service area and for each climate change scenario, an empirical regression between CSO volume and rainfall previously developed by Tetra Tech (Figure 8-5 in Section 8 of the Phase 6 CAST and Watershed Model documentation, Chesapeake Bay Program 2017) was applied to obtain projected CSO volumes under each climate change scenario. For four CSO communities, historical CSO volumes in 1991-2000 were not originally estimated using the Tetra Tech regression because those facilities submitted their own volume data. For these communities, site-specific empirical regressions were developed that captured the relationship between CSO volume and rainfall (*Figure 3-1*), and these site-specific regressions were used instead of the Tetra Tech regression to estimate predicted CSO volumes under climate change scenarios. The four communities for which this approach was used were Washington DC (DC0021199), Lynchburg, VA (VA0024970), Richmond, VA (VA0063177) and Alexandria, VA (VA0087068).
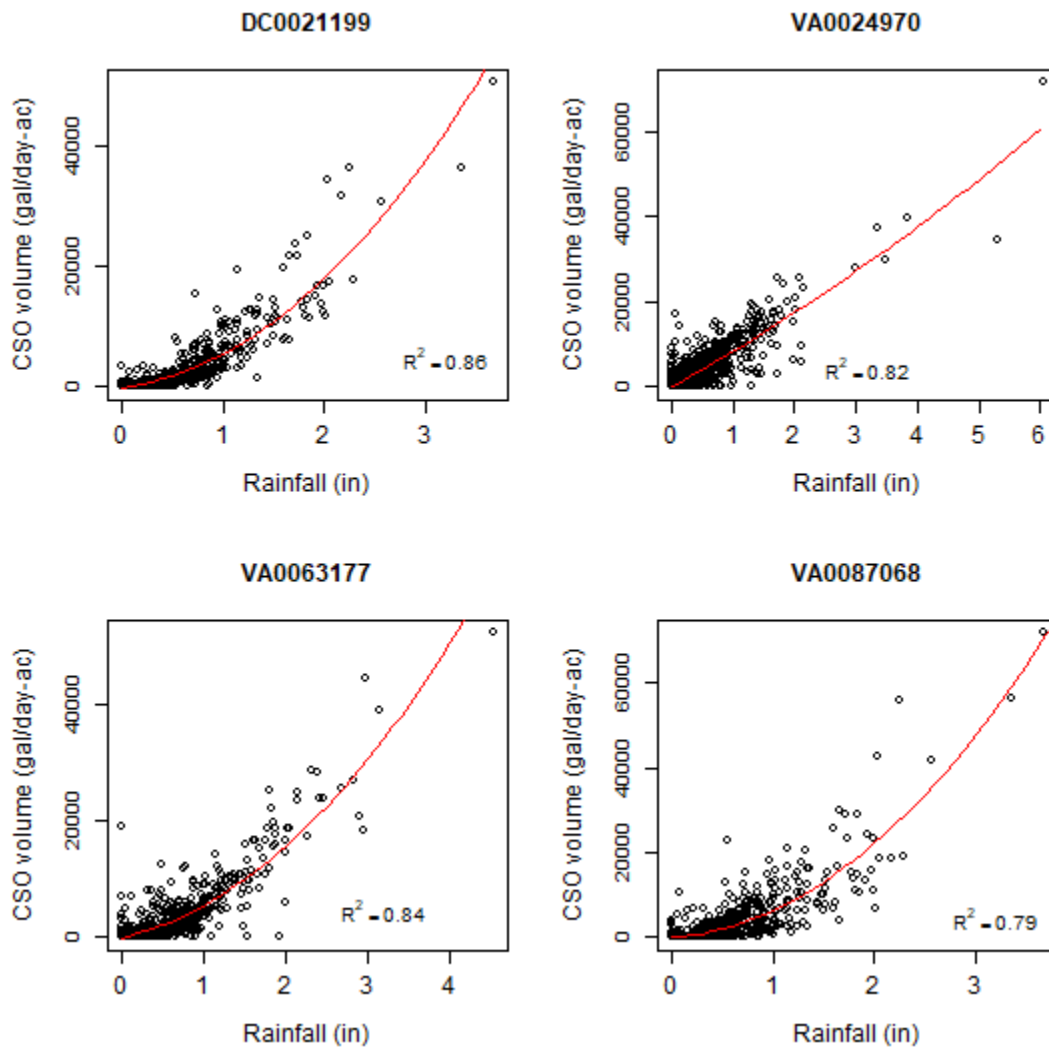
Figure 3-1 Relationship between daily CSO volume per unit area and rainfall at four communities that provided CSO volume data over the period 1991-2000. DC0021199: Washington, DC; VA0024970: Lynchburg, VA; VA0063177: Richmond, VA; VA0087068: Alexandria, VA

Loads of constituents were calculated by multiplying CSO volumes by event mean concentrations (EMC) derived from observations or literature as described in Section 8.5 of the Phase 6 CAST and Watershed Model documentation. Note that because constituent loads are estimated by multiplying CSO volumes by fixed EMC values, for each service area percent changes of constituent loads are identical to percent changes of CSO volumes.

With respect to the 1991-2000 reference period, the estimated average annual percent change in precipitation volume across all CSO service areas was 2.91% under 2025 conditions (estimated through extrapolation of long-term trends), and 4.09, 5.02 and 6.24% under 2035, 2045 and 2055 conditions, respectively (estimated from an ensemble of GCMs).

The corresponding estimated percent changes in average annual CSO volume are reported in *Figure 3-2*. *Figure 3-3* shows time series of total annual CSO volumes estimated for the period 1991-2000 and used for model calibration, together with the corresponding annual values projected under different climate change scenarios. Finally, *Table 3-1* and *Table 3-2* summarize estimated CSO-derived TN and TP loads under different climate change scenarios broken down by state.
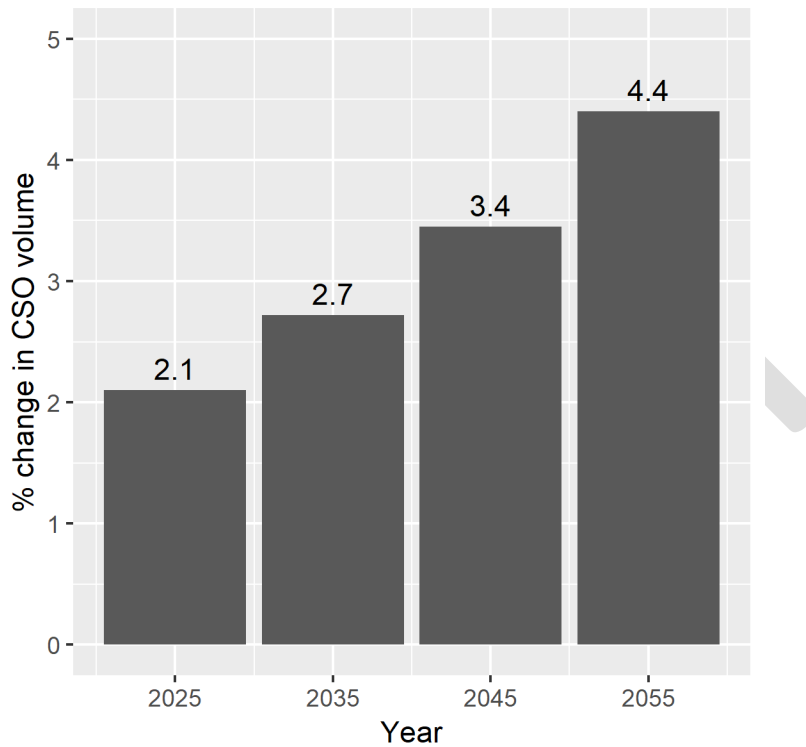

Figure 3-2 Estimated percent change in total CSO volume under different climate change scenarios. Reference period: 1991 – 2000
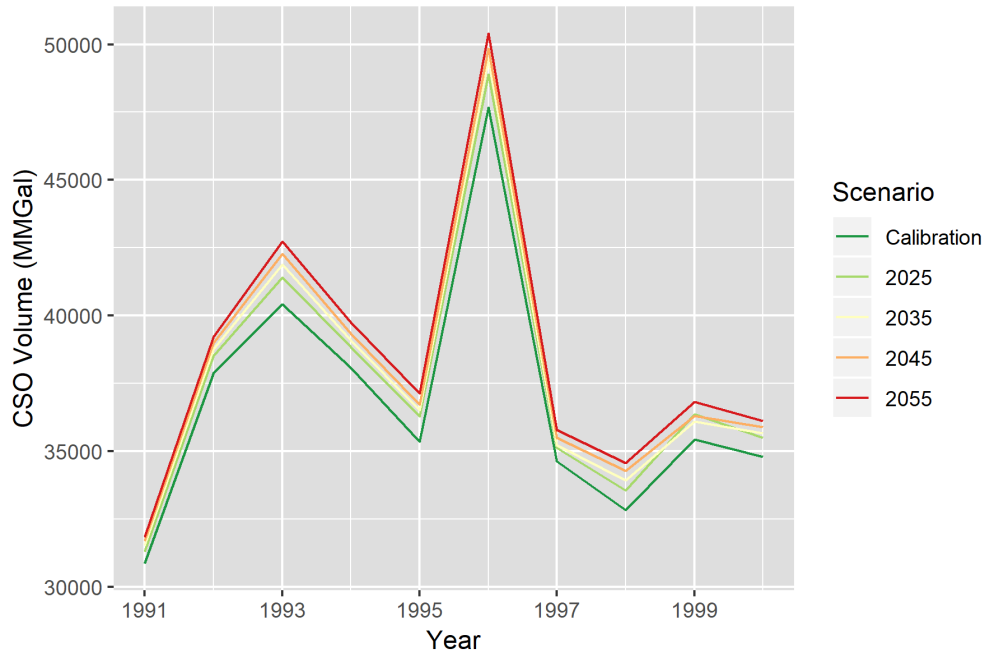
Figure 3-3 Time series of total annual CSO volume across all 64 communities in the Chesapeake Bay watershed. The darkest green line corresponds to CSO volumes used during model calibration, while other lines illustrate the estimated CSO volumes under different climate change projection years

Table 3-1 Mean annual TN loads (Lbs/yr) from CSOs estimated for the historical period 1991-2000 and a set of climate change scenarios

State	# Facilities	1991 – 2000	2025	2035	2045	2055
DC	1	87,414	92,182	93,453	94,890	97,651
DE	1	2,318	2,348	2,350	2,375	2,411
MD	10	31,072	31,675	31,828	32,035	32,465
NY	3	212,015	216,215	217,159	217,419	217,976
PA	40	1,629,861	1,657,892	1,664,987	1,671,681	1,682,526
VA	4	307,901	317,311	322,045	329,372	335,453
WV	5	62,752	63,879	64,317	64,888	65,570

Table 3-2 Mean annual TP loads (Lbs/yr) from CSOs estimated for the historical period 1991-2000 and a set of climate change scenarios

State	# Facilities	1991 – 2000	2025	2035	2045	2055
DC	1	18,599	19,613	19,884	20,189	20,777
DE	1	290	293	294	297	301
MD	10	3,609	3,680	3,698	3,722	3,772
NY	3	26,502	27,027	27,145	27,177	27,247
PA	40	257,694	261,753	262,907	264,028	265,594
VA	4	38,532	39,711	40,303	41,220	41,982
WV	5	7,844	7,985	8,040	8,111	8,196

3.4.2   Other direct loads

MWG Review: Requires review for July

Wastewater treatment plants (WWTPs) may experience operational changes due to climate change. Changes in water use and supply may have an effect on the influent concentrations expected. Increases in influent temperature lead to increased reaction rates associated with biological nutrient removal. However, operators of plants are largely able to control effluent concentrations by altering their processes to meet permit limits. Given the existing permit limits that are expressed in the WIPs, it is unlikely that climate change will have an effect on the effluent of WWTPs in the Chesapeake. Moreover, any changes in wastewater loads due to climate change are already factored into the data supplied to the CBP from 1985 through 2017. Similarly, data for septic systems, rapid infiltration basins, and diversions are inclusive of the period 1985 through the mid-2010s, capturing most of the effects of climate change through 2025. No method has been determined to project climate effects on these systems through 2050.

4   Watershed Model Response to Climate Change

MWG Review: Certain subsections of section 4 require review as marked

Section 0 discussed the calculation of precipitation, temperature, and carbon dioxide changes between the Chesapeake TMDL averaging period of 1991-2000 and future climate scenarios centered around 2025 and 2050. This section discusses simulated watershed responses.

4.1   Simulation of CO$_2$ Concentration Response

MWG Review: Requires review for July

The HSPF model structure does not provide a direct mechanism for simulating the impact of CO$_2$ on water budget through stomatal resistance and decreased plant evapotranspiration. However, Butcher et al. (2014) documents necessary adjustments to HSPF LZETP parameter that can be used for the simulation of CO2 effects on plant stomatal resistance in HSPF and subsequently on the lower vadose zone evapotranspiration. Accordingly, the monthly LZETP
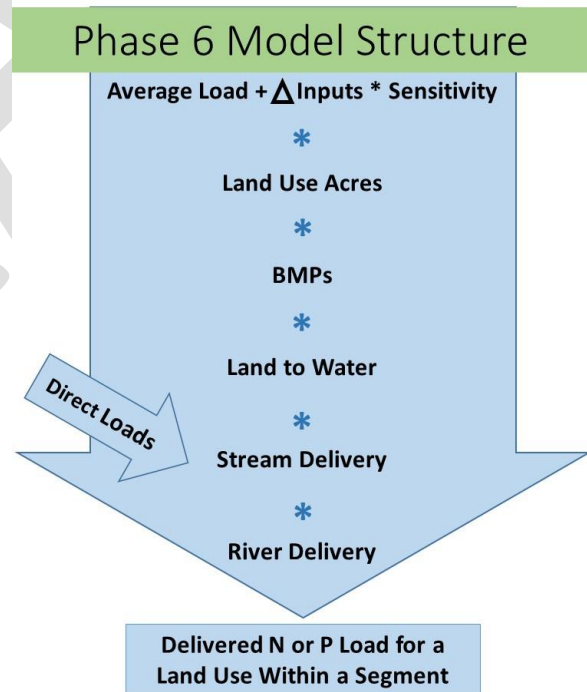
parameter was modified to simulate the effect of increasing CO_2 concentrations as a result of continuing projections of atmospheric contributions from anthropogenic sources.

PETfactor = AET_1 / AET_0

Where,

PETfactor = ratio of actual ET (AET) under new CO2 level and reference

For HSPF: $PETfactor = \dfrac{1/(1-LZETP_1)}{1/(1-LZETP_o)}$

$LZETP_1$ = Max { 1 − (1 − $LZETP_0$) / PETfactor, 0.01 }

Equation 4-1

Where,

LZETP = HSPF lower zone ET parameter

For Penman Monteith: $PETfactor = \dfrac{1/\{\Delta+\gamma(1+r_{s1}/r_a)\}}{1/\{\Delta+\gamma(1+r_{s0}/r_a)\}}$

$$PETfactor = \frac{(\Delta + \gamma)r_a + \gamma r_{s0}}{(\Delta + \gamma)r_a + \gamma r_{s1}}$$

$$\Delta = \frac{4098 \times \left[0.6108\, exp\left(\frac{17.27T}{T + 273.3}\right)\right]}{(T + 273.3)^2}$$

$$\gamma = 0.673645\left(\frac{293 - 0.0065z}{293}\right)^{5.26}$$

T = air temperature (monthly), °C

z = elevation, meter

$$r_{s0} = \frac{r_l}{.5\, LAI} = \frac{100}{.5 \times 24 \times 0.12} = 70$$

$$r_{s1} = \frac{r_l}{.5\, LAI\left(1.4 - 0.4\frac{CO_2}{330}\right)} = \frac{100}{.5 \times 24 \times 0.12\left(1.4 - 0.4\frac{CO_2}{330}\right)} = \frac{70}{\left(1.4 - 0.4\frac{CO_2}{330}\right)}$$

$$r_a = \frac{208}{u}$$

u = wind velocity (monthly), m/s

4.2   Simulation of Hydrology

MWG Review: Requires review for July, asking for approval for direct simulation of hydrologic changes using HSPF.

A new set of precipitation, temperature, potential evapotranspiration, and modified LZETP parameters are inputs for the climate change scenarios. The impact of these climate change variables on the hydrologic response is simulated by the HSPF PWATER, IWATER, SNOW, and HYDR modules for the Phase 6 model. This approach is same as the one used in Phase 5 climate change simulation.

HSPF hydrologic simulation for climate change respond to changes in (a) rainfall volume and rainfall intensity, (b) potential evapotranspiration, (c) CO_2 level, and (d) temperature inputs. Changes in temperature inputs influence snow hydrology by introducing changes in the amount of snow and energy balance for the snowpack. Changes in potential evapotranspiration and adjustments for CO2 level influence the evapotranspiration calculations, subsequently impacting the simulated water budget.

4.3   Simulation of Sediment Loss

MWG Review: Requires review for July, asking for approval for direct simulation of sediment changes using HSPF.

The impact of climate change on the sediment transport is simulated by HSPF SEDMNT, SOLIDS, and SEDTRN modules subroutines for the Phase 6 model. This approach is same as the one used in Phase 5 climate change simulation.

HSPF uses a process-based approach for the production and removal of sediment. The land surface erosion of sediment includes processes for detachment by net rainfall, attachment on days without rainfall, and removal by surface outflow.

As shown in Equation 4-2, the detachment of sediment particles (DET) is simulated due to kinetic energy of falling rain ($RAIN$), which are then available for transport. Changes in rainfall volume and intensity due to climate change will therefore directly impact the net sediment transport. The CR terms in the Equation 4-2 represent the fraction of land covered include coverage by snow. Therefore, any changes in the snow hydrology will also have direct impact on detachment of sediment particles.

$$DET = (1 - CR) \times SMPF \times KRER \times (RAIN)^{JRER}$$

Equation 4-2

Where:

DET = Detachment of particles
CR = fraction covered by vegetation or snow
SMPF = management practice factor (set to 1 for CBP purposes)
KRER = soil detachment coefficient (complex units)
RAIN = Precipitation (inches per hour)
JRER = soil detachment exponent (complex units)

As shown in Equation 4-3, the transport (WSSD) of the detached sediment and the scour of soil is simulated based on surface outflow (SURO) and surface water storage (SURS). The detached sediment storage (DETS) and sediment removal capacity (STCAP) also control the amount of sediment transport. The climate change stressor would impact the surface outflow and surface water storage, and therefore the transport of sediment.

$$WSSD = (DETS \text{ or } STCAP) \times {SURO}/{(SURS + SURO)}$$

Equation 4-3

Where:
WSSD = Sediment Washoff (tons/acre/hour)
DETS = Storage of detached sediment (tons/acre)
STCAP = Sediment removal capacity
SURO = Surface runoff (inches/acre/hour)
SURS = Surface water storage

4.4 Nitrogen Loss Sensitivity to Climate Change

MWG Review: Section 4.4 does not require review for July. This section is mostly complete and left in this July draft for interested members, but changes or additional support are expected for October.

Nitrogen loads do not automatically change in the Phase 6 Watershed Model based on changes in hydrology and sediment. Nitrogen loads are determined by nutrient inputs as discussed in Section 4 and watershed characteristics as discussed in Section 7. Nitrogen loads would be affected by climate change and so additional sensitivities to inputs must be included.

Using the framework of multiple lines of evidence, the modeling team analyzed percent change in nitrogen delivery relative to percent change in flow. Using the Phase 5.3.2 Watershed Model, this ratio was determined to be 0.643 as illustrated in Figure 4-1. In the '20 watersheds' study (U.S. EPA 2013), HSPF and SWAT were used to simulate the effect of climate change on 20 watershed across the contiguous U.S. Figure 4-2 shows the simulated responses for a 20-watershed study using the SWAT model (Butcher et al. 2014, U.S. EPA 2013). This analysis simulated changes in flow (Table 7-7 U.S. EPA 2013) and total nitrogen delivery (Table 7-14 U.S. EPA 2013) in response to the changes in climatic inputs obtained from a set of 6 downscaled climate model projections. The findings suggest that a ratio of 1.14 for the simulated changes

in nitrogen load delivery with respect to changes in flow. For the Susquehanna, out of 20 watersheds the only watershed situated in Chesapeake, the ratio was 7 with a 49 percent increase in TN for a 7 percent increase in flow. However, this ratio was an outlier among the 20 watersheds investigated in U.S. EPA 2013. Given the wide variability in outcomes a ratio of 1 was selected for initial study with additional input being sought for future refinements. This is to suggest an assumption of no changes in time-average nitrogen concentrations with changes in flow or a proportional change in nitrogen load to a change in flow.
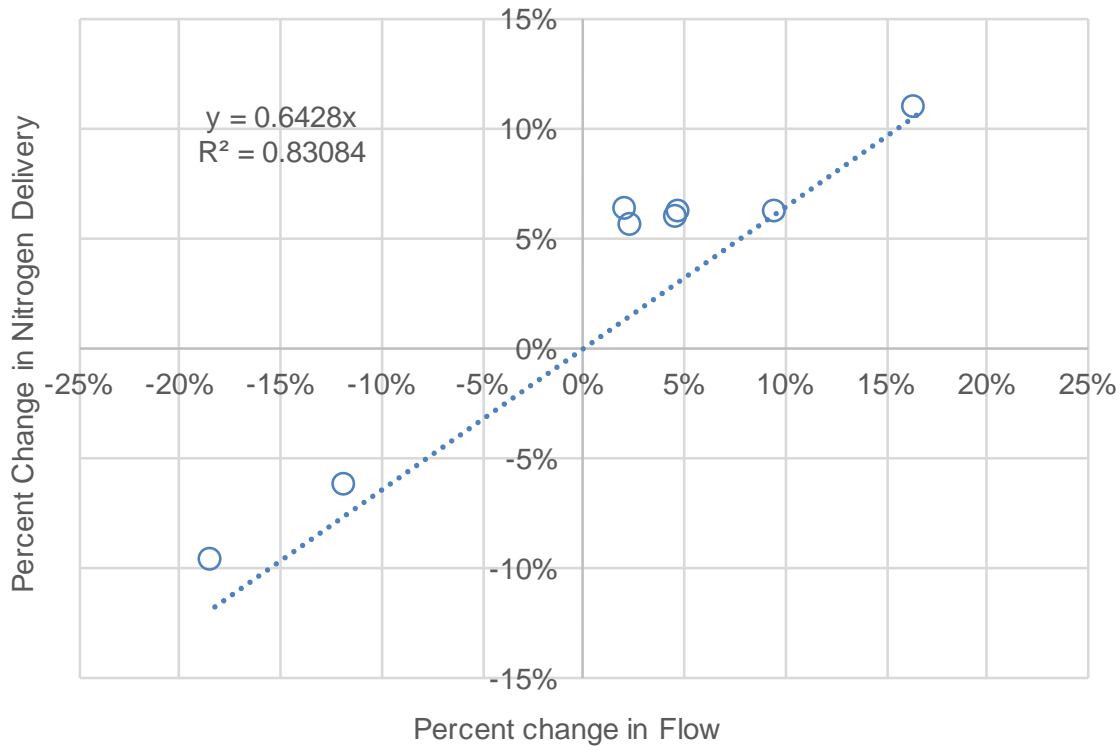
Figure 4-1: Simulated responses for flow and nitrogen from the Phase 5.3.2 Chesapeake Bay Watershed Model. Climate change simulations included in the analysis were based on a CMIP3 ensemble of 6 downscaled Global Circulation Models for the years 2025 and 2050. Six additional sensitivity simulations for rainfall, temperature and potential evapotranspiration, and carbon dioxide were also included.
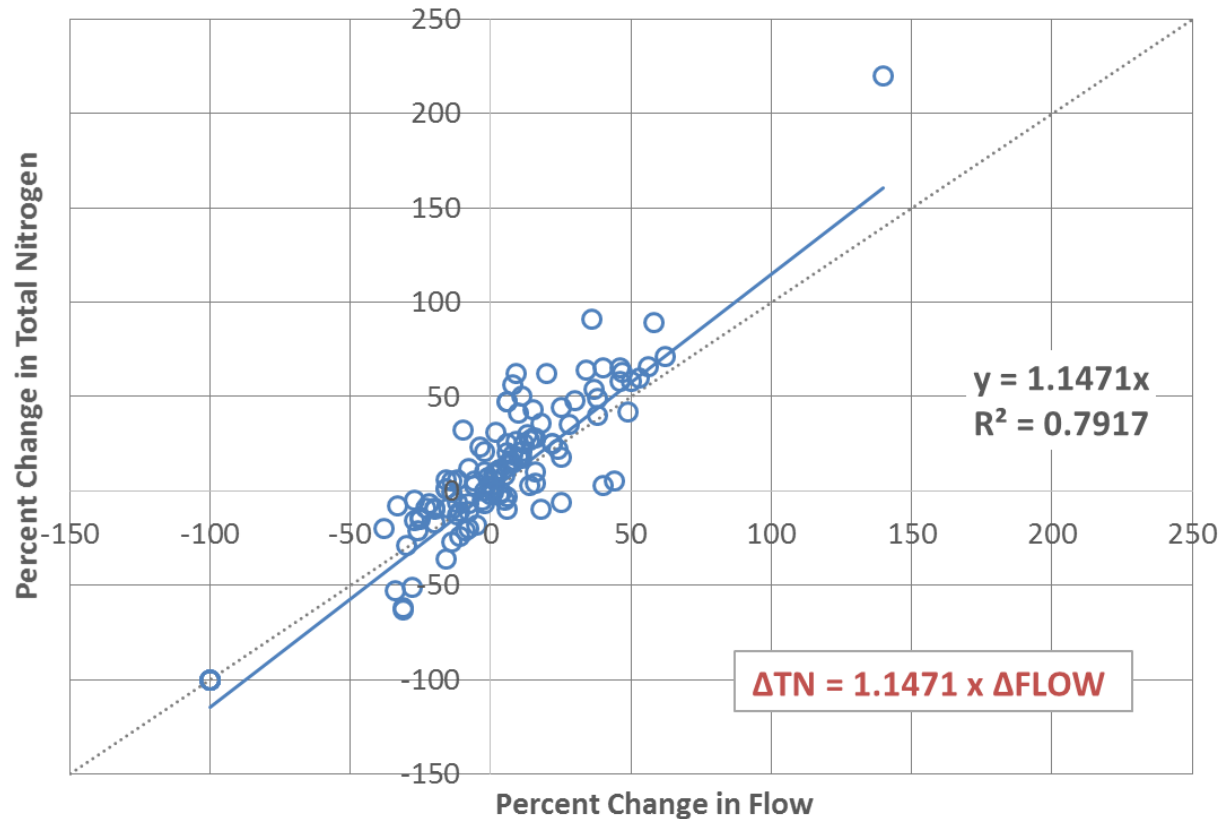
Figure 4-2: The sensitivity of nitrogen load delivery with changes in flow under a wide range of climate change scenarios. The simulated response for 20 watersheds under the climate change scenarios have been shown (From U.S.EPA 2013).

Alam et al. (2017) used the SPARROW model to investigate the effects of climate change on nitrogen delivery. They find relationships between nitrogen load and changes in precipitation and temperature in space and apply those to changes in time. They find an increasing load with precipitation and a decreasing load with temperature. The median effect from multiple SPARROW models of changes in precipitation and temperature in the Chesapeake region was a reduction of 3.6 percent. This finding from an empirical study is consistent with the findings of the Phase 5.3.2 Model.

Studies have been conducted to demonstrate the impacts of climate changes on hydrology and water quality. The relationship between streamflow and nitrate loads are summarized from several papers below. Mehdi et al. (2015a) simulated the impacts of climate change and agricultural land use change on water quality in the Pike River Watershed located in southern Québec/northern Vermont using the hydrological model SWAT for 2050 time horizon. Results showed that climate changes simulations applied to the model caused increase in both streamflow and nitrate loads (up to 80 percent) from November to February. Similar study done in Altmühl River, Germany (Mehdi et al. 2015b) demonstrated that climate change will reduce streamflow but increase nitrate loads. Additionally, nitrate loads increase by three-fold when climate change scenarios coupled with land use change scenarios, comparing to the

climate change simulations alone with decrease. In southern Ontario, Canada, results from El-Khoury et al. (2015) paper reveal that climate change will drive up annual streamflow but show no effect on annual nitrate loads. Wang et al. (2015) utilized Water Erosion Prediction Project-Water Quality (WEPP-WQ) model to simulate the impacts of climate change on nitrogen and phosphorous loss on two small watersheds (Walworth watershed and Green Lake watershed) within the Great Lakes region. Another study done in the Maumee Watershed showed decrease in streamflow and nitrate loads for mid-century and increase in streamflow and nitrate loads for late-century (Verma et al., 2015). Lee et al. (2018) studied the hydrological responses of two sub-watersheds of Chesapeake Bay Watershed to climate change using SWAT model. Result shows that annual streamflow and nitrate loads showed an increase of 70 percent relative to the baseline scenario, due to elevated CO_2 concentrations and precipitation increase over the GCM ensemble mean.

Figure 4-3 is a scatter plot of the percent change in streamflow against the percent change in annual nitrate loads under climate change scenarios only excluding small watersheds. The trendline. The linear extrapolated trendline shows that percent change in nitrate is 100 percent change in streamflow with R square of 0.93. Figure 4-4 shows similar scatter plot of not only climate change scenarios but also land use change scenarios and results from Wang et al. (2015). The trendline in this case is change in nitrate is 67 percent of change in streamflow with R square of 0.30.
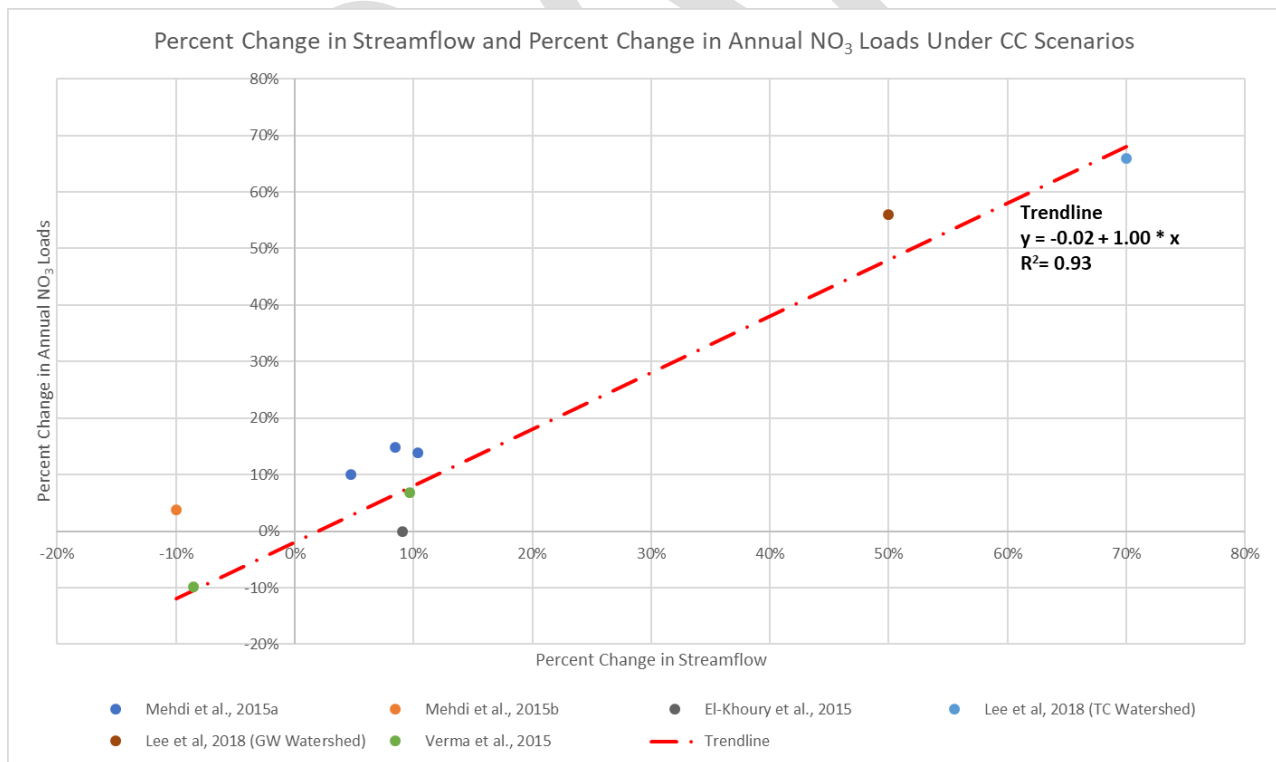

Figure 4-3 Percent Change in Streamflow and Percent Change in Annual Nitrate Loads under Climate Change Scenarios summarized from Literature Studies (excluding Wang et al. (2015))
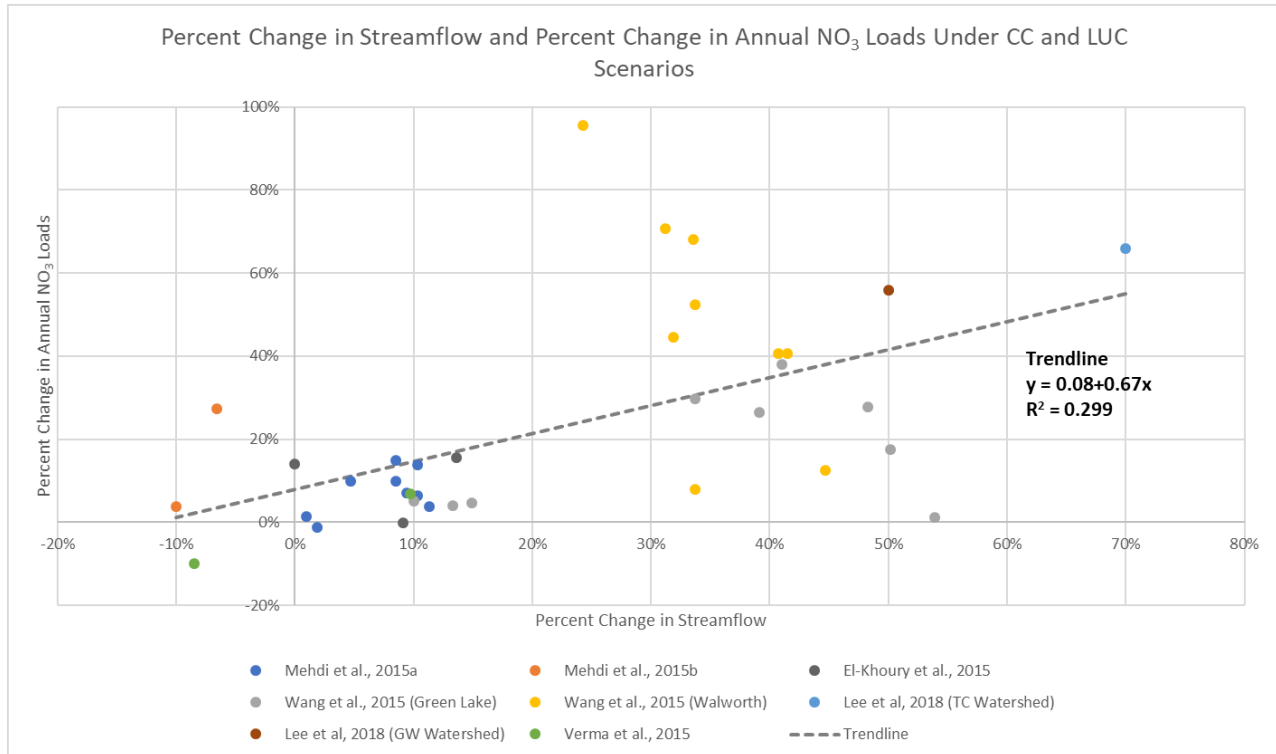
Figure 4-4 Percent Change in Streamflow and Percent Change in Annual Nitrate Loads under Climate Change and Land Use Change Scenarios summarized from Literature Studies

4.5   Phosphorus Loss Sensitivity to Climate Change

MWG Review: Section 4.5 does not require review for July. This section is partially complete and left in this July draft for interested members, but changes are expected for October.

4.5.1   Agricultural Land

Phosphorus transport from land segments and land uses is a function of stormflow, sediment transport, soil phosphorus concentration, and applied water extractable phosphorus as described in Section 4.   Soil concentrations and applications are not altered in a climate change scenario, but stormflow and sediment transport are affected as described above. Stormflow is defined as the sum of HSPF simulated *Surface* and *Interflow outflows*. The time-averaged changes in stormflow and sediment transport for climate change scenarios are estimated using the HSPF simulation. The time-averaged model uses simulated time-averaged changes in stormflow and sediment transport for the estimation of time-averaged changes in phosphorus transport. The sensitivity coefficients for phosphorus transport are based on results from the Annual Phosphorus Loss Estimator (APLE) model. The detailed derivations of these sensitivities are described in Section 4. Table 4-1 provides a brief summary of phosphorus sensitivities to stormflow and sediment losses for major land uses. The sensitivities

show changes in phosphorus transport in pounds per acre corresponding to changes in stormflow (inches/acre) and sediment washoff (tons/acre). These sensitivities are additive.

Table 4-1: Time-averaged phosphorus sensitivities (pounds/acre) of major land uses for stormflow (inches/acre) and sediment washoff (tons/acre). If applicable, the range shows minimum, mean and maximum sensitivity values for the land uses within each category.

Land use Category	Flow Sensitivity Range	Sediment Sensitivity Range
Natural	0.007, 0.019, 0.042	0.012, 0.031, 0.067
Pasture	0.080	0.126
Cropland	0.041	0.121

4.5.2   Developed Land

This section describes preliminary findings of a literature review recently carried out to assess the impact of climate change-driven changes in hydrology on TP loads from developed land uses. These results will be finalized by October 2019 after potentially including results from additional analyses, such as, for example, an upcoming SWAT study on TP sensitivity to climate in two watersheds in Baltimore County (Gwynns Falls and Jones Falls) and an empirical analysis of data from the National Stormwater Quality Database.

4.5.2.1   *Literature review*

To assess the impact of potential climate change-driven changes in hydrology on TP loads from developed land uses, a review of the relevant literature was carried out. To be included in this review a study must have either been conducted in a watershed/site where > 50% of the study area was defined as urban/developed or, if conducted in predominantly agricultural watersheds, reported results of climate change-driven changes in TP loads separately for developed land uses. Both empirical and modeling studies were considered. A total of six studies were found that matched these criteria (Table 4-2), and a brief description of each study`s main characteristics and methods is provided in the following paragraphs.

Alamdari et al. (2017) used EPA`s Storm Water Management Model (SWMM) to assess the impacts of climate change on runoff and water quality in the urbanized Difficult Run watershed (Fairfax, VA). The SWMM model was calibrated and verified to observations from two USGS stream gauges in the watershed. Historical (1971–1998) and future (2041–2068) precipitation and temperature projections from the North American Regional Climate Change Assessment Program (NARCCAP) were used to run the model and compare historical vs. climate change-driven flow and constituent loads. Climate change projections were based on only one of the NARCCAP products (MM51-CCSM, greenhouse gas scenario A2), which was selected based on historical model performance in the study area.

Xiang (2017) quantified the effects of climate change on streamflow and nutrient loads in the suburban Wilde Lake watershed (Columbia, MD) using the Soil and Water Assessment Tool (SWAT). Data from one USGS gauging station were used to calibrate and validate the model, and six downscaled and bias-corrected CMIP5 climate models were selected based on their predictive accuracy over the eastern United States and their representativeness of a broad range of future climates. Predictions corresponding to up to four RCP scenarios were used for each climate model. The SWAT model was run using: 1) precipitation and temperature time series hindcasts of 1965–2015 from each climate model and 2) precipitation and temperature predicted by each climate model x RCP scenario combination for the future period 2016–2099. For each climate model and RCP scenario, annual streamflow and load values averaged over 2080–2090 at the watershed outlet were compared to values averaged over 1970–1989.

Pyke et al. (2011) simulated changes in annual runoff and constituent loads under five precipitation-change scenarios and three hypothetical land use scenarios designed for the redevelopment of a former military base near Boston, MA. Of the three land use scenarios (one representative of low-intensity suburban development, one representative of a mixed-use configuration and one representative of an undeveloped site), only results from the first two scenarios were considered in this review, because the third scenario was more representative of natural rather than developed land. Precipitation scenarios were developed using an observed historical time series (1996–2005) of daily precipitation from a local NOAA weather station. Specifically, five hypothetical future change scenarios were obtained by applying the delta change factor approach. Of the five precipitation change scenarios presented in the manuscript, only three were retained in this review because the other two did not entail a change in precipitation volume but rather only a change in the distribution of precipitation across events with different magnitudes. The three scenarios retained here corresponded to a 20% increase in rainfall volume, a 20% decrease in rainfall volume and a 3% increase in rainfall volume distributed unevenly across rainfall events that ultimately resulted in a 10% increase in the proportion of annual precipitation occurring in the 5% largest events. Potential future changes in temperature were not considered during simulations, which were performed with EPA`s Smart Growth Water Assessment Tool for Estimating Runoff (SG WATER). SG WATER is a simplified stormwater modeling tool designed to provide coarse exploratory information on possible impacts of development scenarios on runoff quantity and quality. It is important to note that, as the authors of the study indicate, "*SG WATER is not calibrated or validated against observed stormwater runoff values, and it is therefore appropriate only for evaluating relative changes resulting from different scenarios and not for providing absolute, quantitative predictions or comparing to simulations from other hydrologic models*".

The work by Munson et al. (2018) differs substantially from the studies mentioned above in that it uses a data-driven approach to estimate the sensitivity of TP loads from an urban stream to changes in a set of variables, including temperature and precipitation. Rather than simulating projected changes in climate variables, the authors used a multivariate regression approach to

model the "elasticity" of historical (2007–2014) monthly TP loads estimated at a USGS gauging station to simultaneous changes in observed monthly precipitation, temperature, streamflow and number of CSO events. Elasticity is defined in the manuscript as the relative change in loads divided by the relative change in each of the predictors that are simultaneously included in the regression model. The work was conducted in the Alewife Brook, a heavily urbanized watershed near Boston, MA. As the authors of the study recognize, this approach has some obvious limitations, including the lack of incorporation of potentially important explanatory variables in the empirical model, such as changes in land use or population growth, or the level of correlation among predictors that makes the separation of their individual effects challenging.

Tong et al. (2006) used EPA`s Better Assessment Science Integrating Point and Nonpoint Sources (BASINS) model to estimate climate-driven changes in runoff quantity and quality in the Lower Great Miami River Basin in southwest Ohio. Although the watershed is predominantly agricultural, results specific to urban land use areas are provided in the manuscript. The watershed model was calibrated over the period 1975–1984 and validated over the period 1985–1994 using data from a USGS gauging station. Observed precipitation and temperature time series were modified to simulate four different future scenarios using delta change factors based on projected climate-related changes from two GCMs (IPCC and UK Hadley Centre`s climate model). The manuscript provides percent changes in TP loads associated with select percent changes in precipitation but does not provide the corresponding percent changes in flow.

Fischbach et al. (2015) used the Chesapeake Bay Phase 5.3.2 watershed model to simulate the impact of different future climate scenarios on streamflow and TP loads from urban land uses within the Patuxent River watershed. The watershed model was run using 1) observed historical (1984–2005) precipitation and air temperature data and 2) downscaled temperature and precipitation projections from six IPCC GCMs, three emission scenarios and two future time periods (2035–2045 and 2055–2065), thereby resulting in a total of 36 climate-altered hydrology projections. Authors of the study kindly provided average annual streamflow and TP load data estimated for the observed historical period and the 36 climate scenarios.

For each study, average flow and TP load estimated under climate change conditions were expressed as percentage change from their corresponding historical baselines. Percentage changes in TP load across all studies were then regressed against percentage changes in flow (Figure 4-5). A hierarchical modeling approach was used, where the regression slope and intercept were assumed to derive from a common hyperdistribution and were allowed to vary across studies, thereby accounting for intra-class correlation arising because observations within each study are not independent.

Although only a limited number of studies were found, they span a relatively broad range in terms of size of the study area, land use characteristics and level of complexity of the modeling approach adopted (Table 4-2). Despite this large inter-study variability, all studies appear to

indicate that a linear relationship exists between climate-driven changes in flow and corresponding changes in TP load, with a 1% change in flow corresponding to an approximately 1% change in TP load when averaging across studies (Figure 4-5).

Table 4-2: Main characteristics of the studies used to assess the impact of climate change-driven changes in hydrology on TP loads from developed land uses. The column "Model" provides the modeling tool used either to simulate TP loads in the study area or to analyze observed load data. The column "Climate simulation approach" reports the method adopted to simulate expected changes in climate variables (Delta change factor: one or more multipliers were applied to historical time series of climate variables to generate modified time series that represent expected future changes; GCM: hourly or daily precipitation and temperature data predicted by one or more GCMs were directly used as input to a watershed model to generate loads expected under future climate scenarios). The column "T change" provides the range of projected temperature increases/decreases that were considered in each study.

| Reference	Site	Area (km²)	Land use	Model	Climate simulation approach	T change
Pyke et al., 2011	Naval Air Station, MA	5.7	Built environment with 64-71% open space	SG WATER	Delta change factor	Not assessed
Easton et al., 2017	Difficult Run watershed, VA	150	57% urban development; 8% commercial/industrial; 11% transportation; 24% open space	SWMM	GCM	-1.2/+4.1 °C
Munson et al., 2015	Alewife Brook watershed, MA	22	61% residential; 11% commercial; 11% open land; 17% other	Multiple regression	Analysis of historical climate variability	+1/+5%
Tong et al., 2006	Lower Great Miami watershed, OH	3600	71% agricultural; 17% forest; 12% urban	BASINS	Delta change factor	+2/+4 °C
Xiang, 2017	Wilde Lake watershed, MD	4.9	Fully built out, 32% impervious	SWAT	GCM	-0.2/+7.2 °C
Fischbach et al., 2015	Patuxent River watershed, MD	2479	22% developed; 18% agricultural; 9% grassland; 50% forest	CBP 5.3.2	GCM	+0.7/+2.8 °C
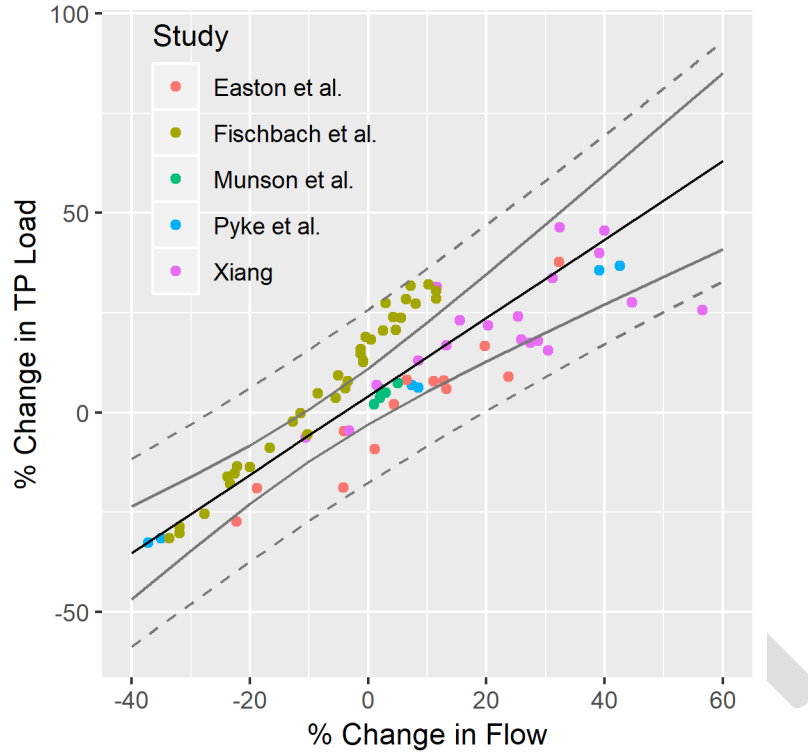
*Figure 4-5: Relationship between % Change in TP Load and % Change in Flow across a set of independent studies. The black line is the average (population-level) fitted line resulting from a hierarchical linear regression where intercept and slope are allowed to vary across studies. The grey lines represent 95% confidence (solid) and prediction (dashed) intervals. Note that results from Tong et al. are not included in this regression because that study reported % changes in rainfall but not % changes in flow. The equation of the population-level regression is: %TP = 4.07 + 0.98 * %FLOW, and the standard errors associated with the intercept and slope estimates are 3.59 and 0.16, respectively.*

4.5.3   Soil P history

Soil phosphorus levels are a primary determinant of phosphorus load. Soil P levels, in turn, are affected by the amount of P runoff. For climate scenarios with increasing P runoff, the levels in the soil will decrease, causing a small negative feedback. The model of changes in soil P levels relative to runoff is an additive model with the coefficients contained in Table 4-3

Table 4-3: Coefficients in the recursive equation for soil P prediction over time

Factor	unit	Coefficient
Solid Manure	pound/acre/year TP	0.151
Liquid Manure	pound/acre/year TP	0.154
Fertilizer	pound/acre/year TP	0.0559
Biosolids	pound/acre/year TP	0.00463
Uptake	pound/acre/year TP	-0.159
Sediment Loss	ton/acre/year	-0.208
Runoff	inches/year	-0.0355

Factor	unit	Coefficient	
Percent Incorporation	percent		0.0479
Percent Mixing	percent		-0.0508
Depth of Incorporation	inches		0.183
Precipitation	inches/year		-0.00152
Clay percent	percent	Clay > 15: Else:	0.160 0.000
Organic Matter	percent	Clay >15: Else:	-0.549 0.000
Local Adjustment	ppm Mechlich 3		Varies

4.6   BMP effectiveness change

MWG Review: Section 4.6 does not require review for July.

To be added by October. The CBP's climate resiliency workgroup and management board have recognized the difficulty in estimating the effects of climate change on BMPs in the near term and it is unlikely that the climate change modeling for 2019 will include this factor.

4.7   Landscape processing effects

4.7.1   Changes in speciation

To be added by October

4.7.2   Land and stream delivery changes

To be added by October

4.7.3   Groundwater Lag

MWG Review: Requires review for July, asking for approval to not consider groundwater lag effect in climate change scenarios.

Groundwater lag times are an important part of the Phase 6 dynamic simulation model but are not simulated in the Phase 6 CAST. CBP management scenarios are run without lag time and are meant to represent the long-term loading based on a static set of management practices. Lag scenarios in the dynamic model are only used for calibration and for specific lag time studies. Given that the CBP 2019-2021 climate assessment is using the CBP management scenarios methodology that excludes lag time, the change in lag time due to climate change will be ignored for the 2019 assessment.

However, some discussion of the potential effects of lag time is helpful if the CBP would like to consider lag scenarios or the effects on calibration. Groundwater systems are expected to be

impacted by climate change. Studies, summarized in Lall, et al. 2018, have found that climate change will have an effect on human uses of groundwater and also on the timing and amount of recharge. Konikow, 2015, in a nationwide study, found long-term depletion in the coastal plain of the Chesapeake region.

The equation found in figure 10-30 of the CAST documentation (CBP 2017) (reproduced here as Figure 4-6, left panel) establishes a relationship between groundwater age and the ratio of water table depth and recharge based on a MODFLOW model of the Potomac. The relationship was used to estimate groundwater age for all non-coastal plain segments the in the Chesapeake Bay watershed in the Phase 6 dynamic model. Using the equation from figure XXX, it is be possible to estimate the change in groundwater age from a climate-change induced change in recharge rate. Figure 4-6, right panel shows the changes in groundwater age based on a 1 inch per year recharge increase.

Figure 4-6: Left panel: Groundwater age as a function of the ration between water table depth and recharge rate [Adapted from Sanford (2015)]. Right Panel: change in groundwater age from a 1 inch per year increase in recharge based on the relationship in the left panel
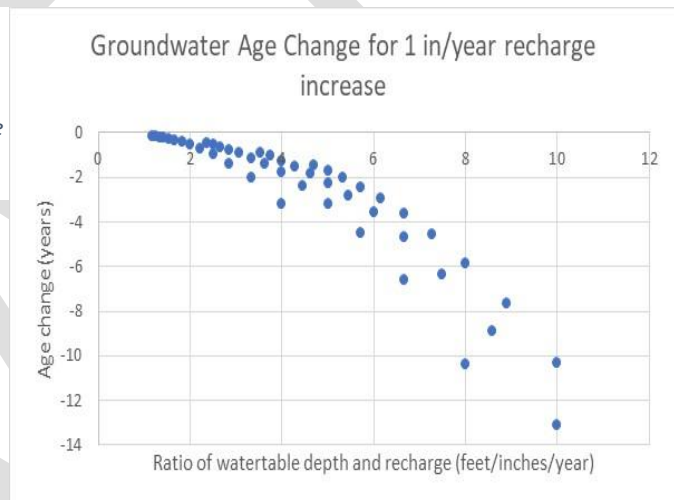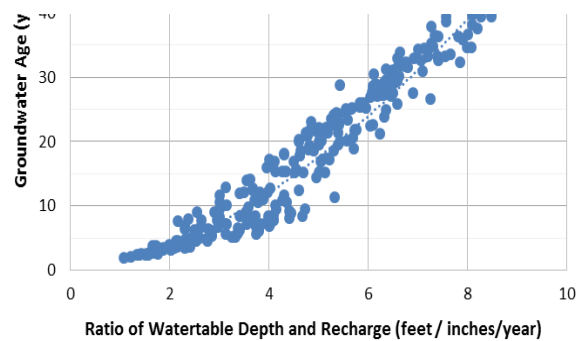
In the coastal plain, figure 10-32 of the CAST documentation (reproduced here as Figure 4-7) found that recharge was a minor portion of the second principle component rather than a major influence. The weights for the 4 most important PCs are shown. Lithological, physiographic, and geological attributes are the main determinant of groundwater age in the Chesapeake Coastal Plain above recharge rate.
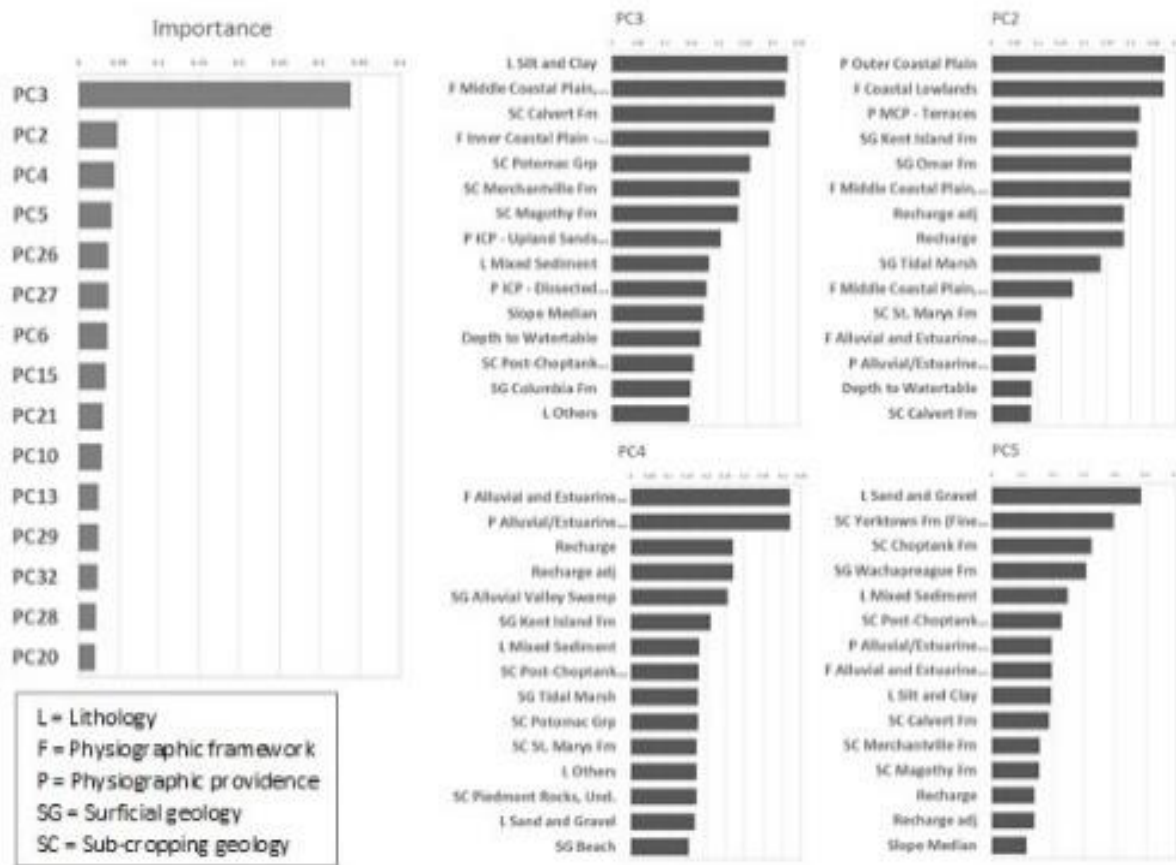
Figure 4-7: Left: Importance of the Principle components (PCs) in the statistical model for explaining the groundwater age in the Chesapeake Coastal Plain. Right: The weights of the watershed attributes in the principle components.

Both of these analyses were aimed at estimating the spatial variability of groundwater lag times and are not necessarily representative of change in lag over time as climate changes. The lack of consistency between the two approaches also causes some concern given that application of the methods may lead to a smaller change in the non-coastal plain regions based on the analysis method rather than real differences that may exist.

4.8   Climate Scenario Model Results

MWG Review: Does not requires review for July. Members and interested parties are welcome to review Section 4.8, however, these results will change with adjustments made before October.

The Phase 6 Watershed Model was used for assessing the impact of climate change on the delivery of flow, nutrients, and sediment. In this assessment, Watershed Implementation Plan Phase 2 (WIP2) Level of Effort scenario was used as the reference scenario for quantifying the impacts of climate change. The estimated change in delivery presented in this section represent anticipated change in watershed response between the 1991-2000 climatology and a future year. Therefore, in reference to 1991-2000, specific scenarios consist of climatic change over a 30-year period for the 2025 scenario and 55 years for the 2050 scenario.

Table 4-4: List of climate change scenarios run and corresponding inputs.

Year	No.	Scenario description	Rainfall	Volume to Intensity	Temperature	CO2
Year 2025	01	Rainfall sensitivity scenario	Extrapolation of 88-year historic trend	Equally between intensity deciles	N/A	N/A
	02	Rainfall sensitivity scenario	Extrapolation of 88-year historic trend	Based on observed trends	N/A	N/A
	03	Temperature sensitivity scenario	N/A	N/A	RCP 4.5 31-member ensemble median (P50)	N/A
	04	CO2 level sensitivity scenario	N/A	N/A	N/A	Change from 363 to 427 ppm
	05	Integrated scenario	Extrapolation of 88-year historic trend	Based on observed trends	RCP 4.5 31-member ensemble median (P50)	Change from 363 to 427 ppm
	06	Integrated scenario	Extrapolation of 88-year historic trend	Based on observed trends	RCP 4.5 31-member ensemble median (P50) – *Hamon Method*	Change from 363 to 427 ppm
	07	Integrated scenario uncertainty	Extrapolation of 88-year historic trend	Based on observed trends	RCP 4.5 10 percentile bound of 31-member ensemble (P10)	Change from 363 to 427 ppm
	08	Integrated scenario uncertainty	Extrapolation of 88-year historic trend	Based on observed trends	RCP 4.5 90 percentile bound of 31-member ensemble (P90)	Change from 363 to 427 ppm
Year 2050	09	Rainfall sensitivity scenario	31-member ensemble median (P50) of RCP 4.5	Equally between intensity deciles	N/A	N/A
	10	Rainfall sensitivity scenario	RCP 4.5 31-member ensemble median (P50)	Based on observed trends	N/A	N/A
	11	Temperature sensitivity scenario	N/A	N/A	RCP 4.5 31-member ensemble median (P50)	N/A
	12	CO2 level sensitivity scenario	N/A	N/A	N/A	Change from 363 to 487 ppm
	13	Integrated scenario	RCP 4.5 31-member	Based on observed trends	RCP 4.5 31-member ensemble median (P50)	Change from 363 to 427 ppm

		ensemble median (P50)			
14	Integrated scenario	RCP 4.5 31-member ensemble median (P50)	Based on observed trends	RCP 4.5 31-member ensemble median (P50) – *Hamon Method*	Change from 363 to 427 ppm
15	Integrated scenario uncertainty	RCP 4.5 10 percentile bound of 31-member ensemble (P10)	Based on observed trends	RCP 4.5 10 percentile bound of 31-member ensemble (P10)	Change from 363 to 427 ppm
16	Integrated scenario uncertainty	RCP 4.5 90 percentile bound of 31-member ensemble (P10)	Based on observed trends	RCP 4.5 90 percentile bound of 31-member ensemble (P10)	Change from 363 to 427 ppm

4.8.1   Effect of rainfall intensity

As described in Section 2.1.5, two different approaches for the changes in rainfall intensity were evaluated in this assessment. In the first approach, the increase in rainfall volume was equally divided amongst the intensity deciles. Whereas in the second approach a large portion of increase was preferentially applied to the rainfall events in the highest decile. For the preferential approach, the proportion for dividing rainfall volume into the intensity deciles were based on Groisman et al. (2004) as shown in the Figure 2-7 that uses observed rainfall data for assessing the change. The latter will result in larger increase in intensity for the higher intensity events. Figure 4-8 shows the simulated changes flow, nitrogen, phosphorus and sediment deliveries. The results for both 2025 and 2050 are shown. As anticipated, for the same change in rainfall volume the simulated flow was slightly higher for the preferential approach, where rainfall volume was divided based on observed intensity trends. Although the differences in simulated flow are almost similar, the resulting changes in nitrogen, phosphorus, and sediment are significant. That response is due to higher delivery of particulate matter with higher intensity events. For the rest of the assessment the approach of increasing rainfall the most in the highest deciles for dividing rainfall volume into rainfall events was used because it is based on observations. It was also corroborated by the analysis of some of the daily climate projection dataset obtained using Bias Correction Constructed Analogues for the Chesapeake Bay region.
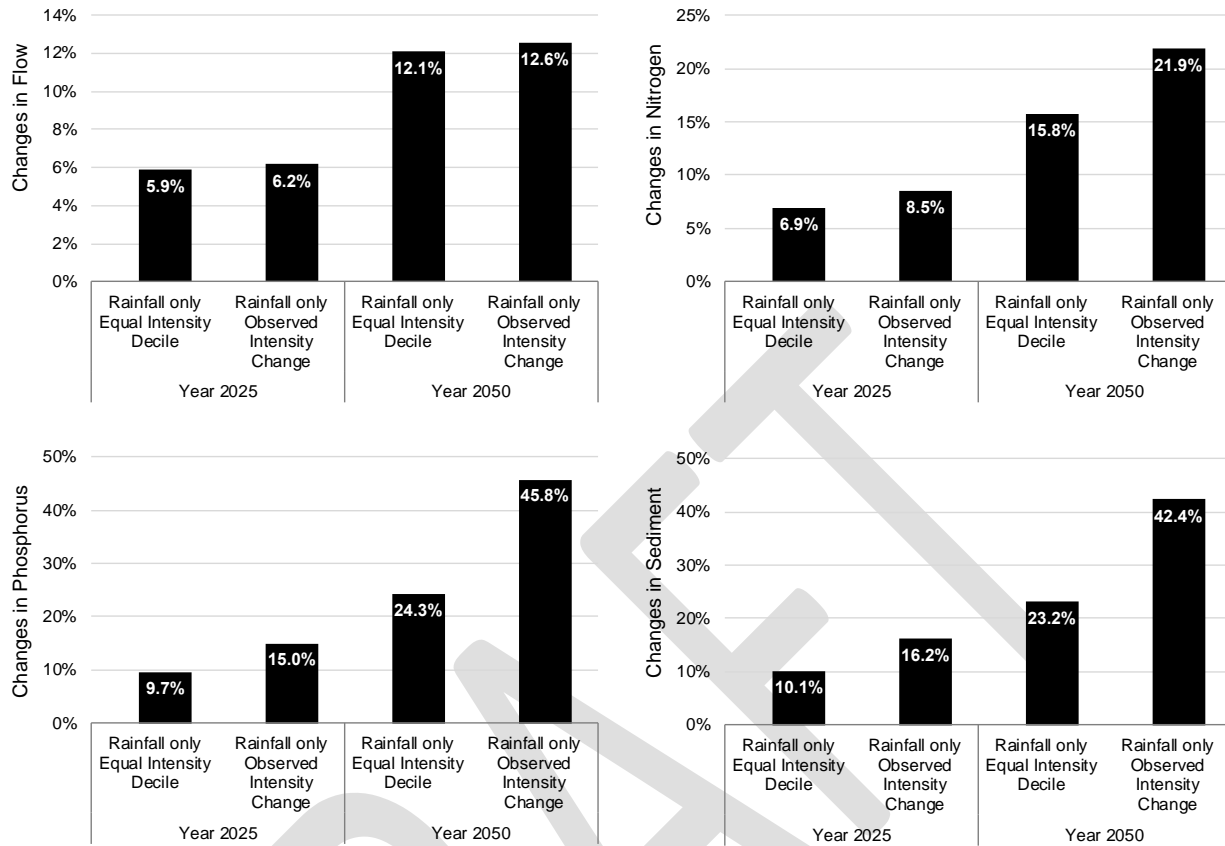
Figure 4-8: Changes in flow, nitrogen, phosphorus, and sediment are shown for the two different methods applied to projected changes in rainfall volume for the year 2025 and 2050.

4.8.2   Climate Change Sensitivity Scenarios

The impact of three climate change drivers incorporated in this climate change assessment were separately analyzed as sensitivity scenarios. The objective of these sensitivity scenarios was to develop better understanding of the watershed response by quantify the relative impact of these climatic drivers on the simulated changes flow, nutrients, and sediment transport. Changes in the delivery of flow, nitrogen, phosphorus, and sediment to the Chesapeake Bay are shown in the Figure 4-9. The results show that for both year 2025 and 2050 the changes in rainfall was the major driver of changes resulting in increased delivery of nutrients and sediment. Temperature and corresponding potential evapotranspiration resulted in a decreased delivery of loads as anticipated and were a close second in terms of impact. The impact of elevated CO_2 levels was relatively minor increases in delivery.
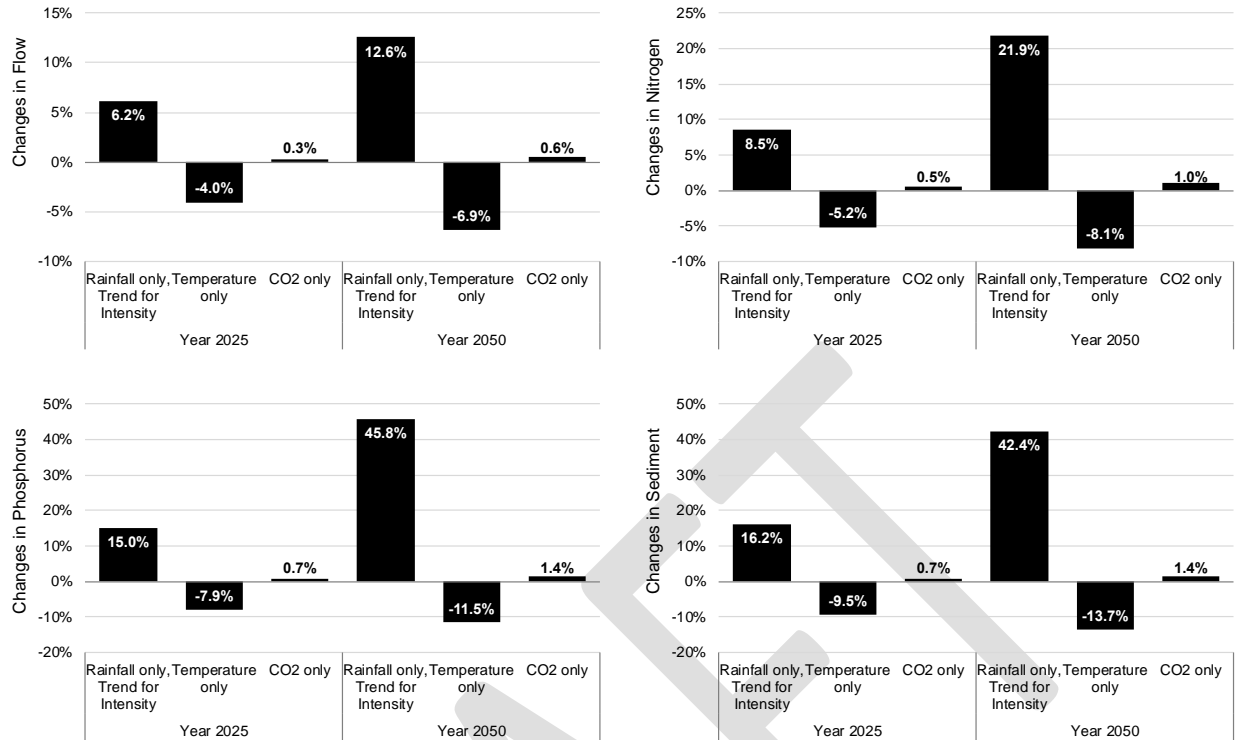
Figure 4-9: Relative impact of projected changes in rainfall, temperature, and CO2 levels were analyzed for the year 2025 and 2050. The changes in the delivery of flow, nutrients, and sediment are shown.

4.8.3   Integrated 2025 and 2050 Scenarios

With the integrated climate change scenarios, the combined impact of rainfall, temperature, and CO2 level were simulated. The integrated scenarios for 2025 and 2050 resulted in increased delivery of flow, nitrogen, phosphorus, and sediment. That is consistent with responses seen for both 2025 and 2050 climate change sensitivity scenarios in the previous section, where the rainfall change dominated the watershed response as compared to changes in temperature and CO2 level. For year 2025, delivery of flow increased by 2.3 percent, nitrogen by 2.4 percent, phosphorus by 3.1 percent, and sediment by 3.3 percent (Figure 4-10). For year 2050, delivery of flow increased by 6.0 percent, nitrogen by 8.3 percent, phosphorus by 15.3 percent, and sediment by 16.2 percent (Figure 4-10).
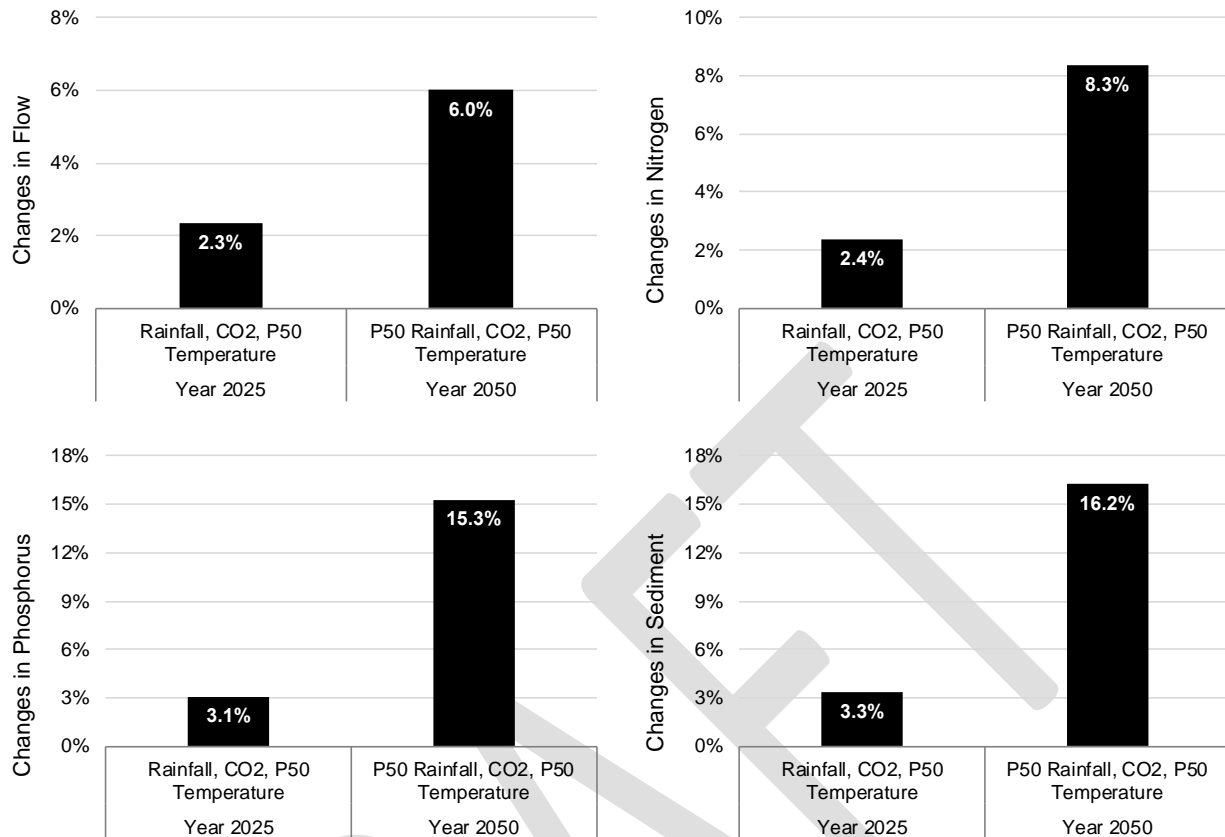
Figure 4-10: Simulated changes in the delivery of flow, nutrients, and sediment to the Chesapeake Bay for year 2025 and 2050 climate change scenarios are shown. For year 2025, rainfall projection from 88-year trends analysis, and temperature using RCP 4.5 31-member ensemble median were used. For year 2050, both rainfall and temperature using RCP 4.5 31-member ensemble median were used.

4.8.4   Changes for the Major Basins

Figure 4-11 shows simulated responses for the major river basins in the watershed. It was shown in the previous section that the increase in watershed delivery for flow, nutrients, and sediment for 2050 was higher than 2025. That behavior is also seen in the simulated responses for the major basins. However, it is noted the model simulation reveal some interesting behavioral differences in the river basin response. For example, the James River basin (JAM) had the lowest percent increase in flow in the 2025 climate changes assessment, but for 2050 it has the largest percent increase in flow. Similarly, percent increase in nitrogen delivery was lowest for James (JAM) in 2025, but it has 3rd largest percent increase for 2050. Similar behavior is seen in phosphorus and sediment response. Such responses are the result of interplay between estimated changes in rainfall (volume and intensity) and temperature that are simulated by the watershed model. For example, James River basin had some of the smallest increases in rainfall volume for 2025, but for 2050 it had higher increases in rainfall as compared to rest of the watershed. Temperature increase on the other hand was higher for

2050 but had pretty much same spatial distribution. As a result, large increase rainfall volume for 2050 in James resulted in a net increase in flow.
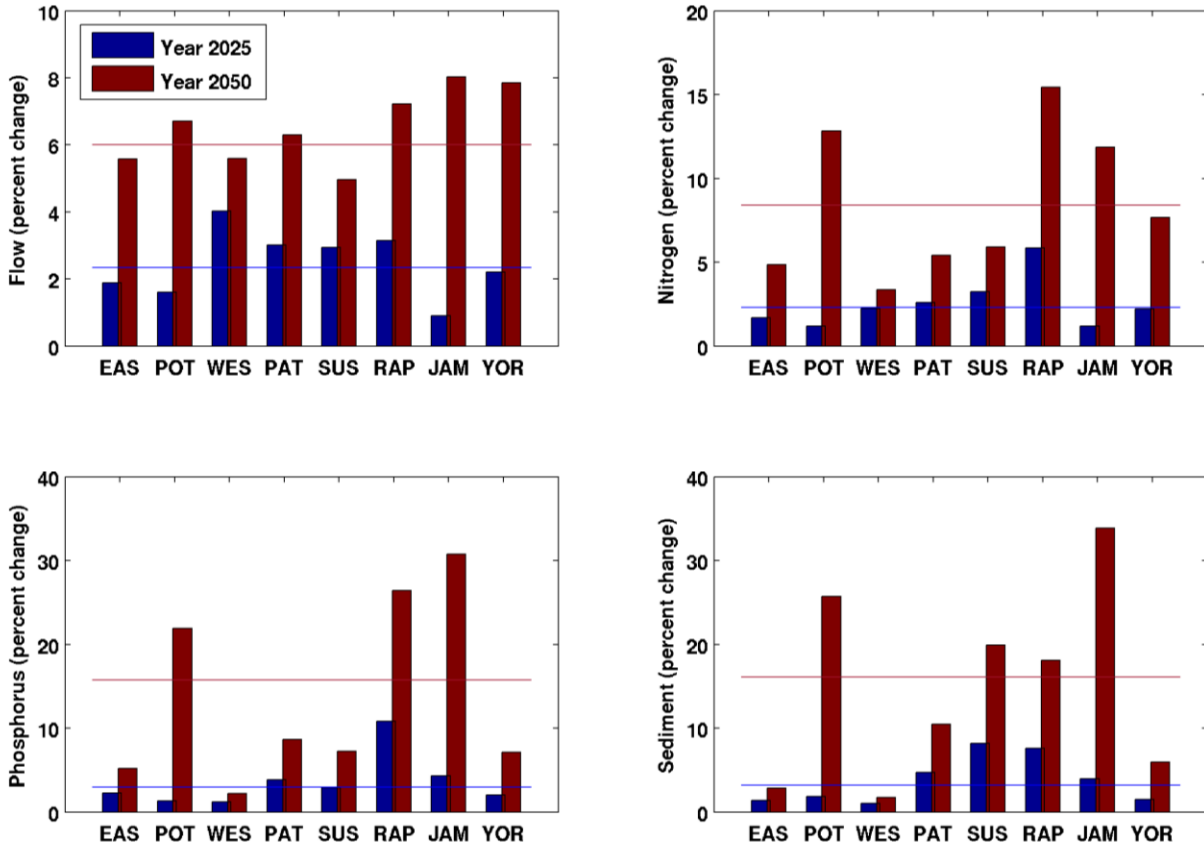

Figure 4-11: Average annual change in flow, nitrogen, phosphorus, and sediment for the major river basins – Eastern Shore (EAS), Potomac (POT), Western Shore (WES), Patuxent (PAT), Susquehanna (SUS), Rappahannock (RAP), James (JAM), York (YOR) are shown. The lines show the change for the entire watershed.

4.8.5   Seasonal Changes for the Watershed
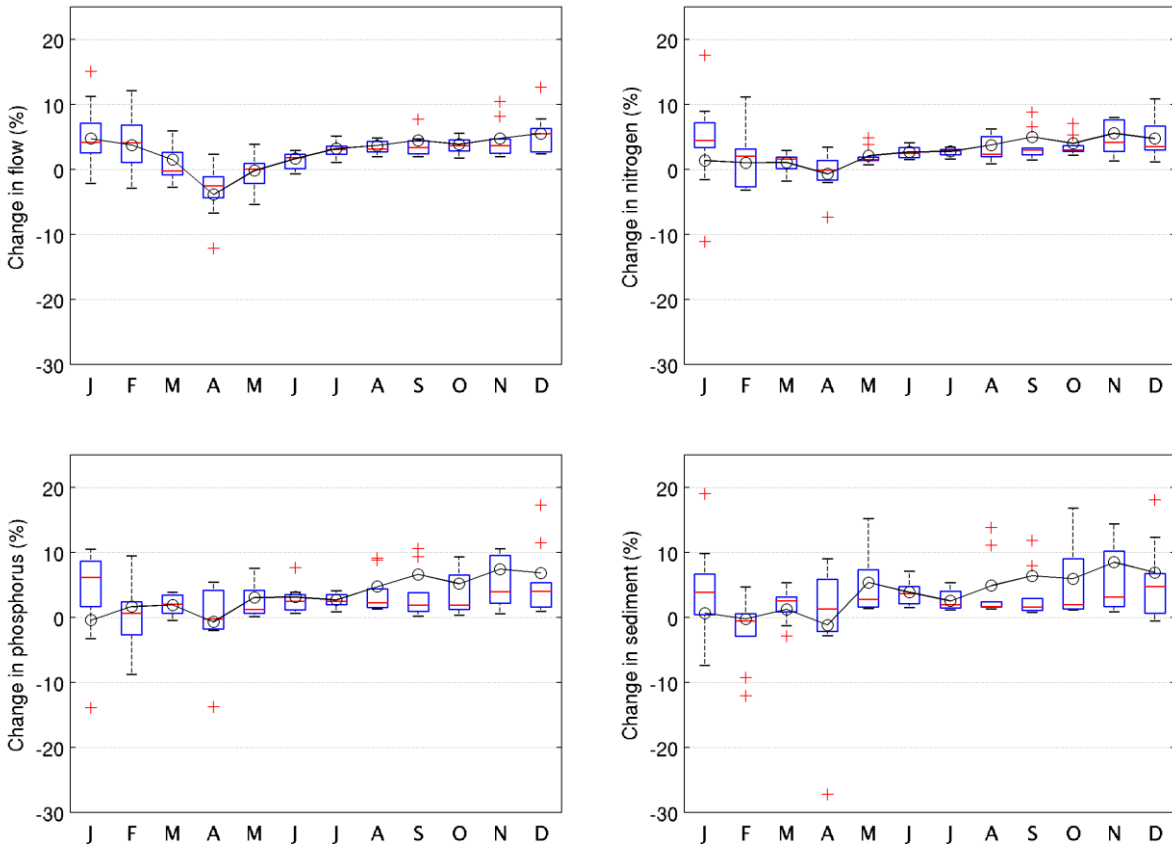
Figure 4-12: Simulated changes in flow, nutrients, and sediment are shown for year 2025 are shown. Box and whiskers show interannual variability, whereas the solid lines show average annual change.
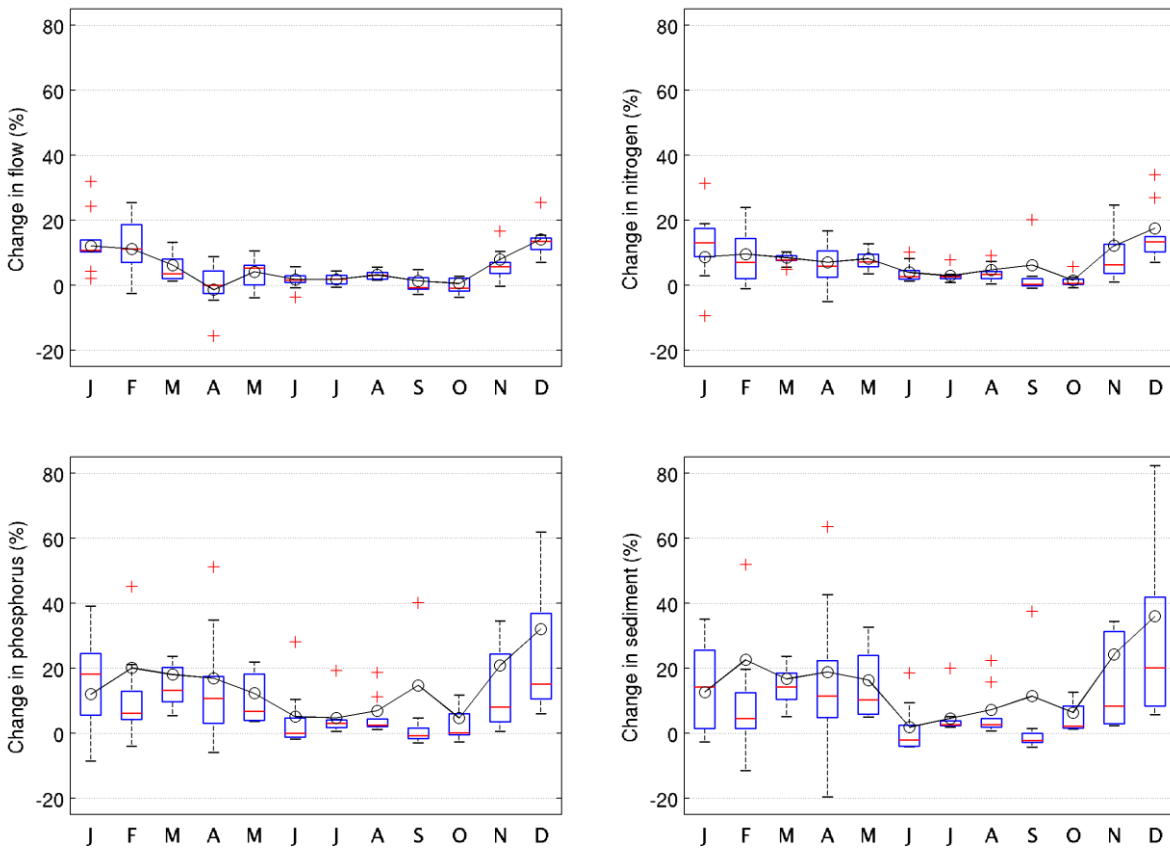
Figure 4-13: Simulated changes in flow, nutrients, and sediment are shown for year 2050 are shown. Box and whiskers show interannual variability, whereas the solid lines show average annual change.

4.8.6   Uncertainty Quantification

There are a number of uncertainties involved in the assessment of climate change impacts on hydrology and water quality. Some of those are (a) uncertainties in the global circulation models, (b) assumptions for the initial conditions in the GCMs and well documented issues of "model drift", (c) the downscaling methods for climate projections, (d) the time-disaggregation of monthly projections to daily or hourly time-steps for use with the watershed model simulation, (e) the methods for the estimation of potential evapotranspiration, and (f) the parameter uncertainty of the watershed model calibration. The technical aspects of the implementations are based on the recommendations of the Chesapeake Bay Program's Modeling workgroup, the Climate Resiliency Workgroup, and the Scientific and Technical Advisory Committee workshop (Johnson et al., 2016).

The uncertainties arising from the climate change inputs used in the assessment were investigated. The 31 downscaled projections for a given period often have differences in the future projections. In the

ensemble analysis, all of the models and the corresponding downscaled data were given same weight, equivalent to an assumption of equal likelihood for any one of them to represent the likely future. The central tendency of the samples was characterized using the ensemble-median values of the dataset. To quantify the uncertainty 10th percentile and 90th percentile bounds of the projections were used.

The setup for uncertainty assessments for 2025 and 2050 were made slightly differently. For year 2025, since the projections for the rainfall was derived from the extrapolation of the long-term observations, only uncertainties due to temperature projections were assessed. For year 2050 scenario, uncertainties in both rainfall and temperature projections were used. And in this case, there are several possible ways the combination of rainfall and temperature can be used in the uncertainty assessment. The combinations for projected changes as "high precipitation – high temperature" and "low precipitation – low temperature" were selected to capture a conservative range for the uncertainty. It is acknowledged that this combination does not capture full range of possible impacts.

As shown in Table 4-5 the range of uncertainties around the 2025 are narrower than 2050. The wider uncertainty for the year 2050 is due to higher variability in the rainfall projections (Figure 4-14), as compared to 2025 where only variability in temperature projections were considered. The 2025 uncertainty assessment suggests change over average 10 year can be anywhere for – flow between no change to 4.8percent increase, nitrogen between 0.6 percent decrease to 6.9 percent increase, phosphorus between 1.6 percent decrease and 11.6 increase, and sediment between 1.8 percent decrease and 13.1 percent increase. The 2050 uncertainty assessment suggests change over average 10 year can be anywhere for – flow between no change to 4.8 percent increase, nitrogen between 0.6 percent decrease to 6.9 percent increase, phosphorus between 1.6 percent decrease and 11.6 increase, and sediment between 1.8 percent decrease and 13.1 percent increase.

Table 4-5: Uncertainty estimates for the climate change scenarios for the year 2025 and 2050. Change shown are difference in average annual delivery over the 10-year period.
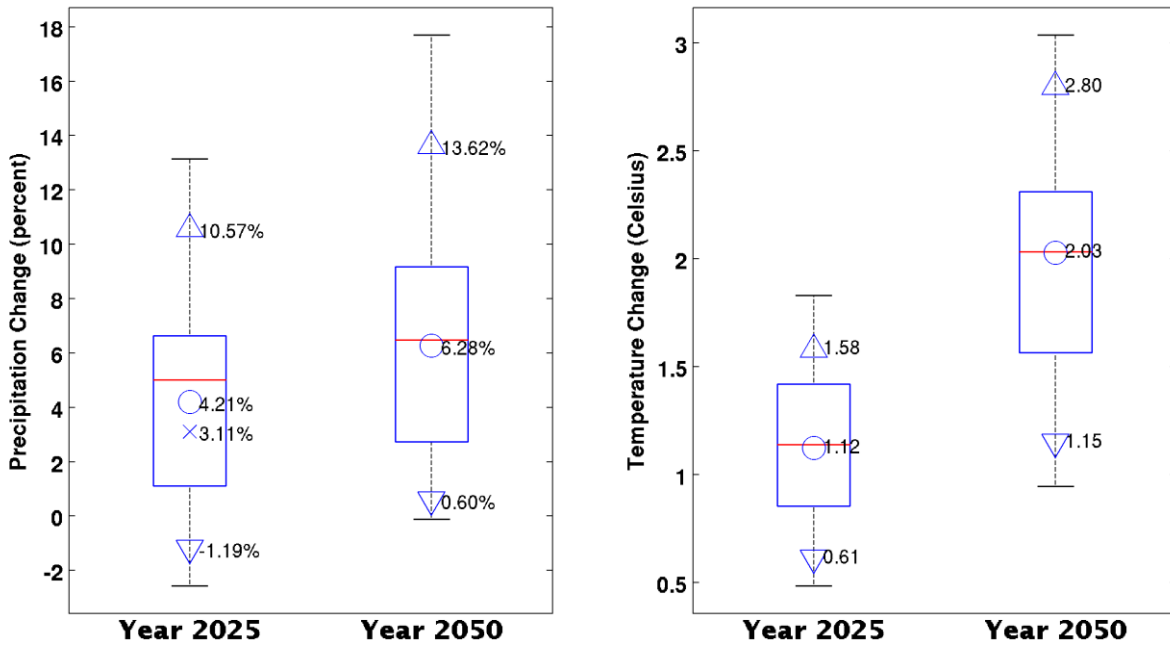
Figure 4-14: Summary of annual RCP4.5 annual rainfall and temperature change for the Chesapeake Bay watershed are shown. Then range for 10th percentile (P10), ensemble median (P50), and 90th percentile (P90) are shown. The estimated change in rainfall volume based on the extrapolation of long-term trends are also shown (with marker symbol x).

The method used for estimating the potential evapotranspiration is an important source of uncertainty. In this assessment two methods were included for quantifying its impact on the delivery of flow, nutrients and sediment. As discussed earlier, for the same delta increase in temperature, Hamon methods estimates higher changes in potential evapotranspiration as compared to Hargreaves Samani. As anticipated higher increase in potential evapotranspiration results in relatively drier conditions and lower delivery of flow and sediment (Figure 4-15).
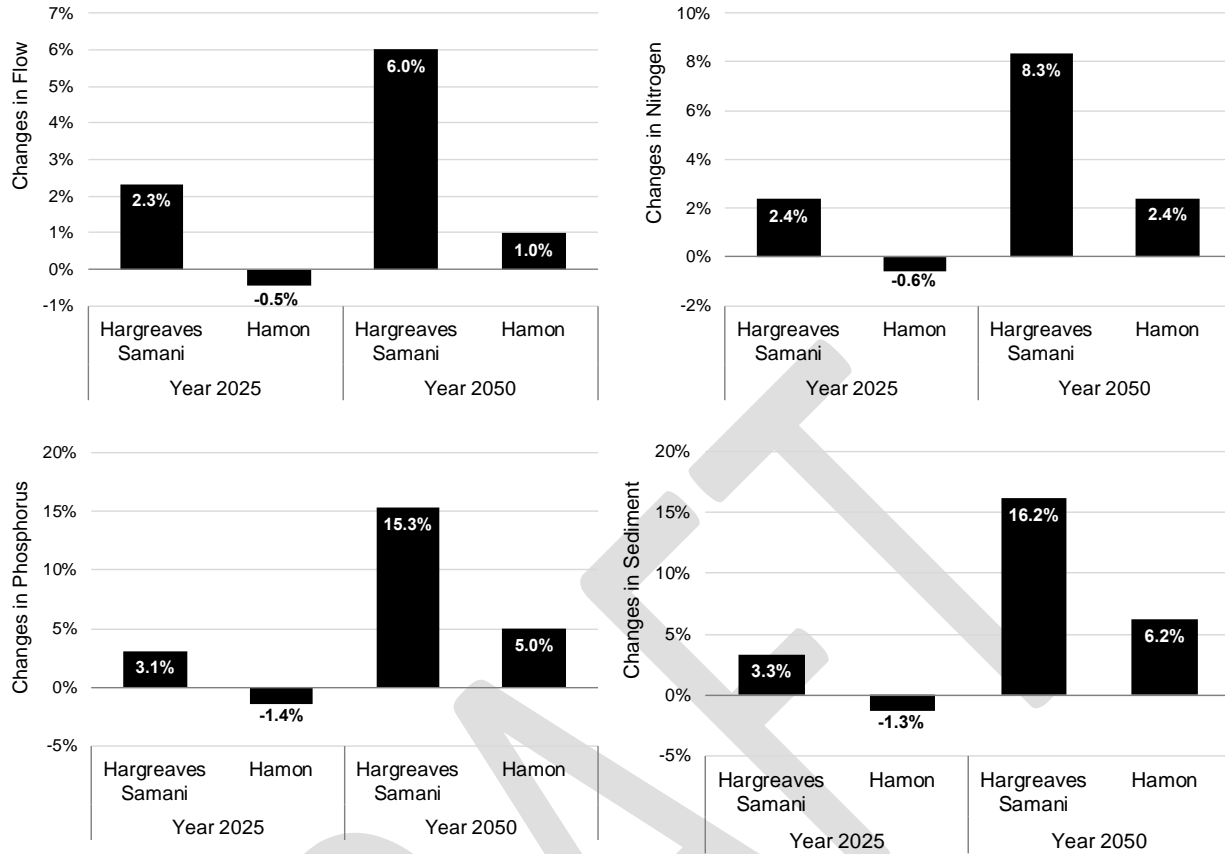
Figure 4-15: Uncertainty due to selection method for estimating potential evapotranspiration for 2025 and 2050 are shown. The uncertainties get higher with increase in temperature.

5   Estuarine Water Quality and Sediment Transport Model Results

MWG Review: Certain subsections of section 5 require review as marked

The guidance for increasing levels of regional sea level rise based upon global tide gauge rates and regional land subsidence rates came from the CRWG. Specifically, the CRWG recommended that sea level rise projections for 2025 be based on long term observations at Sewells Point, VA (0.17 m) and that a range be used for 2050 (0.3 - 0.8 m) be applied in the WQSTM. The approximate median of the 2050 range (0.5 m) was used for initial simulations. Temperatures for riverine inflow were provided by the Watershed Model. Air temperatures were consistent with the Watershed Model for each scenario. Changes in temperatures for the open boundary at the Bay mouth were estimated as a function to changes in air temperature. … Tidal wetland loss was estimated by the GIS analysis of data from Sea Level Affecting Marshes Model (SLAMM).

5.1   Inputs

5.1.1   Wetland losses and gains

To be added by October

5.1.2   Wind effects

MWG Review: Requires review for July, asking for approval to not consider wind effects in climate change scenarios.

The effects of wind on DO aeration and distribution in the Chesapeake Bay are a result of both wind attributes and Bay properties. Variations in wind can alter vertical mixing as well as both along-channel and cross-channel circulation (Scully et al., 2005). Changes not only in wind speed but also in wind direction can modify DO, and these two attributes have the potential to modify DO in different ways (Scully, 2010). It has also been found, through a series of simulations using previous versions of the CBP partnership's WQSTM, that the bathymetry of the Bay plays a significant role in modulating the effect of wind on DO concentration (Wang et al., 2016a). Given the complexity and variability of the Bay's geometry, the potential effects of wind will differ from segment to segment as a function of the local geometry.

Wind speed is the primary metric for wind to influence mixing, circulation and ultimately DO in the Bay. Regardless of which direction it is blowing and how favorable the bathymetry is towards contributing to the wind effect, a slow wind speed, e.g. a few centimeters per second, cannot have a significant effect on the physics and biogeochemistry of the Bay. Wang et al. (2016b) reported sensitivity analyses of hypoxic volume to changes in wind speed and found that anoxic volume (DO < 0.2 mg/l) has a very minor response to wind forcing of 2 meters per second for 2 days (Figure 5-1). Only wind speeds greater than 4 meters per second have substantial influence on DO in the bottom of the Bay. Note that wind events of 2 days duration are relatively rare, and shorter wind durations will have less impact on the Bay.
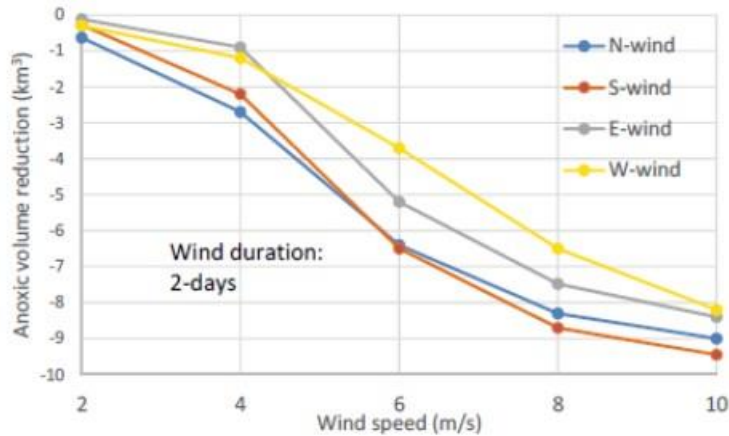
Figure 5-1: Peak anoxia volume reduction in the mainstem Bay, from a no-wind condition to 2-days duration of wind, from the four cardinal directions and at five speeds.

Maria Herrmann of Penn State University has assessed wind speeds under future modeled climate change conditions within the framework of the Chesapeake Hypoxia Analysis and Modeling Program (CHAMP). To generate projections at the Bay scale, the analysis used the downscaling method of MACA, Multivariate Adaptive Constructed Analogs, which is a statistical method for downscaling Global Climate Model (GCM) simulation results from their native coarse resolution to a higher spatial resolution. Twenty GCMs were included in the downscaling

analysis, including 2 from the NOAA Geophysical Fluid Dynamics Laboratory and 1 from the USA National Center for Atmospheric Research (Table 5-1).

Table 5-1: Global Climate Models (GCMs) included in the downscaling analysis of wind speed in Chesapeake Bay (Maria Herrmann, personal communication, April 16, 2019).

Model Name	Model Country	Model Agency	Atmosphere Resolution(Lon x Lat)	Ensemble Used
bcc-csm1-1	China	Beijing Climate Center, China Meteorological Administration	2.8 deg x 2.8 deg	r1i1p1
bcc-csm1-1-m	China	Beijing Climate Center, China Meteorological Administration	1.12 deg x 1.12 deg	r1i1p1
BNU-ESM	China	College of Global Change and Earth System Science, Beijing Normal University, China	2.8 deg x 2.8 deg	r1i1p1
CanESM2	Canada	Canadian Centre for Climate Modeling and Analysis	2.8 deg x 2.8 deg	r1i1p1
CCSM4	USA	National Center of Atmospheric Research, USA	1.25 deg x 0.94 deg	r6i1p1
CNRM-CM5	France	National Centre of Meteorological Research, France	1.4 deg x 1.4 deg	r1i1p1
CSIRO-Mk3-6-0	Australia	Commonwealth Scientific and Industrial Research Organization/Queensland Climate Change Centre of Excellence, Australia	1.8 deg x 1.8 deg	r1i1p1
GFDL-ESM2M	USA	NOAA Geophysical Fluid Dynamics Laboratory, USA	2.5 deg x 2.0 deg	r1i1p1
GFDL-ESM2G	USA	NOAA Geophysical Fluid Dynamics Laboratory, USA	2.5 deg x 2.0 deg	r1i1p1
HadGEM2-ES	United Kingdom	Met Office Hadley Center, UK	1.88 deg x 1.25 deg	r1i1p1
HadGEM2-CC	United Kingdom	Met Office Hadley Center, UK	1.88 deg x 1.25 deg	r1i1p1
inmcm4	Russia	Institute for Numerical Mathematics, Russia	2.0 deg x 1.5 deg	r1i1p1
IPSL-CM5A-LR	France	Institut Pierre Simon Laplace, France	3.75 deg x 1.8 deg	r1i1p1
IPSL-CM5A-MR	France	Institut Pierre Simon Laplace, France	2.5 deg x 1.25 deg	r1i1p1
IPSL-CM5B-LR	France	Institut Pierre Simon Laplace, France	2.75 deg x 1.8 deg	r1i1p1
MIROC5	Japan	Atmosphere and Ocean Research Institute (The University of Tokyo), National Institute for Environmental Studies,and Japan Agency for Marine-Earth Science and Technology	1.4 deg x 1.4 deg	r1i1p1
MIROC-ESM	Japan	Japan Agency for Marine-Earth Science and Technology, Atmosphere and Ocean Research Institute (The University of Tokyo), and National Institute for Environmental Studies	2.8 deg x 2.8 deg	r1i1p1
MIROC-ESM-CHEM	Japan	Japan Agency for Marine-Earth Science and Technology, Atmosphere and Ocean Research Institute (The University of Tokyo), and National Institute for Environmental Studies	2.8 deg x 2.8 deg	r1i1p1
MRI-CGCM3	Japan	Meteorological Research Institute, Japan	1.1 deg x 1.1 deg	r1i1p1
NorESM1-M	Norway	Norwegian Climate Center, Norway	2.5 deg x 1.9 deg	r1i1p1

The downscaling analysis was conducted on a monthly basis (Figure 5-2). Winter months from January through March show greater variability, with more outliers than in the summer months from July through September. In particular changes in July and August wind speed are very small. In other months, the median changes in wind speed, under projected climate change conditions, are mostly a few centimeters per second.
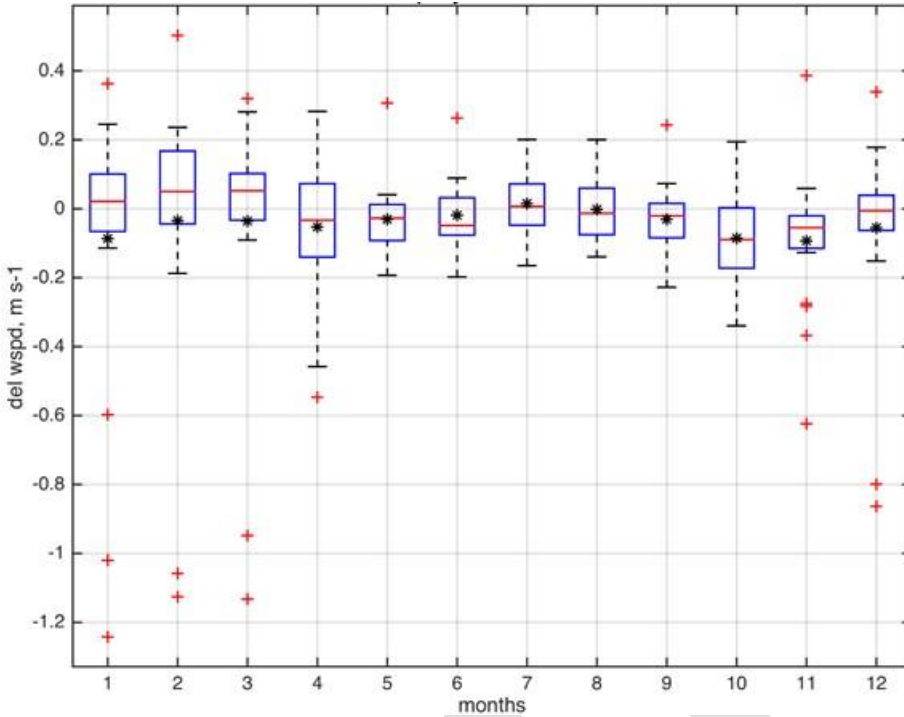
Figure 5-2: Results of wind speed downscaling analysis from 20 Global Climate Change Models (GCMs) to the Chesapeake Bay local scale for the year 2050 using the Multivariate Adaptive Constructed Analogs (MACA) method (Maria Herrmann, personal communication, April 16, 2019)

As mentioned above, modeling sensitivity analysis show that wind speeds below 2 meters per second have a small influence on anoxia volume in the Bay. Significant change in anoxia volume requires wind forcing greater than 4 meters per second. Based on these sensitivity results using the Chesapeake Bay partnership model, wind speed changes under future climate conditions, up to the year 2050, are approximately 2 orders of magnitude lower than what is needed to have a significant impact on bottom DO in the Bay. Given this large difference, it is unlikely that the Chesapeake Bay partnership model will show significant water quality effects of weak changes in wind speed. Additionally, the uncertainties of the change in wind speed are greater than the mean during the summer months. Consequently, further assessment of the climate effects on wind in our assessment of climate change impact on water quality in the Bay is not being pursued.

5.1.3 Sea level rise

MWG Review: Requires review for July.

Sea level rise is a major element in the climate change array of factors affecting water quality and ecosystem function in the Bay. Sea level rise can alter the gravitational circulation, stratification, saltwater intrusion, and DO advection fluxes. Robust projection of the magnitude of sea level rise contributes to the correctness and reliability of water quality assessment under

future climate change conditions. Two methods of sea level rise projection for the Bay area were assessed: The quadratic function method and the probabilistic projection method.

Boon and Mitchel (2015) fitted a quadratic function to tidal gauge data and successfully projected sea level rise magnitude up to 2055 at a large number of North America tidal gauge sites. The quadratic function is shown in Equation 5-1. Readers are referred to Boon and Mitchel (2015) for detailed description of the method.

Equation 5-1: Quadratic sea level rise equation

$$h = \beta_0 + \beta_1 t + \frac{1}{2}\beta_2 t^2 + \varepsilon$$

where:
h = sea surface level
t = time in years relative to the reference point
β_0 = intercept, i.e. the sea surface level at the reference point
β_1 = rate of sea level rise (m·yr^{-1})
β_2 = acceleration rate of sea level rise (m·yr^{-2})
ε = error of the prediction or the residual between the quadratic function projection and the observation data.

The tidal gauge site of Sewells Point, Norfolk, VA is located at the entrance of the Chesapeake Bay. The Climate Resiliency Workgroup recommended using data at this site to drive the estuarine partnership model for the assessment of climate change impact on water quality in the Bay. Sea surface level data over 50 years from 1969 to the present are available, which provides a sound basis for model fitting and projection (Figure 5.1.3.1). With data from 2018 included and 1992 as the reference point when the sea surface level is assumed at 0, the fitted sea level rise rate β_1 is 5.2 mm·yr^{-1} and the acceleration rate β_2 is 0.12 mm·yr^{-2}. Note that the sea level rise rate at Sewells Point is more than double the global ocean surface level rise of about 2 mm·yr^{-1}. A linear function fitting is comparable with the quadratic function with a coefficient of determination R^2 0.51 versus 0.52 of the quadratic function. However, the linear function does not take the acceleration of sea level rise into account. It can be seen in Figure 5-3 that the residuals of the linear function are consistently positive at the starting and ending periods and more often negative in the central period of the data, indicating that the linear function cannot adequately predict sea level rise for a long period of time within which the acceleration of sea level rise is significant. No trend in the distribution of the residuals of the quadratic function prediction (Figure 5-4) can be determined by inspection over the 50 years of data. The ability of the quadratic function in predicting the acceleration of sea level rise make it appropriate to predict sea level rise into the near future.
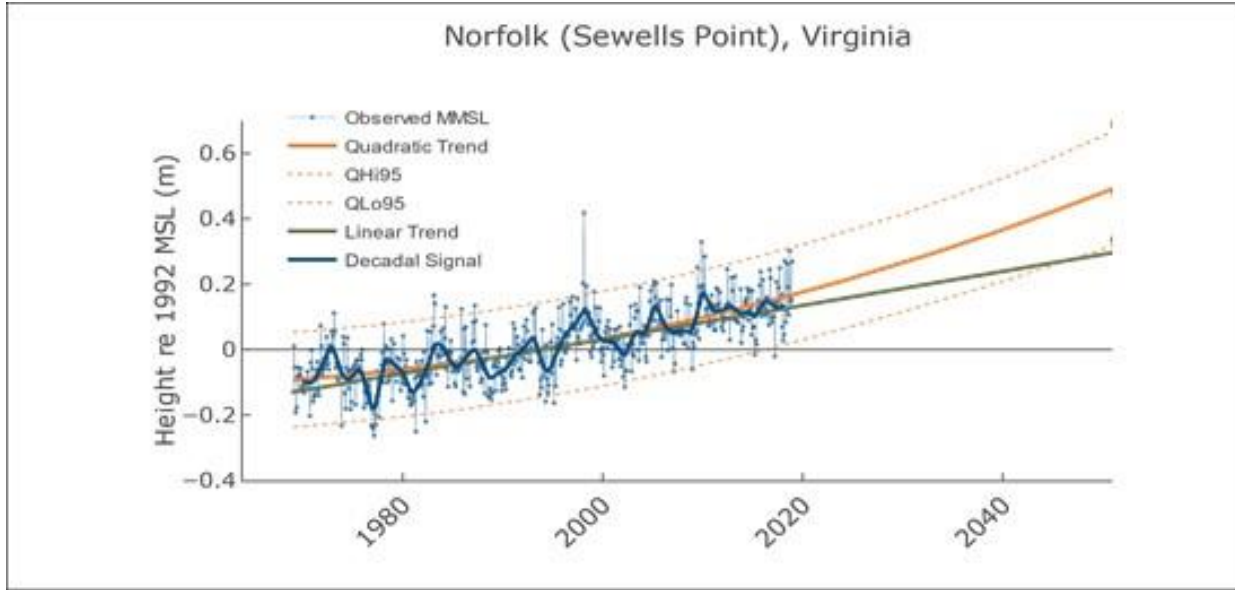
Figure 5-3: Quadratic function fitting and projection at Sewells Point, Norfolk, VA. The red solid line is the fitted quadratic function, the dashed lines are the 95% confidence interval and the black line is the fitted linear function as a comparison. (modified from Boon and Mitchel, https://www.vims.edu/research/products/slrc/localities/nova/index.php).
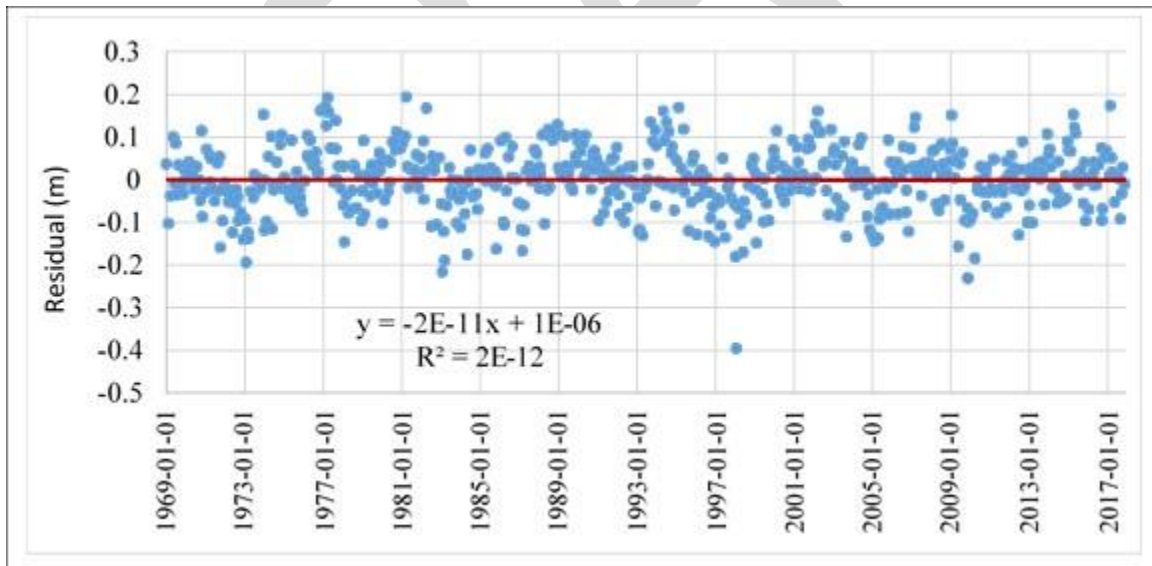
Figure 5-4: Residuals between quadratic method and observations and Sewell's Point, VA

The probabilistic method, known as the K14 method (Kopp et al., 2014), combines the IPCC projection of global seal level rise based on projections from GCMs with local tidal gauge data through a Gaussian process model for prediction at the local scale (Figure 5-5). Glacier and ice cap (GIC), ice sheet melt, oceanographic processes, local land water storage and local non-

climatic background are all taken into account for sea level rise projection at local tidal gauge sites. Detailed information can be found in the original reference (Kopp et al., 2014).
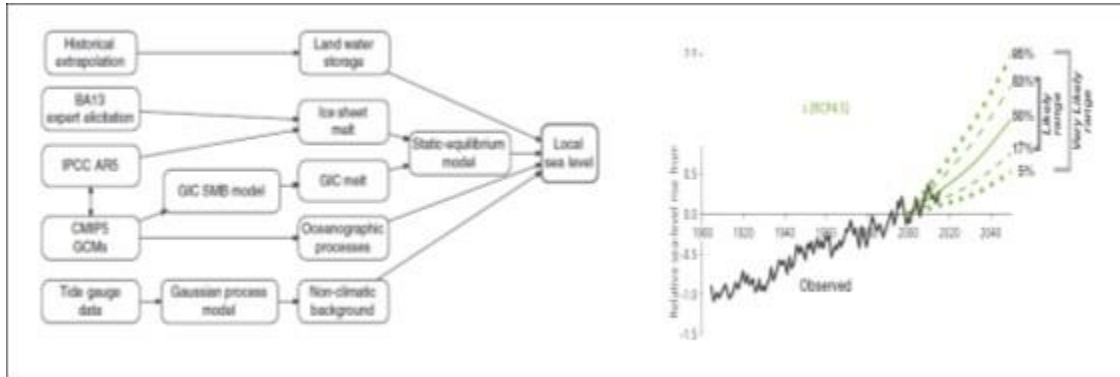

Figure 5-5: Probabilistic projection of future sea surface level at tide-gauge sites Sewells Point (Kopp et al. 2014, Boesch et al., 2018). BA13: Bamber and Aspinall [2013]. GIC: glacier and ice cap. SMB: surface mass balance.

The two projections at the Sewells Point are quite similar (Figure 5-6, left panel). Using 1995 as the reference point, the central year of the standard hydrology period used in the Chesapeake Bay Program, sea surface level will rise 0.22 m by 2025 based on the Quadratic Function projection and by 0.23 m based on the K14 projection, with a difference of 4.5%. The difference between the two methods are all within 5% up to 2055: 0.31 m versus 0.32 m by 2035, 0.42 m versus 0.41 m by 2045, 0.48 m versus 0.46m by 2050, and 0.54 m versus 0.52 m by 2055, respectively. It can be seen that the Quadratic Function projection is slightly lower than the K14 projection till 2035 and slightly higher after. *Based on the recommendation of the Climate Resiliency Workgroup, the CBP will use the average of the two methods for the analysis of climate change impacts on water quality in the Bay (Figure 5-6, right panel): 0.22 m for 2025, 0.31 m for 2035, 0.42 m for 2045 and 0.53 m for 2055, respectively*. The sea level rise numbers for 2050 are displayed in Figure 5.1.3.4 to facilitate comparison with other applications, but the Bay Program does not plan to do an assessment for 2050, rather every decade from 2025

through 2055.
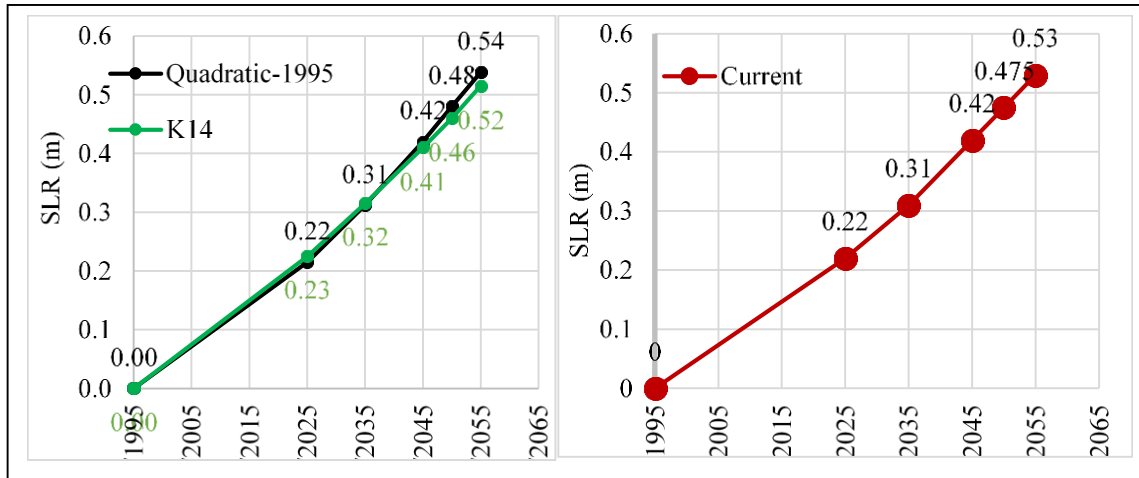
Figure 5-6: Projection of sea level rise by 2025, 2035, 2045 and 2055 as compared to 1995 using the probabilistic method (K14) and the Quadratic Function (left panel) and the average between the two (right panel) which are the final numbers that the Climate Resiliency Working Group recommended to use for assessing climate change impact on water quality in the Bay.

5.1.4   Temperature and Salinity at the Ocean Open Boundary

MWG Review: Requires review for July for Section 5.1.4 and its subsections

The oceanic open boundary conditions represent an additional forcing of the CBP partnership model. As with other model forcings, robust estimation of climatic changes at the ocean boundary is important for producing a reliable assessment of projected water quality impacts in the Bay. An assessment of historical changes in sea surface temperature and modeled air temperature changes provides a relationship between air and ocean temperatures that is then applied across seasons and depths at the ocean boundary. The results of a modeling study relating salinity to sea level rise is applied do the ocean boundary.

5.1.4.1   *Observed Ocean Temperature Change*

Regional temperature changes are happening in the context of a global ocean that has been warming, as evidenced by global sea surface temperature (SST) increases of approximately 0.13 °F per decade from 1990 to 2015, which is equivalent to 0.072 ℃ increase per decade (Figure 5-7, left panel). However, SST trends vary over space and time, and there is evidence that global warming has tended to accelerate in recent decades as compared to temperature changes in the early 20th century. The National Oceanic and Atmospheric Administration (NOAA) conducted a comprehensive analysis of historical temperature trends for coastal waters of the United States, and the Northeast Continental Shelf ranging from Maine to Maryland constituted a part of the investigation (Dupigny-Giroux et al., 2018). Results for this region showed that SST from 1982 to 2016 increased by 0.6 °F per decade on average, which is equivalent to 0.33 ℃

increase per decade, more than 4 times the rate of the global SST increase (Figure 5-7, right panel).
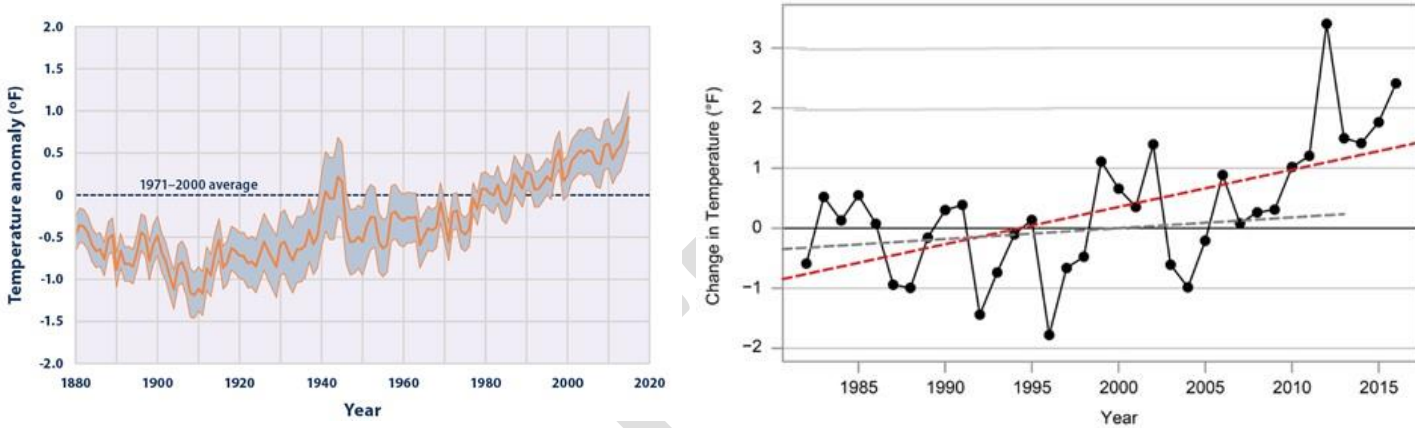

Figure 5-7: Left Panel: Average global sea surface temperature from 1880 to 2015 (from U.S.EPA, 2016b). Right Panel: Annual average sea surface temperature (SST) anomaly from the 1982–2011 average (plotted data and red line) over the period 1982–2016, on the Northeast Continental Shelf of USA (Dupigny-Giroux et al., 2018).

Thomas et al. (2017) conducted a similar historical trend analysis on the northeast continental shelf of the United States using SST data from 1982 to 2014, with a region extending from the Nova Scotian Shelf in the north to Cape Hatteras in the south. The authors were able to analyze the data separately for each major basin: Nova Scotian Shelf, Gulf of Maine and the Mid-Atlantic Bight. They found that SST has a faster pace of increase in the northern region than in the southern region. Over the 33 years of analyzed data, SST increased approximately 0.6 ℃ per decade on the Nova Scotian Shelf, 0.4 ℃ in the Gulf of Maine and about 0.3 ℃ in the Mid-Atlantic Bight. These numbers are in coherence with the NOAA analysis presented earlier, i.e. 0.33 ℃ per decade, while also fully including both the Gulf of Maine and the Mid-Atlantic Bight. The agreement between these two large-scale comprehensive analyses provides mutual support for the findings, and consequently, these results provide a sound basis for our specification of temperature at the WQSTM's ocean boundary in the CBP climate change assessment.

These results provide a reliable reference for our determination of the Chesapeake Bay model ocean boundary condition. Our simulation is based on the standard hydrology period from 1991 to 2000, with 1995 being the central reference year, which is close to the central reference year of the NOAA investigation, which was 1996. The first period for the climate change assessment is a three-decade span from 1995 to 2025. Based on the NOAA trend analysis, SST will increase 1.0 ℃ from 1995 to 2025. The data in the NOAA analysis continued until 2016, which is only 9 years earlier than our target year. As in the watershed model simulation, observational data are

preferred over GCM projections for 2025, because this target year is considered to be the near future relative to the most recent available observations.

5.1.4.2   *Modeled air temperature change*

Heat flux forcing for the WQSTM is computed from air temperature observations at the U.S. Naval Air Station located at the Patuxent River mouth (38.28N; -76.40W). For climate change application, a downscaling analysis of 31 GCMs was carried out to county scale using the Bias Corrected and Spatially Disaggregated method (BCSD; See Table 2-1 and Section 2.1.3 for details). The Naval Air Station is located at the boundary between the Maryland counties of St. Mary's and Calvert, and downscaled air temperature change for future climate conditions averaged between the two counties is used for the ICM forcing. Figure 5-8 displays the monthly air temperature change from 1995 to projections for 2025, with an annual average change of 1.058 ℃. To reproduce the surface water temperature change observed in the Mid-Atlantic Bight, the air temperature change was multiplied by a factor of 0.9 to produce the ocean boundary condition; this yielded a surface water temperature change of 0.95 ℃ over 30 years. This water temperature change at the ocean open boundary is the average between the two large scale analyses of historic data presented earlier (Dupigny-Giroux et al., 2018 and Thomas et al., 2017).
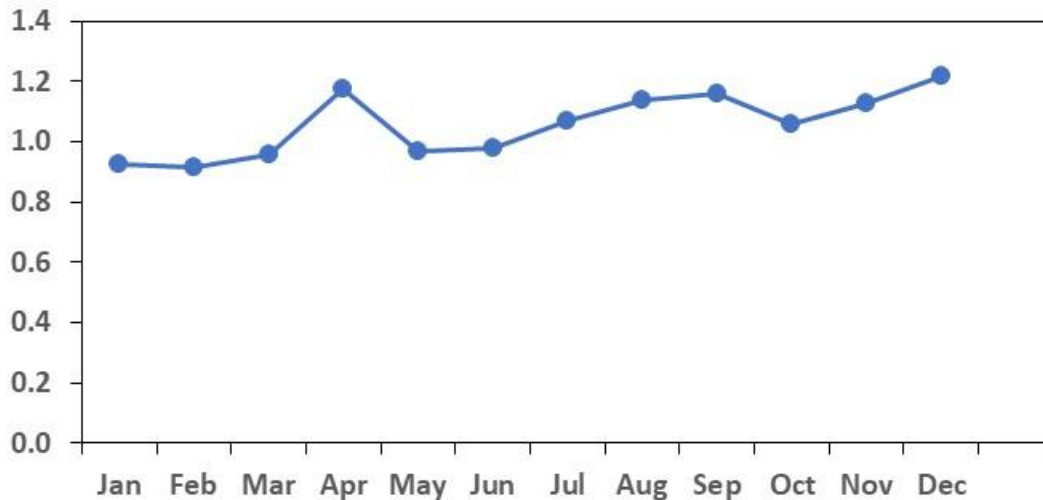

Figure 5-8: Air temperature change from 1995 to 2025 projected from downscaling analysis of 31 GCMs to the St Mary's and Calvert counties, with an annual average of 1.058 ℃ (data from climate models as described in Section 2.1)

5.1.4.3   *Generation of the ocean boundary temperature*

Water temperature below the surface was modified in proportion to the ratio of water temperature at depth and the surface water temperature:

Equation 5-2: Relationship between water temperature at depth and air temperature

$$\Delta T_{water} = 0.9 \bullet \Delta T_{air} \bullet T_{water} / T_{surface}$$

Where

T_{water} = water temperature

$T_{surface}$ = surface water temperature

ΔT_{air} = air temperature change under climate change conditions from downscaled GCM ensemble projection,

ΔT_{water} = water temperature change at the ocean open boundary under climate change conditions.

An example is given in Figure 5-9 for September 1, 1993. Air temperature change from 1995 to 2025 is 1.16 ℃ for September based on the downscaled GCM ensemble projection, leading to a change in surface water temperature of 1.04 ℃ (0.9*1.16 ℃). The observed surface water temperature at the ocean boundary is 22.3 ℃ and the modified temperature for 2025 is 23.34 ℃ (22.3+1.04 ℃). The observed bottom temperature is 21.3 ℃, which leads to a change in bottom water temperature of 0.996 ℃ (0.9*1.16*21.3/22.3 ℃) and a resulting modified bottom temperature for 2025 of 22.30 ℃.

The advantage of linking water temperature change to air temperature change is that it facilitates the generation of projections for other climate change scenarios, i.e. 2035, 2045 and 2055, that the Bay Program is charged to evaluate. Moreover, the acceleration of air temperature warming, which is included in the GCM simulations, propagates into the water column boundary condition values and is thus taken into account. The same coefficient (0.9) between air and water temperature change will therefore be used for the above future periods of time.
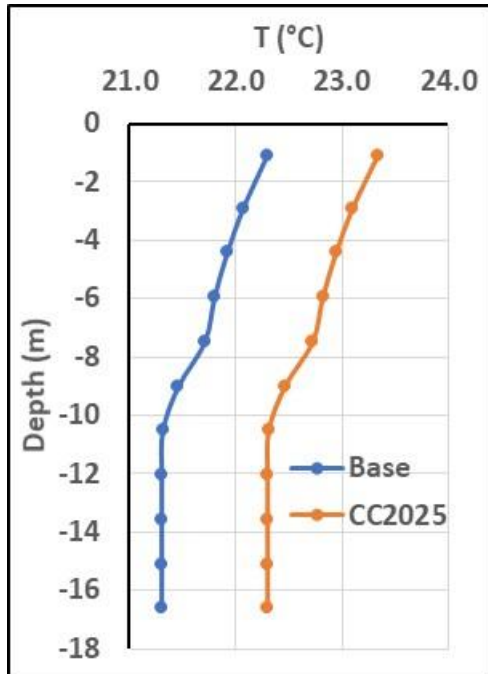
Figure 5-9: Example of modified vertical temperature profile (orange line) from the calibration conditions (blue line) at the ocean open boundary in September 1, 1993 under 2025 climate change conditions.

5.1.4.4   *Salinity Changes at the Open Boundary*

Salinity at the Bay mouth where the simulation boundary is located can increase with sea level rise and changes in oceanic circulation. Saba et al. (2016) conducted a high-resolution model projection (10 km, versus 100 km in IPCC GCMs; IPCC, 2013) under future climate change conditions for the Northwest Atlantic. They reported salinity increases under future climate change conditions due to the retreat of the Labrador Current, the northerly shifting of the Gulf Stream, the weakening of the Atlantic Meridional Overturning Circulation (AMOC), and an increase of Warm Slope Water entering the Northwest Atlantic Shelf.

Hong and Shen (2012) conducted a modeling analysis of sea level rise impact on salinity in the Chesapeake Bay (Figure 5.1.4.5). In their analysis, the model domain extended offshore, therefore the simulated salinity change can provide guidance for our specification of salinity change at the CBP model's open boundary. At the entrance of the Bay where the WQSTM ocean open boundary is located, salinity increased approximately 0.4 psu with a 0.5 m sea level rise. Assuming a linear relationship between sea level rise and salinity change at the entrance of the Bay, as indicated by the previous study, specification of salinity change at the ocean open boundary can be determined as:

Equation 5-3: Salinity changes as a function of sea level rise.

$$\Delta S = 0.4\Delta\zeta/0.5$$

where
ΔS = salinity change at the ocean open boundary,

$\Delta\zeta$ = sea surface level rise (m).

Based on the Climate Resiliency Working Group's recommendation, sea surface level is projected to rise 0.22 m by 2025, 0.31 m by 2035, 0.42 m by 2045 and 0.53 m by 2055, which will lead to a salinity increase at the ocean open boundary of 0.18, 0.25, 0.34 and 0.42 psu, respectively. As shown in Figure 5-10, no significant stratification of salinity changes was projected at the boundary, and therefore a constant salinity change was specified over the entire water column.
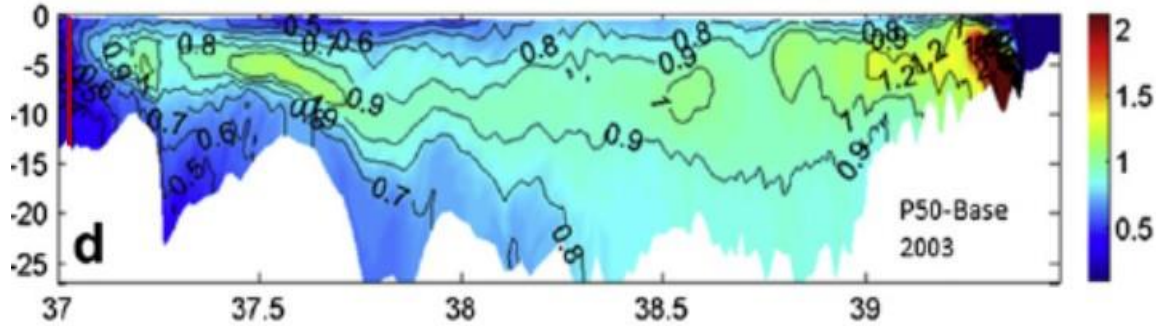

Figure 5-10: Longitudinal (x-axis) and depth (m; y-axis) distribution of projected salinity changes in Chesapeake Bay after a sea surface level rise of 0.5 m. A vertical red line indicates the entrance of the Bay where the ICM ocean open boundary is located, where the ICM ocean open boundary is located, where there is a 0.4 psu increase (from Hong and Shen, 2012)

Before adding the salinity change, salinity was re-interpolated to the new, sea-level rise expanded grid based on the new depth of each layer (Figure 5-11). such that the base salinity at each depth remained the same even though the depth of the cell centroids had changed.
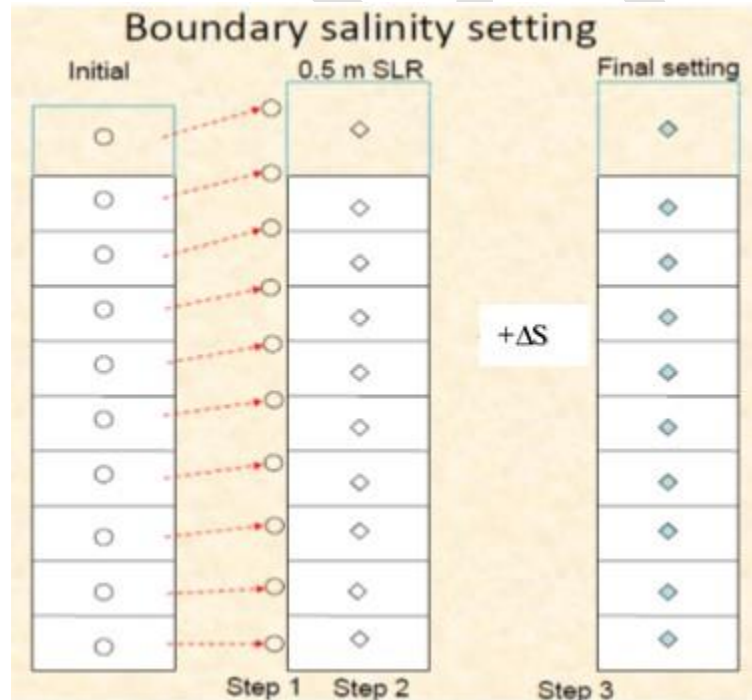

Figure 5-11: Interpolation of salinity to the new grid before adding the salinity change (ΔS) at the ocean open boundary.

5.2   Growth and Respiration Curve Modification

MWG Review: Requires review for July for Section 5.2 and its subsections

Water temperature increase is one of the projected effects of climate change on the ocean and coastal embayments, such as the Chesapeake Bay. Increased phytoplankton production, which can be driven by eutrophication as well as higher temperatures, leads to greater amounts of organic material, oxygen demand, and ultimately hypoxia in the Bay. As such, an adequate simulated response of phytoplankton growth and respiration to temperature increase is essential for a robust assessment of the climate change impact on water quality in the Bay.

5.2.1   Growth Curve Modification

The response of phytoplankton growth rate to temperature increase is usually expressed as the Q10 coefficient, which is the growth rate increase over a 10℃ temperature increase. The value of this coefficient can differ from species to species and from region to region. Lomas et al. (2002) carried out an extensive study of the temperature effect on phytoplankton growth rate and microbial processes in the Chesapeake Bay and found values of Q10 ranging from 1.7 to 3.4. A Q10 of 2, which means that phytoplankton growth rate will double over 10 ℃ increase in water temperature, is commonly used in the literature and particularly in the modeling community (Eppley, 1972; Tian et al., 2014). Irby et al., (2018) used a Q10 of 2.1 in their modeling study of potential climate change impacts in Chesapeake Bay.

The CBP partnership's estuarine water quality sediment transport model (WQSTM) was calibrated for the period 1991 to 2000, the standard hydrology period used in the Chesapeake Bay TMDL. The phytoplankton growth curves used in the calibration were appropriate for temperatures observed in the Bay during that period. At the STAC workshop "Chesapeake Bay Program Climate Change Modeling 2.0" held on September 24-25, 2018, it was recommended to revise the temperature-related coefficients for phytoplankton growth and respiration to adequately reflect phytoplankton assemblage characteristics over the range of water temperatures expected in the Bay due to climate change.

In the ICM model, the response of phytoplankton growth rate to temperature increase is formulated in Equation 5-4:

Equation 5-4: Phytoplankton growth rate

$$g(T) = g_{max}e^{-K1 \cdot (T - Topt)2} \quad \text{when } T \leq Topt$$
$$ = g_{max}e^{-K2 \cdot (Topt - T)2} \quad \text{when } T > Topt$$

Where:

$g(T)$ = growth rate as a function of temperature (g C (g chl)$^{-1}$day^{-1})

g_{max} = theoretical maximum growth rate (g C (g chl)$^{-1}$day^{-1})

T = temperature ($^{\circ}$C)

T_{opt} = optimal temperature for algal growth ($^{\circ}$C)

K_1 = effect of temperature below T_{opt} on growth ($^{\circ}$C^{-2})

K_2 = effect of temperature above T_{opt} on growth ($^{\circ}$C^{-2})

Parameter values are listed in Table 5.2.1. There are three groups of phytoplankton in the model: cyanobacteria, diatoms, and green algae. These terms represent integrated phytoplankton groups rather than phytoplankton species. The cyanobacteria group represents fresh water species in the tidal fresh zone of the tributaries, diatoms represent transitional groups in the spring, and green algae represent all other species that succeed diatoms in the summer and fall. Initially, the optimal temperatures (Topt) was set to 29 $^{\circ}$C for cyanobacteria and 25 $^{\circ}$C for green algae, temperatures over which growth for these phytoplankton groups would decrease or remain static. With these optimal temperature values, the model can underestimate the impact of climate change on phytoplankton production and ultimately dissolved oxygen.

As recommended from the STAC workshop, the optimal temperatures for cyanobacteria and green algae are both revised to 37 $^{\circ}$C, a value that it is unlikely water temperature will reach even under climate change conditions (Table 5-2). The optimal temperature for diatoms was kept the same as in the calibration run because it is a transitional group in spring and succeeded by green algae. Diatoms are known to be a cold-water species, and theoretically it is poorly understood how they will respond to water temperature increases. The optimal temperature for diatoms in the model only affects the timing of when the diatom group is succeeded by other species, and not the total primary production and ultimately oxygen demand, which is the purpose of our assessment.

Once the optimal temperatures were revised, the theoretical maximum growth rate and the exponential coefficient were altered in such a way that the simulated growth rate is comparable with the original calibration during the growth season from 10 to 30 $^{\circ}$C for cyanobacteria and from 10 to 25 $^{\circ}$C for green algae (Figure 5-12). Given the equation of phytoplankton growth with respect to temperature presented above, the simulated growth rate is not linear with temperature change and, as such, the simulated Q10 is not a constant. The simulated Q10 for green algae is 2.02 from 5 to 15 $^{\circ}$C and 1.92 from 10 to 20 $^{\circ}$C. This group is the dominant group in the main stem of the Bay and the robustness of its simulation is the most relevant to water quality simulation. Cyanobacteria is treated as a warm species in the tidal fresh zone in the model with higher optimal temperature up to 29 $^{\circ}$C in the calibration. The simulated Q10 after the revision is 2.02 from 20 to 30 $^{\circ}$C and 2.5 from 15 to 25 $^{\circ}$C. All these

numbers show that the revised model has an adequate response of phytoplankton growth to temperature increase and thus is suitable for climate change simulation.

Table 5-2: Coefficients of phytoplankton growth and respiration response to temperature increase. g_{max}: Theoretical maximum growth rate of phytoplankton (g C (g chl)$^{-1}$day^{-1}), T_{opt}: Theoretical optimal temperature; K_1: Exponential coefficient for phytoplankton growth increase with temperature increase below T_{opt}, K_2: Exponential coefficient for phytoplankton growth decrease with temperature increase above T_{opt}, K_r: Exponential coefficient for phytoplankton respiration response to temperature increase (Carl Cerco, personal communication, March 29, 2019)

| Coefficient	Cyanobacteria			Diatom			Green Algae	
	Calibration	Revision		Calibration	Revision		Calibration	Revision
g_{max}	200	250		300	300		450	600
T_{opt} (°C)	29	37		16	16		25	37
K_1	0.005	0.0022		0.0018	0.0018		0.0035	0.0013
K_2	0.004	0.0		0.0022	0.002		0	0
K_r	0.0322	0.069		0.0322	0.069		0.0322	0.069
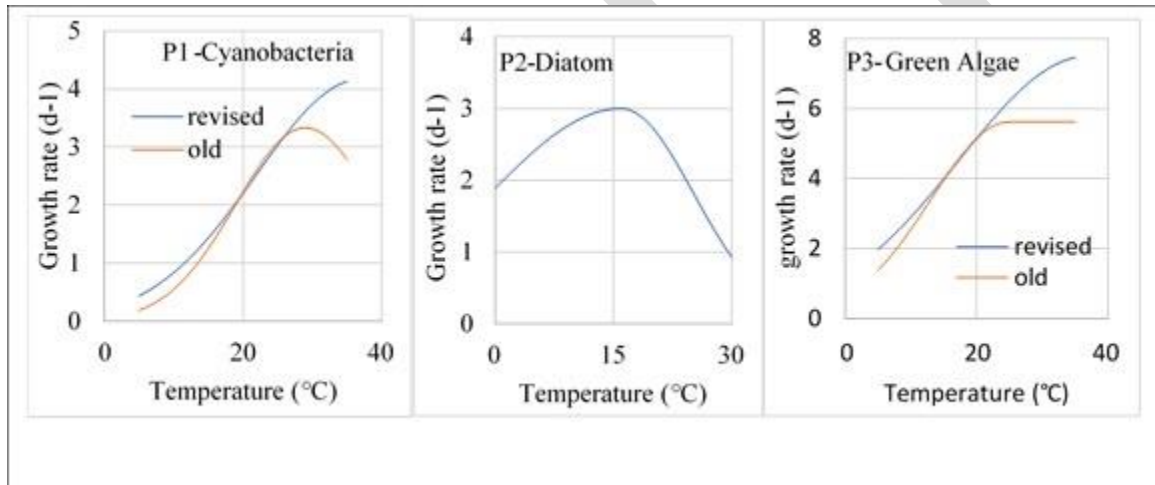
Figure 5-12: . Phytoplankton growth curve in function of water temperature (Red line: Original calibration curve; Blue: Revised curve for climate change assessment; From Carl Cerco, 2017)

5.2.2   Respiration Curve Modification

Base phytoplankton respiration is a complex formulation that varies spatially. The temperature dependence of the respiration is represented in Equation 5-5:

Equation 5-5: phytoplankton respiration multiplier

$$f(T) = e^{k_r(T - T_0)}$$

where:
f(T) = multiplier to the respiration rate (dimensionless),
k_r = exponential coefficient of response to temperature change (°C^{-1}),
T = temperature (°C),
T_0 = reference temperature at which respiration rate is equal to the base rate.

In the calibration, k_r was assigned a value of 0.0322, which leads to a Q10 of 1.38. This is relatively low as compared to the values reported for the Chesapeake Bay and in the literature (Lomas et al., 2002). For the climate change anlysis, k_r was revised to 0.069, yielding a Q10 of 2, in coherence with the literature and what is reported in Chesapeake Bay. The original and revised curves are shown in Figure 5-13.
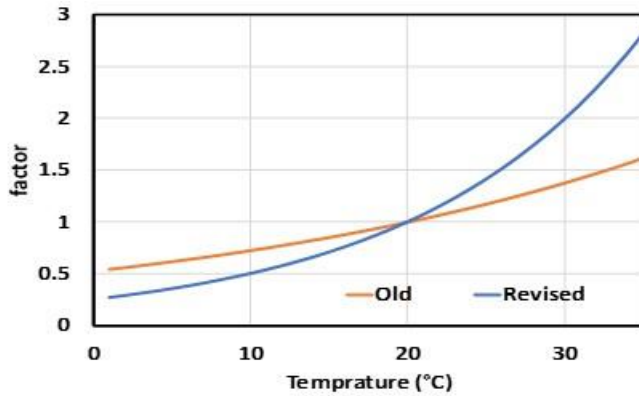

Figure 5-13: Response of phytoplankton respiration rate to temperature increase. The orange line is the calibration and the blue line is the revised curve for climate change application.

5.2.3   Test of Calibration

The temperature parameter values were modified after the calibration for the climate change application. A key question is whether these modifications significantly altered the calibration in such a way that simulation drifts away from the data. To address this question, a simulation was conducted with all forcing files and parameter values the same as in the calibration except the modified temperature parameters as shown in Table 5-2, and its results were compared with the results of the original calibration run. Mean difference (MD) and absolute mean difference (AMD), calculated as shown in Equation 5-6 were computed for both runs across the array of state variables used routinely during the calibration (Cerco and Noël, 2017):

Equation 5-6: Calibration metrics for the WQSTM

$$MD = \frac{\sum_{i=1}^{N}(P_i - O_i)}{N}$$

$$AMD = \frac{\sum_{i=1}^{N}|P_i - O_i|}{N}$$

Where:
P = prediction
O = observation
N = number of observations.

Time-series data comparison and whisker box plots of bottom DO at the central station CB4.2C are given as an example in Figure 5-14, followed by AMD and MD plots for DO (Figure 5-15),

chlorophyll (Figure 5-16), total nitrogen TN (Figure 5-17) and total phosphorus TP (Figure 5-18). On the time-series plot of bottom DO at CB4.2C, the two simulations are superimposed on each other (Figure 5-14 left panel). Both simulations match well with the data in terms of magnitude, seasonal variation, and hypoxia events with DO < 2 mg/l during the summer season. Similarity between the two solutions dominates on the whisker plots in term of the median, the first and the fourth quartiles and even the extrema (Figure 5-14 right panel). The new solution with modified temperature-related parameter values even show some slightly better results as compared to the original calibration solution, with the simulated median closer to the data median, such as in 1991, 1994, and 1997.
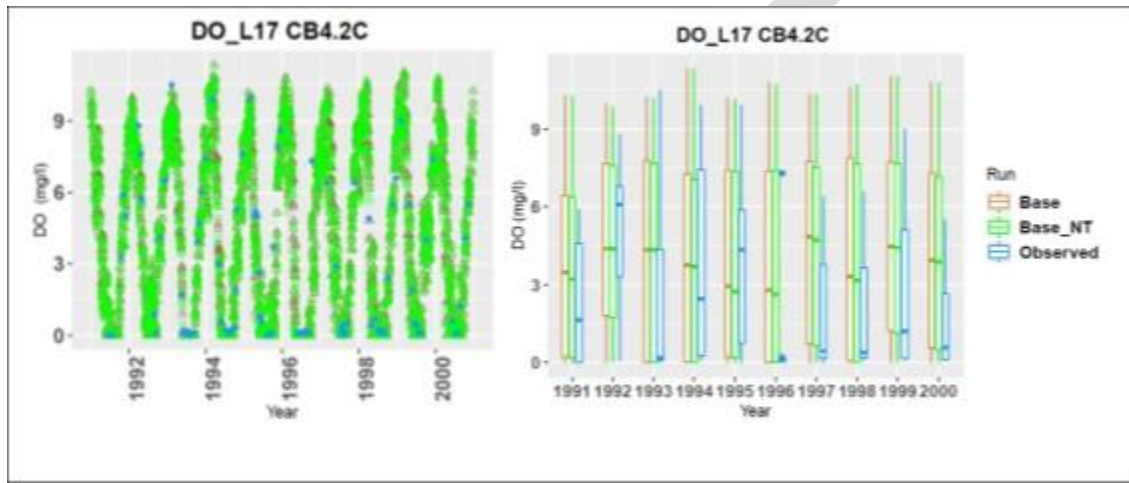

Figure 5-14: Bottom DO at the central Station CB4.2C in segment CB4MH (Base: Calibration run; Base_NT: Simulation with revised parameter values for the phytoplankton growth function and respiration rate with temperature).

In terms of AMD and MD of DO in the entire water column, the new solution with modified temperature parameter values generated slightly lower AMD in the main stem than the original calibration, but slightly higher in the tributaries (Figure 5-15, left panel). Nonetheless, all differences are within 5% of the original solution. The MD plot shows that both solutions slightly underestimate DO in the Eastern Shore and overestimate DO in the tributaries on the western shore, with the best solution for the main stem of the Bay resulting in the smallest MD over all the tributaries.
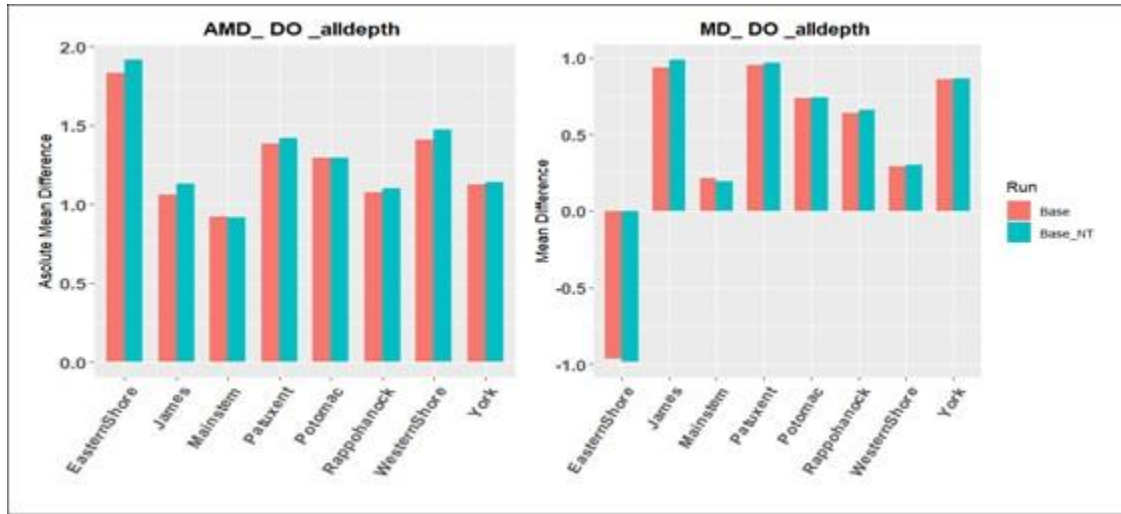
Figure 5-15: Absolute mean difference AMD (left panel) and mean difference MD (right panel) between simulation and data of DO in the major tributaries and the main stem of the Bay (Base: Calibration run; Base_NT: Simulation with revised parameter values for the phytoplankton growth and respiration functions with temperature).

The chlorophyll results are quite similar between the two solutions in the main stem (Figure 5-16), and the AMD of the new solution with the modified temperature parameter values is slightly higher than the original calibration solution in most of the tributaries. The differences are mostly below 15% of the original solution. Usually chlorophyll has greater variability in space, time and in the vertical profile than DO, which can help to explain its larger AMD than DO. Both model solutions underestimate chlorophyll in the James River and on the Western Shore, but tend to slightly overestimate chlorophyll concentration in other tributaries. Similarity is even more apparent for total nitrogen (TN) and total phosphorus (TP) between the two model solutions (Figure 5-17 and Figure 5-18). For TN and TP, AMD is practically identical between the two model simulations in the main stem of the Bay, the James, Potomac, Rappahannock and the York rivers. The new solution has a slightly higher AMD than the original simulation in the western and eastern shore and in the Patuxent River, but the differences are minimal. Given the high similarity between the two model runs, the modification of the parameter values controlling phytoplankton growth and respiration rate to temperature increase did not significantly alter the calibration, and these parameter values can lead to adequate simulation of phytoplankton response to temperature under future climate change conditions.
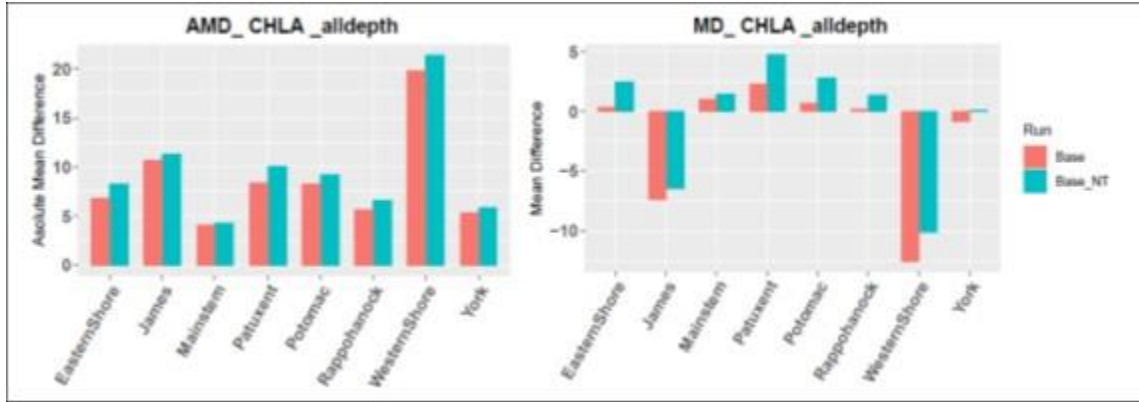
Figure 5-16: Absolute mean difference AMD (left panel) and mean difference MD (right panel) between simulation and data of chlorophyll in the main tributaries and the main stem of the Bay (Base: Calibration run; Base_NT: Simulation with revised parameter values for the phytoplankton growth and respiration functions with temperature).
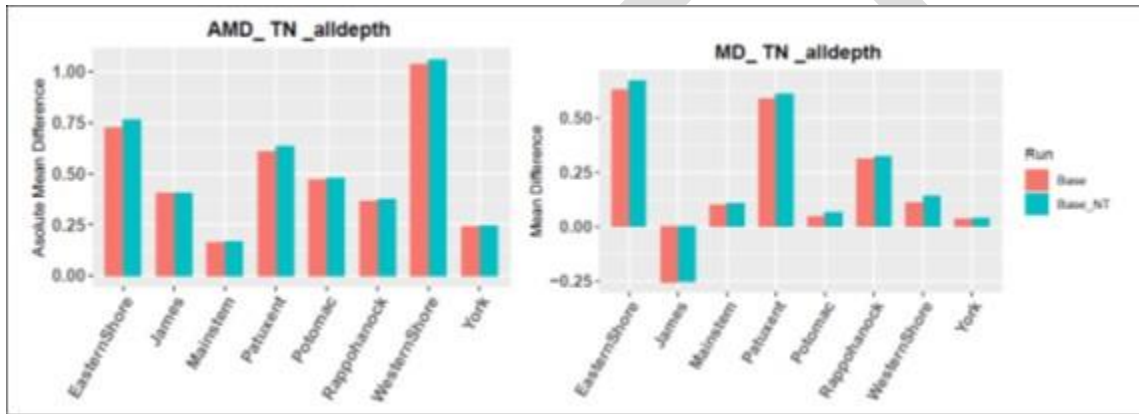

Figure 5-17: Absolute mean difference AMD (left panel) and mean difference MD (right panel) between simulation and data of total nitrogen TN in the main tributaries and the main stem of the Bay (Base: Calibration run; Base_NT: Simulation with revised parameter values for the phytoplankton growth and respiration functions with temperature).
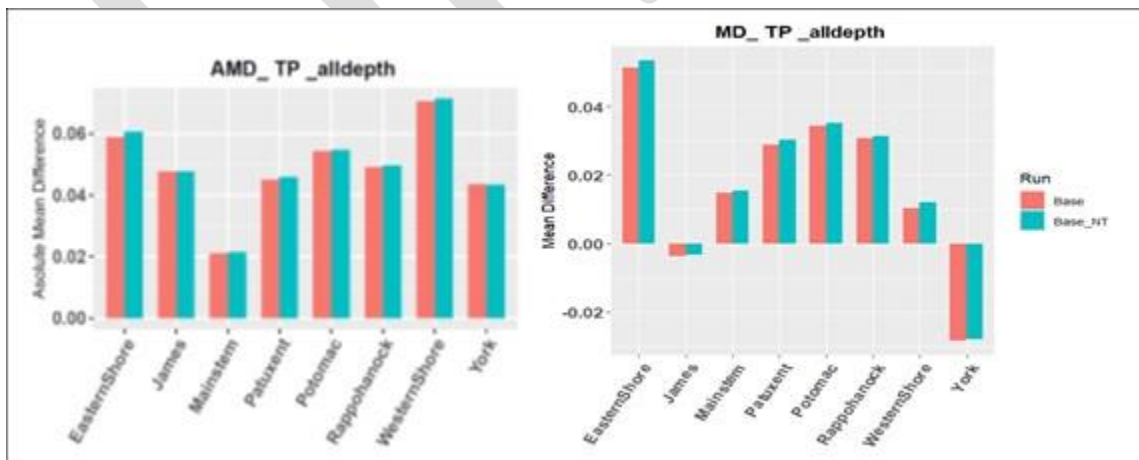

Figure 5-18: Absolute mean difference AMD (left panel) and mean difference MD (right panel) between simulation and data of total phosphorus TP in the main tributaries and the main stem of the Bay (Base: Calibration run; Base_NT: Simulation with revised parameter values for the phytoplankton growth and respiration functions with temperature).

5.3 Validation of model response

5.3.1 Reasonable response to Sea Level Rise

To be added by October

5.3.2 Reasonable Response to Temperature Change

To be added by October

5.4 Simulation Results

To be added by October

6 Findings

To be added by October

6.1 Effect on water quality standards

6.2 Management effort adjustment

7 References

Abatzoglou, J.T. and T.J. Brown 2011. A comparison of statistical downscaling methods suited for wildfire applications. International Journal of Climatology 32: 772-780.

Alamdari, N., D.J. Sample, P. Steinberg, A.C. Ross, Z.M. Easton. 2017. Assessing the effects of climate change on water quantity and quality in an urban watershed using a calibrated stormwater model. Water 9 (7): 464.

Boesch, D.F., W.C. Boicourt, R.I. Cullather, T. Ezer, G.E. Galloway, Jr., Z.P. Johnson, K.H. Kilbourne, M.L. Kirwan, R.E. Kopp, S. Land, M. Li, W. Nardin, C.K. Sommerfield, W.V. Sweet. 2018. Sea-level Rise: Projections for Maryland 2018, 27 pp. University of Maryland Center for Environmental Science, Cambridge, MD.

Boon, J.D. and M. Mitchell 2015. Nonlinear Change in Sea Level Observed at North American Tide Stations. Journal of Coastal Research, 31(6):1295-1305.

Brown, D. G., C. Polsky, P. Bolstad, S. D. Brody, D. Hulse, R. Kroh, T. R. Loveland, and A. Thomson, 2014: Ch. 13: Land Use and Land Cover Change. Climate Change Impacts in the United States: The Third National Climate Assessment, J. M. Melillo, Terese (T.C.) Richmond, and G. W. Yohe, Eds., U.S. Global Change Research Program, 318-332. doi:10.7930/J05Q4T1Q. http://nca2014.globalchange.gov/report/sectors/land-use-and-land-cover-change (accessed 6/14/2019)

Butcher, J.B., T.E. Johnson, D. Nover, and S. Sarkar. 2014 Incorporating the effects of increased atmospheric CO2 in watershed model projections of climate change impacts. Journal of hydrology 513:322-334, http://dx.doi.org/10.1016/j.jhydrol.2014.03.073

Chanat, J.G and G. Yang, 2018. Exploring Drivers of Regional Water-Quality Change Using Differential Spatially Referenced Regression—A Pilot Study in the Chesapeake Bay Watershed. Water Resources Research. 54:10, October 2018. https://doi.org/10.1029/2017WR022403.

Chesapeake Bay Program, 2016. Climate Resiliency Workgroup. Recommendations on Incorporating Climate-Related Data Inputs and Assessments: Selection of Sea Level Rise Scenarios and Tidal Marsh Change Models. August 2016. https://www.chesapeakebay.net/channel_files/24216/crwg_mid_point_assessment_climate_data_recommendations_final_080516.pdf Last accessed 4/2019.

Chesapeake Bay Program, 2017. Chesapeake Assessment and Scenario Tool (CAST) Version 2017d. Chesapeake Bay Program Office, http://cast.chesapeakebay.net/ Last accessed 4/2019.

Chesapeake Executive Council, 2014. Chesapeake Bay Watershed Agreement. June 16, 2014.

Deryng, D., Elliott, J., Folberth, C., Müller, C., Pugh, T. A. M., Boote, K. J., et al. (2016). Regional disparities in the beneficial effects of rising CO2 concentrations on crop water productivity. Nat. Clim. Change 6, 786–790. doi: 10.1038/nclimate2995

DiPasquale, N., 2014. EPA-CBPO Response to STAC report re: climate change April 22, 2014. US EPA Chesapeake Bay Program Office. http://www.chesapeake.org/pubs/319_DiPasquale2014.pdf last accessed 4/2019.

Dupigny-Giroux, L.A., E.L. Mecray, M.D. Lemcke-Stampone, G.A. Hodgkins, E.E. Lentz, K.E. Mills, E.D. Lane, R. Miller, D.Y. Hollinger, W.D. Solecki, G.A. Wellenius, P.E. Sheffield, A.B. MacDonald, and C. Caldwell, 2018: Northeast. In Impacts, Risks, and Adaptation in the United States: Fourth National Climate Assessment, Volume II [Reidmiller, D.R., C.W. Avery, D.R. Easterling, K.E. Kunkel, K.L.M. Lewis, T.K. Maycock, and B.C. Stewart (eds.)]. U.S. Global Change Research Program, Washington, DC, USA. doi : 10.7930/NCA4.2018.CH1.

Eppley, R.W., 1972. Temperature and phytoplankton growth in the sea. Fish. Bull. 70, 1063–1085.

Fischbach J.R., R.J. Lempert, E. Molina-Perez, A.A. Tariq, M.L. Finucane, F. Hoss. 2015. Managing Water Quality in the Face of Uncertainty: A Robust Decision Making Demonstration for EPA's National Water Program. Santa Monica, CA: RAND Corporation.

Gammas, Matthew; Mérel, Pierre; Ortiz-Bobea, Ariel. "Negative Impacts of Climate Change on Cereal Yields: Statistical Evidence from France" Environmental Research Letters. 12 (2017): 054007

Gowda, P., J.L. Steiner, C. Olson, M. Boggess, T. Farrigan, and M.A. Grusak, 2018: Agriculture and Rural Communities. In Impacts, Risks, and Adaptation in the United States: Fourth National Climate Assessment, Volume II [Reidmiller, D.R., C.W. Avery, D.R. Easterling, K.E. Kunkel, K.L.M. Lewis, T.K. Maycock, and B.C. Stewart (eds.)]. U.S. Global Change Research Program, Washington, DC, USA, pp. 391–437. doi: 10.7930/NCA4.2018.CH10 (accessed 6/21/2019)

Grimm, N., Chapin, F., Bierwagen, B., Gonzalez, P., Groffman, P., Luo, Y., Melton, F., Nadelhoffer, K., Pairis, A., Raymond, P., Schimel, J., Williamson, C. 2013. The impacts of climate change on ecosystem structure and function. Frontiers in Ecology and the Environment. 2013; 11(9): 474–482, doi:10.1890/120282

Hatfield, J., G. Takle, R. Grotjahn, P. Holden, R. C. Izaurralde, T. Mader, E. Marshall, and D. Liverman, 2014: Ch. 6: Agriculture. Climate Change Impacts in the United States: The Third National Climate Assessment, J. M. Melillo, Terese (T.C.) Richmond, and G. W. Yohe, Eds., U.S. Global Change Research Program, 150-174. doi:10.7930/J02Z13FR. http://nca2014.globalchange.gov/report/sectors/agriculture (accessed 6/21/2019)

Hong, B. and J. Shen 2012. Responses of estuarine salinity and transport processes to potential future sea-level rise in the Chesapeake Bay. Estuarine, Coastal and Shelf Science 104-105: 33-45

IPCC, 2013: Summary for Policymakers. In: Climate Change 2013: The Physical Science Basis. Contribution of Working Group I to the Fifth Assessment Report of the Intergovernmental Panel on Climate Change [Stocker, T.F., D. Qin, G.-K. Plattner, M. Tignor, S.K. Allen, J. Boschung, A. Nauels, Y. Xia, V. Bex and P.M. Midgley (eds.)]. Cambridge University Press, Cambridge, United Kingdom and New York, NY, USA.

Irby, I.D., A.M. Marjorie Friedrichs, D. Fei, and K.E. Hinson 2018. The competing impacts of climate change and nutrient reductions on dissolved oxygen in Chesapeake Bay. Biogeosciences, 15, 2649–2668.

Johnson, Z., M. Bennett, L. Linker, S. Julius, R. Najjar, M. Mitchell, D. Montali, R. Dixon. 2016. The Development of Climate Projections for Use in Chesapeake Bay Program Assessments. STAC Publication Number 16-006, Edgewater, MD. 52 pp. http://www.chesapeake.org/pubs/360_Johnson2016.pdf last accessed 4/2019.

Konikow, L. F., 2015: Long-term groundwater depletion in the United States. Groundwater, 53 (1), 2–9. doi:10.1111/gwat.12306

Kopp R.E., R.M. DeConto, D.A. Bader, C.C. Hay, R.M. Horton, S. Kulp, M. Oppenheimer, D. Pollard, and B.H. Strauss 2014. Evolving Understanding of Antarctic Ice-Sheet Physics and Ambiguity in Probabilistic Sea-Level Projections. Earth's Future 2, 383-406

Lall, U., T. Johnson, P. Colohan, A. Aghakouchak, C. Brown, G. McCabe, R. Pulwarty, and A. Sankarasubramanian, 2018: Water. In Impacts, Risks, and Adaptation in the United States: Fourth National Climate Assessment, Volume II [Reidmiller, D.R., C.W. Avery, D.R. Easterling, K.E. Kunkel, K.L.M. Lewis, T.K. Maycock, and B.C. Stewart (eds.)]. U.S. Global Change Research Program, Washington, DC, USA, pp. 145–173. doi: 10.7930/NCA4.2018.CH3

Linker, L.C., G.W. Shenk, P. Wang, K.J. Hopkins, S. Pokharel. 2002. A Short History of Chesapeake Bay Modeling and the Next Generation of Watershed and Estuarine Models Proceedings of the Water Environment Federation, Watershed 2002 , pp. 569-582(14) Water Environment Federation. Alexandria, VA.

Lomas, M. W., Gilbert, P. M., Shiah, F. K., and Smith, E. M.: Microbial processes and temperature in Chesapeake Bay: current relationships and potential impacts of regional warming, Glo. Change Biol., 8, 51–70, 2002.

Munson, K.M., R.M. Vogel, J.L. Durant. 2018. Climate sensitivity of phosphorus loadings to an urban stream. Journal of the American Water Resources Association 54 (2): 527-542.

Office of the President. 2009. Executive Order: Chesapeake Bay Protection and Restoration. Office of the President, Washington, DC

Pyke, C., 2012. STAC Letter to the Chesapeake Bay Program Management Board re: Adapting to Climate Change in the Chesapeake Bay, June, 2012. STAC. http://www.chesapeake.org/pubs/288_Pyke2012.pdf last accessed 4/2019.

Pyke, C., M. Bennett, R. Najjar, M. Raub, K. Sellner, S. Stiles, D. Wardrop. (2012). Adapting to Climate Change in the Chesapeake Bay: A STAC workshop to monitor progress in addressing climate change across the Chesapeake Bay Watershed (CRC# STAC 12-01). STAC. http://www.chesapeake.org/pubs/287_Pyke2012.pdf last accessed 4/2019.

Pyke, C.R., R.G. Najjar, M.B. Adams, D. Breitburg, M. Kemp, C. Hershner, R. Howarth, M. Mulholland, M. Paolisso, D. Secor, K. Sellner, D. Wardrop, and R. Wood. 2008. Climate Change and the Chesapeake Bay: State-of-the-Science Review and Recommendations. Chesapeake Bay Program Science and Technical Advisory Committee, Annapolis, MD. http://www.chesapeake.org/pubs/Pubs/climchangereport.pdf last accessed 4/2019

Pyke C., M.P. Warren, T. Johnson, J.Jr. LaGro, J. Scharfenberg, P. Groth, R. Freed, W. Schroeer, E. Main. 2011. Assessment of low impact development for managing stormwater with changing precipitation due to climate change. Landscape and Urban Planning 103: 166-173.

Karen C. Rice, Douglas L. Moyer, and Aaron L. Mills, 2017. Riverine discharges to Chesapeake Bay: Analysis of long-term (1927 - 2014) records and implications for future flows in the Chesapeake Bay basin *JEM* 204 (2017) 246-254

Saba, Vincent S., Stephen M Griffies, Whit G Anderson, Michael Winton, M A Alexander, Thomas L Delworth, J A Hare, Matthew J Harrison, Anthony Rosati, Gabriel A Vecchi, and Rong Zhang 2016. Enhanced warming of the northwest Atlantic Ocean under climate change. Journal of Geophysical Research, 121(1), DOI:10.1002/2015JC011346.

Sanford, W. E., Pope J. P., Selnick, D. L., and Stumvoll, R. F., 2012, Simulation of groundwater flow in the shallow aquifer system of the Delmarva Peninsula, Maryland and Delaware: USGS Open-File Report 2012-1140, 58 p.

Scully M.E., C. Friedrichs and J. Brubaker 2005. Control of estuarine stratification and mixing by wind-induced straining of the estuarine density field. Estuaries 28: 321-326.

Scully M.E. 2010. The importance of climate variability to wind-driven modulation of hypoxia in Chesapeake Bay. Journal of Physical Oceanography 40: 1435-1440.

STAC Report to the Executive Council 2011. http://www.chesapeake.org/pubs/162_E.C.Krome1990.pdf last accessed 4/2019.

Thomas, A.C., A.J. Pershing, K.D. Friedland, J.A. Nye, K.E. Mills, M.A. Alexander‖, N.R. Record, R. Weatherbee and M.E. Henderson 2017 Seasonal trends and phenology shifts in sea surface temperature on the North American northeastern continental shelf. Elem Sci Anth, 5: 48, DOI: https://doi.org/10.1525/elementa.240

Tong, S.T.Y., A.J. Lie. 2006. Modelling the hydrologic effects of land-use and climate changes. International Journal of Risk Assessment and Management 6: 344-368.

Tian, R., Chen, C., Qi, J., Ji, R., Beardsley, R. C., and Davis, C. 2014. Model study of nutrient and phytoplankton dynamics in the Gulf of Maine: patterns and drivers for seasonal and interannual variability. ICES Journal of Marine Science, doi: 10.1093/icesjms/fsu090.

Wainger, L., 2016. STAC Letter to CBP re: Climate Change Workshop Report. STAC. http://www.chesapeake.org/pubs/361_Wainger2016.pdf last accessed 4/2019.

Wang, P., H. Wang, L. Linker, R. Tian 2016a. Effects of cross-channel bathymetry and wind direction on destratification and hypoxia reduction in the Chesapeake Bay. Estuarine, Coastal and Shelf Science 178: 168-188.

Wang, P., H. Wang, L. Linker, K. Hinson 2016b. Influence of Wind Strength and Duration on Relative Hypoxia Reductions by Opposite Wind Directions in an Estuary with an Asymmetric Channel. Journal of Marine Science and Engineering 4, 62; doi:10.3390/jmse4030062.STAC, 2011.

U.S. Department of Agriculture-National Agricultural Statistics Service. Census. 2012 Census of Agriculture. Volume 1, Geographic Area Series (CD ROM). Washington, D.C.: USDA. 2014. Cerco, C.F. and M.R. Noel, 2017. The 2017 Chesapeake Bay Water Quality and Sediment Transport Model: A Report to the US Environmental Protection Agency Chesapeake Bay Program May 2017 Annapolis, 108 pp.

U.S. EPA (U.S. Environmental Protection Agency). 2010. Chesapeake Bay Total Maximum Daily Load for Nitrogen, Phosphorus, and Sediment. USEPA, Philadelphia, PA <http://www.epa.gov/chesapeake-bay-tmdl/chesapeake-bay-tmdl-document>. Accessed 1/8/2016

U.S. EPA (Environmental Protection Agency). (2013) Watershed modeling to assess the sensitivity of streamflow, nutrient, and sediment loads to potential climate change and urban development in 20 U.S. watersheds. National Center for Environmental Assessment, Washington, DC; EPA/600/R-12/058F. Available from the National Technical Information Service, Alexandria, VA, and online at http://www.epa.gov/ncea

U.S. EPA. 2016a. Climate change indicators in the United States. www.epa.gov/climate-indicators; https://www.epa.gov/sites/production/files/2016-08/documents/climate_indicators_2016.pdf

U.S. EPA. 2016b. "Climate Change Indicators: Sea Surface Temperature." Accessed August 16, 2019 https://www.epa.gov/climate-indicators/climate-change-indicators-sea-surface-temperature.

Xiang Z. 2017. Hydrologic response of a suburban watershed to climate models. Master Thesis, University of Maryland, College Park, MD.